Experimental Investigations into the Role of Geosynthetic Inclusions on the Earth Pressure Acting on Buried Structures

Mahmoud Ahmed

Department of Civil Engineering and Applied Mechanics
McGill University, Canada

March 2016

A thesis submitted to McGill University in partial fulfillment of the requirements of the degree of Doctor of Philosophy in Engineering

ABSTRACT

The design of subsurface structures associated with transportation and other underground facilities, such as buried pipes and culverts, requires an understanding of soil-structure interaction. These structures are usually subjected to heavy loads from the backfill material in addition to substantial traffic loads, particularly when the structure is buried at shallow depth below ground surface. The soil-structure interaction of these systems depend on several factors including the method of construction and the relative stiffness between the structure and the surrounding backfill material. To reduce earth pressure acting on buried structures, different techniques have been proposed by researchers including the installation of geosynthetic material above the structure to either reinforce the backfill soil (using geotextile or geogrid sheets) and distribute the earth loads away from the structure or to mobilize shear strength of the soil above the buried structure by installing a compressible material (e.g. EPS geofoam) immediately above the structure. This thesis is devoted to investigate the behavior of these composite soil-geosynthetic-structure systems using laboratory experiments focusing on buried rigid structures. The experimental results are compared with some of the available theoretical solutions, typically used in design. The investigations involved designing and building a test chamber and utilizing the tactile sensing technology to measure the changes in earth pressure distribution on the walls of the buried structures. The research results have been published and submitted for publication in refereed journals and conference proceedings amounting to three journal and two conference papers. The papers are compiled to produce six chapters and one appendix presented in this thesis.

The role of geogrid in reducing earth loads on circular pipes buried at shallow depth and subjected to a strip load is first investigated to illustrate that this installation method can be effective only if sufficient surface movement is allowed to mobilize geogrid resistance. The rest of the thesis is devoted to study the effect of placing EPS geofoam blocks above buried conduits of circular and square shapes on the magnitude and distribution of earth pressures acting on the walls of the structure. Significant reduction in pressure was found for the case of shallow circular pipes installed with EPS geofoam inclusion and subjected to repeated surface loading. This is attributed to the compressibility of the geofoam material compared to the surrounding backfill that leads to differential ground movement and the generation of upward shear stresses above the EPS material. Lastly, The behavior of a square shaped structure overlain by geofoam material under deep burial condition is also examined and the changes in pressure as well as the drag forces developed along the sides of the box section are evaluated. A comparative study is then performed between the experimental results and the existing theoretical solutions to evaluate the validity of these solutions in designing buried conduits under different conditions.

RÉSUMÉ

La conception des ouvrages et installations souterrainnes en lien avec les transports, tel que les conduites enfouies et caniveaux, nécessite une compréhension avancée des interactions sol-structure. Ce type de structure est habituellement exposé à de lourdes charges provenant des matériaux de remblais en plus d’importantes charges de trafic, plus particulièrement lorsque la structure est enfouie de façon superficielle. L’interaction sol-structure de ces systèmes dépend directement de nombreux facteurs, incluant la méthode de construction de l’ouvrage ainsi que la rigidité relative de la structure par rapport au matériel de remblayage employé. Pour réduire la pression de la terre agissant sur les structures enterrées, différentes techniques ont été proposées par des chercheurs, incluant l'installation de matières géo synthétiques au-dessus de la structure, à la fois pour renforcer le sol de remblai (en utilisant des géotextiles ou des feuilles géogrilles) et répartir les charges de terre loin de la structure ou déplacer la résistance au cisaillement du sol au dessus de la structure enterrée en installant un matériau compressible (par exemple Geofoam EPS) directement au-dessus de la structure. Cette thèse est consacrée à l’étude détaillée du comportement d’un système composite avec une structure sol-geosynthétique à l’aide de d’expériences de laboratoire effectuées sur des structures rigides enfouies. Les résultats expérimentaux sont comparés avec quelques solutions analytiques disponibles, généralement utilisées dans la conception. Les enquêtes comprenaient la conception et la construction d’une chambre d’essai et l’implantation de la technologie de senseurs tactiles pour enregistrer les variations dans la distribution de la pression des terres sur les parois de la structure enfouie. Les résultats de la recherche ont été publiés et soumis pour publication dans des revues arbitrées et

actes de conférence, pour un total de trois papiers et deux documents de conférence. Les documents sont compilés pour produire six chapitres et une annexe présentée dans cette thèse.

Le rôle des géogrilles dans la réduction des pressions des terres sur des conduites circulaires enfouies peu profondément et assujetties à une charge linéaire est tout d'abord étudié afin d'illustrer que cette méthode d'installation n'est efficace seulement lorsqu'un déplacement suffisant pour mobiliser la résistance du géogrille est possible.

La seconde partie de ce mémoire est consacrée à l'effet que peut avoir l'installation de blocs de géofoam en polystyrène expansé au-dessus de conduites de forme circulaire et carré sur l'amplitude et la distribution des pressions des terres agissant sur la structure.

Une réduction significative de la pression a été constatée pour le cas de conduites circulaires à faible profondeur installées avec des inclusions en Geofoam PSE et exposées à des charges de surface répétitives. Ceci est attribué à la compressibilité du matériau Geofoam par rapport au remblai qui mène un mouvement différentiel de masse ainsi que la génération des forces de cisaillement ascendantes au-dessus du matériau PSE. Le comportement d'une structure de forme carrée recouverte par un matériau Geofoam, sous condition d'enfouissement profond, est également examiné ainsi que les changements de pression et les forces de traînée développées le long des côtés de la section de la boîte sont évalués. Une étude comparative est ensuite effectuée entre les résultats expérimentaux et les solutions analytiques existantes pour évaluer la validité de ces solutions dans la conception de conduits enterrés dans des conditions différentes.

ACKNOWLEDGEMENTS

I would like to deeply thank my parents for their continuous support throughout the duration of my studies. This would not have been possible without my father's full trust and advice. I would like to deeply thank my PhD supervisor, Professor M.A. Meguid, for the support and training provided during my stay at McGill. This helped me broaden my learning experience over and above what was expected when I started the research program.

I would like to thank Mr. John Bartczak, Chief Shop Technician for all his effort in the laboratory particularly with the experimental setup and the preparation for the experiments. I also wish to thank Dr. William Cook for his help with the laboratory equipment throughout the study. Thanks is also due to Mr. Jorge Sayat, the IT person in the Department, for his prompt help whenever needed. I would thank my colleagues in the Geo-Group research team who assisted with the laboratory work, including, Zkaria Omeman, Sherif Kamal, Gholamreza Saghaee, Hubert Peloquin, Derek Lu and Cheehan Leung.

A special thanks to Prof. Susan Gaskin, the former Graduate Program Director, for the encouragement and guidance and making herself available whenever needed.

This thesis is dedicated to my lovely daughters Farida, Nadine and Mona.

PUBLICATIONS TO DATE

Journal Papers

[J1] Ahmed, M. and Meguid, M.A. (2009). Patents and techniques of contact pressure measurement in geotechnical engineering. Recent Patents on Engineering, Bentham Science Publishers, 3(3), 210-219.

[J2] Ahmed, M.R., V.D.H. Tran, and M.A. Meguid (2015). On the role of geogrid reinforcement in reducing earth pressure on buried pipes: experimental and numerical investigations. Soils and Foundations, 55(3), 588–599.

[J3] Ahmed, M.R., Omeman, Z., Meguid, M.A., (2016). Investigation of soil-structure interaction under deep embankments using induced trench installation. Soils and Foundations. (Submitted)

Conference Papers

[C1] Ahmed, M. and Meguid, M.A. (2009). The effect of subsurface volume loss on the bearing capacity of reinforced granular material. 62nd Canadian Geotechnical Conference, Halifax, September 2009, CD, 6 pages

[C2] Ahmed, M.R., Meguid, M.A. and Jim Whalen (2013). Laboratory measurement of the load reduction on buried structures overlain by EPS geofoam. 66th Canadian Geotechnical Conference, September 2013, Montreal, Quebec, CD, 7 pages.

CONTRIBUTION OF AUTHORS

This thesis was written according to the rules and regulations of the Faculty of Graduate Studies and Research of McGill Guidelines for a Manuscript Based Thesis, where-in it is stated the following:

“As an alternative to the traditional thesis format, the thesis can consist of a collection of papers of which the student is an author or co-author.

These papers must have a cohesive, unitary character making them a report of a single program of research. The structure for the manuscript based thesis must conform to the following:

1. Candidates have the option of including, as part of the thesis, the text of one or more papers submitted, or to be submitted, for publication, or the clearly-duplicated text (not the reprints) of one or more published papers. These texts must conform to the "Guidelines for Thesis Preparation" with respect to font size, line spacing and margin sizes and must be bound together as an integral part of the thesis. (Reprints of published papers can be included in the appendices at the end of the thesis.)

2. The thesis must be more than a collection of manuscripts. All components must be integrated into a cohesive unit with a logical progression from one chapter to the next. In order to ensure that the thesis has continuity, connecting texts that provide logical bridges preceding and following each manuscript are mandatory.

3. The thesis must conform to all other requirements of the "Guidelines for Thesis Preparation" in addition to the manuscripts.

The thesis must include the following:

1) A table of contents;

2) A brief abstract in both English and French;

3) An introduction which clearly states the rationale and objectives of the research;

4) A comprehensive review of the literature (in addition to that covered in the introduction to each paper);

5) A final conclusion and summary;

4. As manuscripts for publication are frequently very concise documents, where appropriate, additional material must be provided (e.g., in appendices) in sufficient detail to allow a clear and precise judgement to be made of the importance and originality of the research reported in the thesis."

Manuscripts J1, J2, J3, C1 and C2 (please refer to the previous section) are included in the thesis. Papers J1, C1 and C2 are the candidate's original work. All the experimental preparation, testing and manuscripts preparation were completed by the student under the supervision of Dr. Mohamed Meguid, his thesis advisor. Mr Jim Whalen, the industrial partner representative in the project, helped in revising of paper C2 and suggested some sections in the manuscript.

The author carried out all experimental work, writing of literature and the related results in the Manuscript of paper J2. Dr. V.D.H. Tran, conducted the numerical analysis and wrote the sections related to it in the manuscript under the supervision of Dr. Meguid, the authors thesis supervisor.

The experimental work in paper J3 was conducted by the author and Dr Z. Omeman, The manuscript material including introduction, literature and analysis were completed by the author under the supervision of the thesis advisor Prof Meguid. The comparison with available solutions in the code and literature was suggested by Dr. Meguid and conducted by the author. Dr. Meguid wrote some sections and finalized the paper for submission.

Table of Contents

1 Introduction 1

1.1 Overview 1

1.2 Research motivation 5

1.3 Objectives and methodology 6

1.4 Statement of originality 7

1.5 Thesis organization 8

2 Contact pressure measurement on buried structures* 9

2.1 Abstract 9

2.2 Introduction 9

2.3 Load Cells 11

2.4 Fiber optic sensors 18

2.5 Tactile Sensors 22

2.5.1 Digitacts sensors 27

2.5.2 Capacitive Sensing Technology 28

2.5.3 Tactile Sensors Protection 31

2.5.4 Validation of the sensing pads readings 32

2.5.5 Effect of protection layers on pressure readings 33

2.5.6 Advantages and Disadvantages 35

2.6 Other Techniques 36

2.6.1 Piezoresistive cells: 37

2.6.2 Normal and tangential pressure cells: 37

2.7 Current and future developments 37

2.8 Summary and Conclusions 41

3 Experimental investigation of the effect of geogrid inclusion on the earth pressure acting on buried pipes* 43

3.1 Abstract 43

3.1 Introduction 43

3.1.1 Footings on reinforced soils 46

3.1.2 Buried structures in geosynthetic reinforced soil 49

3.1.3 Scale effects 51

3.2 Experimental Setup 52

3.2.1 Test Chamber 52

3.2.2 Instrumented pipe 53

3.2.3 TactArray sensors 54

3.2.4 Backfill soil 54

3.3 Testing procedure 56

3.4 Results and Discussions 57

3.4.1 Load-displacement relationship 57

3.4.2 Initial pressure distributions on the pipe 59

3.4.3 Pressures on the pipe due to the applied footing load 60

3.5 Summary and Conclusions 64

4 Investigating the role of EPS geofoam in reducing earth load on buried pipes subjected to static and cyclic loading* 65

4.1 Abstract 65

4.2 Introduction 66

4.3 Literature review 67

4.4 Objectives 70

4.5 Experimental Setup 70

4.6 Methodology 71

4.6.1 Placement procedure 73

4.6.2 Load application 73

4.7 Measured Earth Pressure Distributions 74

4.7.1 Initial Radial Pressure on the Pipe 74

4.7.2 At the crown: 80

4.7.3 At 45 degrees (upper haunch): 81

4.7.4 At 90 degrees (springline): 83

4.7.5 At 135 degrees (lower haunch): 84

4.7.6 At 180 degrees (Invert): 85

4.8 Summary and Conclusions 85

5 Contact pressure distribution on buried box sections installed with geofoam inclusion 88

5.1 Abstract 88

5.2 Introduction and literature review 89

5.2.1 Marston-Spangler theory 90

5.2.2 Previous experimental work 90

5.2.3 Drag down forces on box sections 93

5.3 Objectives 95

5.4 Experimental Setup 95

5.4.1 Test chamber 96

5.4.2 Air pressure system 103

5.4.3 Instrumented buried box 104

5.4.4 TactArray sensors ... 105

5.4.5 Backfill soil ... 106

5.4.6 Geofoam ... 106

5.5 Methodology ... 106

5.6 Measured Earth Pressure Distributions ... 114

5.6.1 Upper Slab ... 117

5.6.2 Lower Slab ... 118

5.6.3 Side Slab ... 119

5.7 Drag down forces ... 120

5.8 Comparison with ACPA code and Marston/Spangler design theory: ... 121

5.8.1 ACPA 2011 equations ... 121

5.8.2 Marston/Spangler equations ... 122

5.8.3 Observations ... 125

5.9 Summary and Conclusions ... 125

6 Conclusions and Recommendations ... 127

6.1 Summary and Conclusions ... 127

6.1.1 Effect of geogrid reinforcement on cylindrical conduits: ... 127

6.1.2 Effect of EPS geofoam on cylindrical conduits: ... 128

6.1.3 Effect of EPS geofoam on square-shaped conduits: 129

6.2 Limitations and Future Recommendations; 130

7 Appendix 131

8 References 135

LIST OF FIGURES

Figure 1.1 Distribution of Experimental Contact Pressure (Hoeg, 1968)...................................... 1

Figure 1.2 Installation techniques for buried conduits... 2

Figure 1.3 Soil arching induced by negative projecting installation 4

Figure 2.1 Hydrualic load cell (Ahmed and Meguid, 2009)... 12

Figure 2.2 A schematic of the centrifuge experiment used to study induced trenching method (McGuigan and Valsangkar, 2010)... 13

Figure 2.3 Side and front views of a vibrating wire load cell (Ahmed and Meguid, 2009) 14

Figure 2.4 Cylindrical load cell with bonded strain gauges (Ahmed and Meguid, 2009)............ 15

Figure 2.5 Integrated strain gauge load cells to measure contact pressure on model tunnels (Tobar and Meguid, 2009) 16

Figure 2.6 Null soil pressure sensor (Talesnick, 2005) 17

Figure 2.7 Instrumented pipe section in test cell (Talesnick et al., 2011) 18

Figure 2.8 Fabry-Perot interferometer sensor (Inaudi and Glisic, 2007)..................................... 19

Figure 2.9 Fiber Bragg grating sensor (Bhalla et al., 2005) 20

Figure 2.10 Fiber Brag grating principle (White and Boltryk, 2007).. 21

Figure 2.11 Multiplexing of FBG sensors (Inaudi and Glisic, 2007) 22

Figure 2.12 Resistive tactile transducer (Girao et al., 2007) 23

Figure 2.13 Tactile sensing sheets around deformed pipelines (Choo et al., 2007) 25

Figure 2.14 Tactile sheets around a pipe in the lab (O'Rourke et al., 2008) 26

Figure 2.15 TekScan tactile sensors (https://www.tekscan.com/products-solutions/systems/i-scan-system).. 27

Figure 2.16 Digitacts tactile sensors 28

Figure 2.17 TactArray tactile sensors (PPS).. 29

Figure 2.18 Testing the precision and repeatability of TactArray Sensors.................................. 30

Figure 2.19 Capacitive technology based tactile sensors (PPS) 30

Figure 2.20 Instrumented cylindrical pipe 32

Figure 2.21 Verification of sensors accuracy and repetition in similar to experiment setup........ 33

Figure 2.22 Effect of protective layers on the measured pressure 34

Figure 2.23 Results of investigation of protective layer effect 35

Figure 2.24 Sample Data showing 3D plot of pressure distribution captured by TactArray Tactile Sensors 36

Figure 3.1 The load-displacement curves for unreinforced sand and geogrid-reinforced sand supporting a strip foundation (Das, 1993) 44

Figure 3.2 Schematic of the test chamber and the buried pipe 45

Figure 3.3. Test apparatus using aluminum rods stacked as soil medium (Yamamoto and Kusuda, 2001) 50

Figure 3.4 Translation and rotation of aluminum rods (Yamamoto and Ottani, 2002) 51

Figure 3.5 Details of the experimental setup 52

Figure 3.6 Instrumented pipe with protective layers 53

Figure 3.7 Particle size distribution of the backfill material 55

Figure 3.8 A snapshot of the measured earth pressure distribution around the pipe 57

Figure 3.9 Load-displacement relationship due to footing load over reinforced and unreinforced soil 58

Figure 3.10 Initial pressure distribution on the pipe (units kPa)...................................... 59

Figure 3.11 Changes in radial pressure at the crown 60

Figure 3.12 Changes in radial pressure at the upper haunch 61

Figure 3.13 Changes in radial pressure at the lower haunch 61

Figure 3.14 Changes in radial pressure at the invert.. 62

Figure 3.15 Augmented role of geogrid in reducing crown contact pressure at higher surface loads 63

Figure.3.16 Augmented role of geogrid in reducing upper haunch contact pressure at higher surface loads.. 63

Figure 4.1 Positive projecting versus induced trench installations.................................. 66

Figure 4.2 Culvert at Vieux Comptoir (Lefebvre et al., 1975) 68

Figure 4.3 Induced trench test (McAffee and Valsankar, 2008)..................................... 69

Figure 4.4 Experimental setup 70

Figure 4.5 Schematic of the test setup 72

Figure 4.6 Compression of a geofoam block due to induced trench installation........................ 72

Figure 4.7 Testing procedure 74

Figure 4.8 Initial earth pressure distribution (without geofoam) 75

Figure 4.9 Snapshot of the earth pressure around the pipe after geofoam installation 75

Figure 4.10 Initial earth pressure distribution on the pipe 79

Figure 4.11 Changes in earth pressures under cyclic loading (at the crown) 80

Figure 4.12 Changes in earth pressures under cyclic loading (at the upper haunch).................... 81

Figure 4.13 Changes in earth pressures under cyclic loading (at the springline) 83

Figure 4.14 Earth pressures in cyclic loading (lower haunch).. 84

Figure 4.15 Earth pressures in cyclic loading (invert).. 85

Figure 5.1 Problem Description.. 89

Figure 5.2 A schematic of the box culvert installation methods.. 94

Figure 5.3 Schematic showing dimensions of setup.. 95

Figure 5.4 Detailed schematic of setup.. 97

Figure 5.5 Lateral confining system 98

Figure 5.6 Test chamber top view (showing reinforced restraining cover)................................. 99

Figure 5.7 Vertical restraining system 100

Figure 5.8 Assembled test chamber 101

Figure 5.9 Dial Gauges for monitoring bulging during loading 102

Figure 5.10 Air pressure system 103

Figure 5.11 Instrumentation of the buried structure 104

Figure 5.12 (a) instrumented box wrapped in protective layer (b) tactile sensor pads orientation on the box.. 105

Figure 5.13 The buried box and geofoam installation process layout 1: (a) HSS placed over bedding layer; (b) geofoam layer placed over the HSS; (c) backfill placed.............................. 108

Figure 5.14 and geofoam installation process layout 2: (a) HSS placed over bedding layer; (b) geofoam layer placed on the sides; (c) backfill placed (d) sides covered with backfill (e) top layer of geofoam placed.. 109

Figure 5.15 The test setup and acqusition system during the experiment 110

Figu 5.16 Contact pressure when the buried box is placed resting on soil................................ 112

Figure 5.17 (a) initial condition (airbag empty), (b) positive projecting (Test 3), induced trench (c) stiff geofoam on Top (Test 5), (d) soft geofoam on top (Test 6), (e) (stiff geofoam top/sides (Test 10), (f) soft geofoam top/sides (Test 12) 113

Figure 5.18 Typical pressure readings on the top wall under applied surface pressure of 140 kPa 114

Figure 5.19 Average contact pressure on the upper wall (EPS on top only)............................. 117

Figure 5.20 Average contact pressure on the upper wall (EPS on top and side walls) 117

Figure 5.21 Average contact pressure on the lower wall (EPS on top only)............................. 118

Figure 5.22 Average contact pressure on the lower wall (EPS on top and side walls) 118

Figure 5.23 Average contact pressure on the side wall (EPS on top only)................................. 119

Figure 5.24 Average contact pressure on the side wall (EPS on top and side walls)................. 119

Figure 5.25 Comparison of normalized contact pressures using different methods.................. 124

LIST OF TABLES

Table 2-1 Tactile sensors 31

Table 2-2 Comparison between selected contact pressure measurement techniques 40

Table 2-3 Selected applications of different contact pressure measurement cells........................ 42

Table 3-1 Footings on soils with reinforcement and/or induced voids.. 48

Table 3-2 Recommended parameters for geogrid reinforcement 49

Table 3-3 Properties of the backfill material 55

Table 4-1: Properties of GeoSpec EPS 22 geofoam (Plasti-Fab Ltd).. 71

Table 4-2 Measured pressure changes after Geofoam Installation 87

Table 5-1 Parametric studies in the literature for box culverts.. 92

Table 5-2 Geofoam physical properties 106

Table 5-3 Conducted tests.. 107

Table 5-4 Pressure changes recorded for different EPS arrangement around the structure 120

Table 6-1 Measured pressure changes after geofoam installation 128

LIST OF SYMBOLS

λ_B	Resonance value
η_{ref}	Refractive index
Λ	Grating pitch
C_n	Embankment load coefficient
B_{cr}	Bearing capacity ratio
N_γ	bearing capacity factor due to self-weight
γ_s	Soil unit weight
B	Trench width
ν	The medium Poisson's ratio
k	The lateral pressure factor
r	The pipe radius
C	The compressibility ratio
F	The flexibility ratio
M^*	The constrained modulus
E_c	The conduit Young's modulus
D	Pipe diameter

t	Pipe wall thickness
ν_c	The conduit Poisson's ratio
E	Material stiffness
w	Geofoam width
h	Geofoam height
H	Culvert box height
W	Culvert box width
Υ_s	Soil unit weight
D_o	Outside diameter
B_d	Width of trench
K	Ratio of active lateral unit pressure to vertical unit pressure
μ'	Coefficient of friction between fill material and sides of trench
$K_{\mu'}$	0.165 Max for sand and gravel
H_e	Height of plane of equal settlement
C_n	Embankment load coefficient
c_d	Trench load coefficient
w	Vertical load

Chapter 1

Introduction

1.1 Overview

Buried pipes and culverts are critical infrastructures used under highways, roads, levees, and dams to convey water, utilities or pedestrians. These structures carry significant vertical and lateral earth pressures and are often subjected to temporary loading during construction and more complex permanent loading during service life. The magnitude and distribution of these pressures depend mainly on the construction method and the relative stiffness between the pipe and the surrounding soil. Figure 1.1 shows the contact pressure for buried pipes based on the experimental investigations conducted by Hoeg (1968) on embankment installations. It can be seen that for rigid pipes on the left side of the figure, the maximum contact pressure is reached at the invert (bottom) followed by crown (top) and its minimal at the spring line (middle).

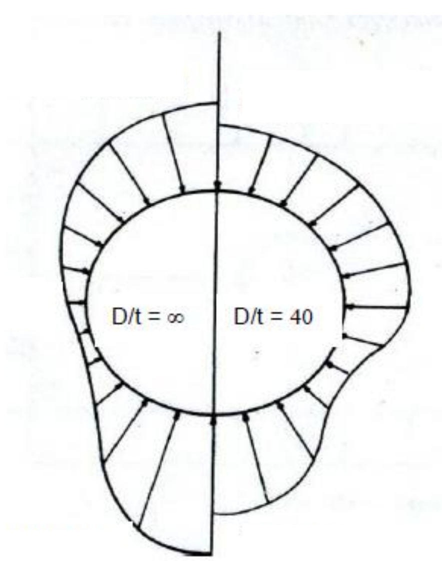

Figure 1.1 Distribution of Experimental Contact Pressure (Hoeg, 1968)

There are different installation techniques for rigid structures. The selection of the technique depends on the geography, location and expertise available. In addition to that, the Code might specify which techniques are permitted. Figure 1.2 illustrates such techniques where each has its own advantages and equations which are mainly related to the contact pressures transferred to the buried structure as will be explained later in more details.

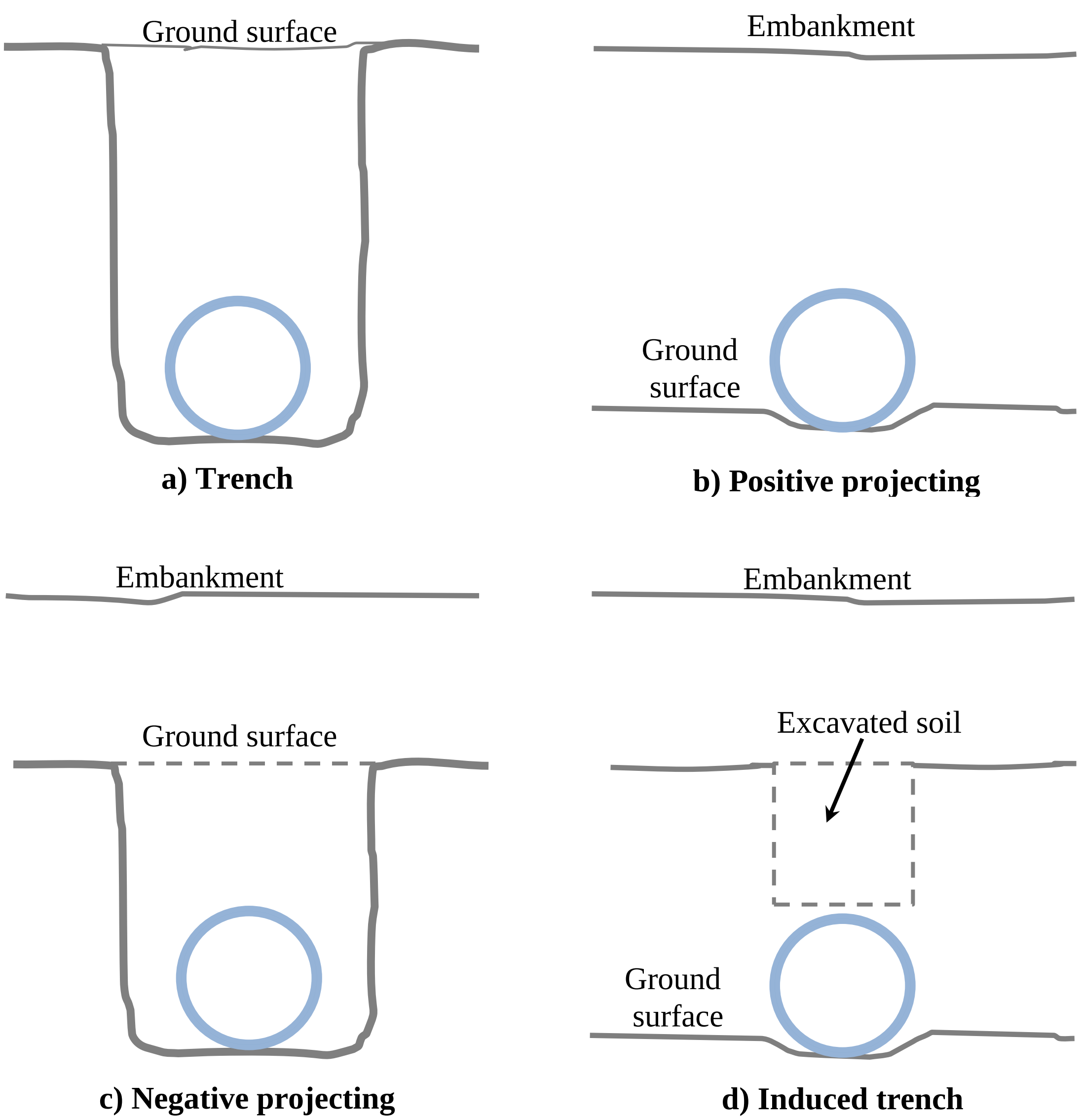

Figure 1.2 Installation techniques for buried conduits

When the relative movement of the soil prism above the structure is more than that of the adjacent soil (e.g. trench installation), upward shear forces develop along the trench walls resulting in a reduction in earth pressure on the pipe. Similarly, when the relative movement of the soil prism above the pipe is less than that of the adjacent soil (e.g. embankment installation), downward shear forces develop increasing the earth pressure on the structure to a value even more than the overburden pressure at a similar depth. The theory of external loads on buried pipes was first published by Marston and Anderson (1913). Marston (1930) discussed the loads on rigid conduits and the shear forces developing above the structure considering the stress-strain characteristics and other soil properties (e.g. density, cohesion and friction angle). Spangler (1950) quantified the load distribution phenomenon around buried conduits by measuring the settlement ratios of different highway culverts.

These studies led to the Marston-Spangler design equation for calculating earth loads on buried structures (Equation 1.1) for negative projecting installations. The corresponding earth load on the structure is determined using the following equation:

$$W_n = (C_n w B_d^2) \tag{1.1}$$

Where,

W_n is the backfill load for negative projecting embankment installations,

C_n is the load coefficient for negative projecting embankment installations,

w is unit weight of backfill material and B_d is the trench width.

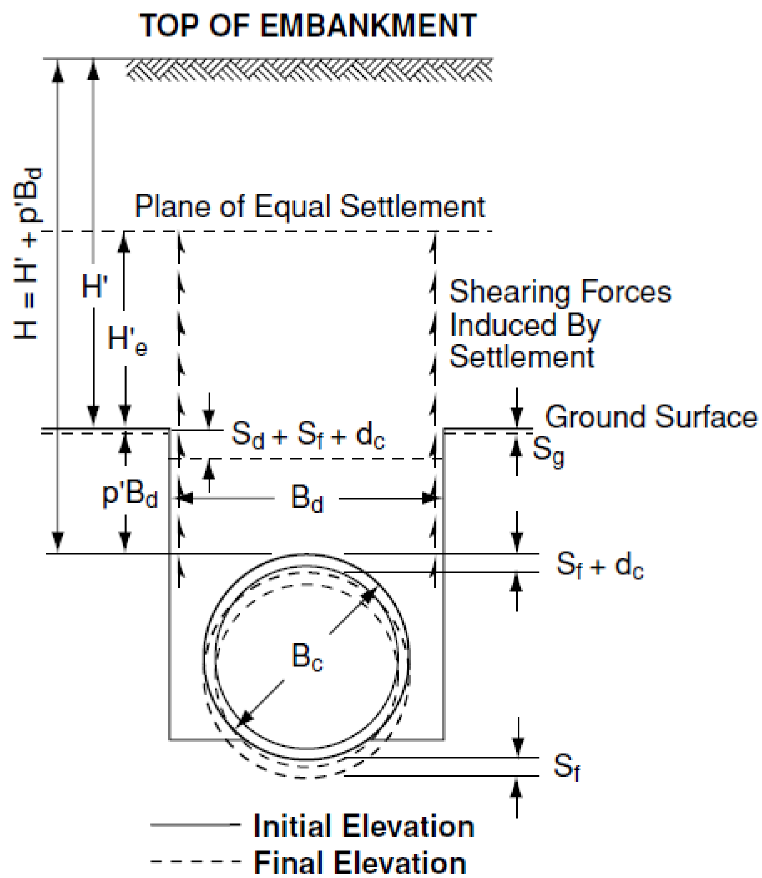

Figure 1.3 Soil arching induced by negative projecting installation (ACPA, 2011)

Figure 1.3 illustrates the various terms used to calculate the load coefficient, C_n, and the backfill load, W_n, on the pipe. The load coefficient is calculated from a set of charts provided by Marston-Spangler using the settlement ratio (r_{sd}) (Equation 1.2), projection ratio (ρ') and the location of the plane of equal settlement (H_e') which are hard to determine in advance. Some recommended values were provided by Spangler and Handy (1982).

$$r_{sd} = \frac{S_g - (S_d + S_f + d_c)}{S_d} \tag{1.2}$$

The induced trench method is one of the effective installation techniques in reducing earth pressure on buried conduits (Figure 1.2d). The addition of a light-weight material above the pipe installed under embankment was found to promote relative movement and consequently the development of upward shear stresses. It has been recently found (McAffee and Valsangkar, 2008) that EPS geofoam is considered suitable as a compressible lightweight material for induced trench applications above buried conduits installed using the embankment technique.

Another way of reducing the earth pressure on buried structures is to transfer the vertical loads laterally away from the conduit using a high tensile geosynthetic sheet placed above the pipe. (Bueno et al. 2005). The shear resistance developing at the interface between the geosynthetic sheet and the backfill material due to relative soil movement results in lateral spreading of the vertical pressure in the horizontal direction.

This research work is an attempt to understand the load transfer mechanisms on rigid conduits overlain by different geosynthetic materials through experimental investigation and comparison with existing analytical and empirical solutions.

1.2 Research motivation

Evaluating the earth pressure distribution on buried pipes and culverts requires direct measurement of the contact pressure transferred to the walls of the structure. Previous experimental work relied mainly on load cells placed at selected locations at the outer perimeter of the buried structure. Although this method might work well for rectangular culverts, it becomes complicated for circular pipes. Therefore, there is a need for other pressure measurement techniques that are suitable for measuring contact pressure distribution on subsurface structures particularly for physical modeling experiments conducted in the laboratory.

AASHTO (2010) has recognized induced trench construction as one of the acceptable pipe installation techniques, however, since there were no clear guidelines or procedure provided for engineers to apply the method, AASHTO suggested that accepted test methods or soil-structure interaction analyses would be needed to determine the earth load on the culverts. Additional experimental investigations (such as those presented in this thesis) and field data are therefore needed to confirm the existing design methods. Experimental data are also essential for the validation of numerical models. It is also worth noting that the work reported here is supported by the industry and the final results can be used to confirm design.

1.3 Objectives and methodology

The objectives of this research is to experimentally investigate the effect of installing geosynthetic materials above buried conduits on the earth loads transferred to the walls of the structure. A test chamber was designed and built to host the buried structure and the backfill material simulating two-dimensional loading condition. Two different types of load-reduction techniques are examined in this study, namely, the inclusion of geogrid reinforcement and the use of EPS geofoam. The laboratory tests are conducted for both circular and square shaped cross sections. Emphasis is placed on the following:

1. The influence of geogrid reinforcement on the contact pressure acting on shallow circular pipes subjected to strip loading parallel to the pipe axis.
2. The effect of placing a geofoam block immediately above a circular pipe subjected to static and cyclic loading on the contact pressure distribution on the pipe.

3. The role of geofoam inclusion on the contact pressure distribution on square shaped conduit. A comparison between the measured pressures and the analytical solution of Marston-Spangler theory as well as the ACPA procedure is made.

1.4 Statement of originality

The research reported in this thesis investigated important aspects related to improving the performance of buried rigid structures using two different techniques. A laboratory setup is designed and built to allow for the instrumented buried structures to be hosted in a test chamber and subjected to various types of surface loading. A new earth pressure measurement technique utilizing TactArray flexible sensors was developed and used throughout this study. The key contributions of this thesis are listed below.

- Examining the role of reinforcing the backfill material above cylindrical buried pipes using a geogrid sheet on the earth load reaching the pipe wall.
- Investigating the response of cylindrical buried pipes installed at a shallow depth using induced trench method to cyclic loading.
- Studying the soil-structure interaction and the development of drag down forces associated with rigid conduits of squared cross-section installed using the induced trench method under high embankment loading.
- Evaluating the effect of placing geofoam blocks around the buried structure on the earth pressure distribution as compared with conventional installation methods.
- Comparing the measured earth pressure at the top wall of the buried conduit with theoretical solutions used in the ACPA code as well as Marston-Spangler theory.

1.5 Thesis organization

This thesis is divided into three parts. The first part, Chapter 2, reviews contact pressure measurement techniques with emphasis on measuring earth pressure on subsurface structures. Conclusions were made regarding the suitability of each method for application in geotechnical engineering to measure the magnitude and distribution of earth pressure on various structures.

The second part is presented in Chapter 3 and investigates the effect of geogrid reinforcement on the contact pressure distribution on circular pipes. The design of the experimental setup is first presented and the test procedure, including the calibration of the tactile sensors, is discussed. Results and comparison with unreinforced condition are presented.

The third part, Chapters 4 and 5, investigates induced trench installation of buried conduits of circular and square sections, respectively, using EPS geofoam material. In Chapter 4, the effect of cyclic loading on pipes of circular cross-section installed near the surface is investigated. Chapter 5 focuses on the response of square-shaped conduits buried under deep embankment and overlain by a geofoam block. The drag forces associated with induced trench installation is discussed. In addition, the effect of EPS density and location around the buried conduit is examined. A comparison between the experimental results and two different theoretical solutions (ACPA code and Marston-Spangler theory) is made and the applicability of these methods is evaluated. Chapter 6 presents the conclusions of the research described in this thesis, recommendations for future research and limitations of the reported results are highlighted as well.

Chapter 2

Contact pressure measurement on buried structures*

2.1 Abstract

Measuring the contact pressure between a structure and the surrounding ground is essential for the analysis and design of different geotechnical engineering systems (e.g. foundations, underground tunnels, buried pipes, vertical shafts and retaining walls). Several devices and techniques have been developed to facilitate the measurement of contact pressure in small scale experiments and large scale field tests. These devices range from stiff pressure cells that measure the soil pressure against a structure at specific locations to flexible tactile sensors that can track the pressure changes continuously over large contact areas of various geometrical shapes.

This Chapter presents a review of selected techniques commonly used to measure contact pressure in different soil-structure interaction problems. A comparison between the different techniques with respect to their theoretical background, applicability and limitations is also presented. The pressure measurement method used in this study is then introduced.

2.2 Introduction

Pressure measurements in soil fall into two basic categories: measurements within the soil mass and measurements at the interface between a structural element and the surrounding soil. Conventionally, embedded load cells have been used to determine the magnitude and distribution

*A version of this chapter has been published in Recent Patents on Engineering, Bentham Science Publishers, 3(3), 210-219.

of in-situ stress within embankments and backfill material in addition to the measurement of contact pressure against retaining walls, culverts and shallow foundations.

Carlson (1939) is considered to be among the first to measure compressive stresses in concrete using load cells and showed that a cell stiffer than the surrounding material would indicate a higher stress state. Taylor (1947), Monfore (1950) and Peattie and Sparrows (1954) investigated the effects of shape and internal construction of the cell on the measured pressure. Comprehensive surveys of the use of pressure cells to measure in-situ stresses have been made by Selig (1964), Hanna (1985) and Dunnicliff (1988). These studies aimed at understanding the behaviour of large pressure cells when placed “in concrete” or “in soil”. An important criterion required for rating an earth pressure measuring instrument is that it should be capable of determining pressure or a related parameter (e.g. displacement) without distortion resulting from the presence of the instrument in the soil as a foreign material.

Lazebnik and Tsinker (1997) reviewed the different monitoring techniques used in soil-structure interaction problems focusing on developing, calibrating and installing soil pressure measuring devices. This application requires a device that is rigid enough such that the sensing surface is not deformable during the loading process. It was concluded based on field studies that the best results can be achieved when multiple pressure cells are flush-mounted with the underside of a footing or the backside of a retaining structure. This was found to average out the soil reaction or lateral pressure and local discontinuities in the soil over the larger contact area of the plate.

The above studies, among others, provided engineers and researchers with guidelines as to the suitability of different classical devices to a given application. A brief summary of pressure measurement devices commonly used for soil-structure interaction applications is given below.

2.3 Load Cells

A load cell is a transducer that converts force into a measurable electrical output. Load cells have been widely used for measuring contact soil pressures in different geotechnical engineering applications including foundations, retaining walls, pavements, buried pipes and tunnels

The main advantage of using load cells is the accumulated experience for more than 70 years. In addition, there are various types of commercially available transducers with application-specific documentation and installation procedure. Load cells consist mainly of a disc of certain stiffness connected to a transducer. This disc is then placed atop of the surface where soil pressure is to be measured. Once the deformable face is pressed, a signal is sent to the transducer and converted into an equivalent earth pressure reading using the connected data acquisition system.

Load cells are often distinguished according to the type of output signal generated. Four different types of commonly used load cells are discussed below.

Hydraulic and Pneumatic Cells: Hydraulic load cells are force-balance devices measuring the change in pressure of the internal filling fluid (Lazebnik and Chemysheva, 1968). The applied pressure is usually transferred to a piston that in turn compresses the filling fluid confined in a diaphragm chamber as shown in Figure 2.1. Since such sensor has no electric components, it is ideal for use in hazardous areas.

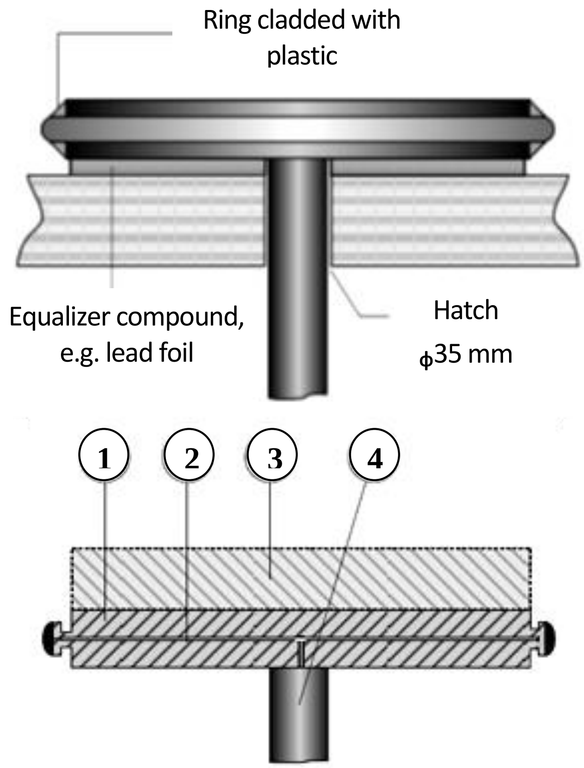

System and construction:

1 Piston pad
2 Hydraulic fluid
3 Distribution plate
4 Electric pressure converter

Figure 2.1 Hydrualic load cell (Ahmed and Meguid, 2009)

Pneumatic load cells operate similarly, however it contain no fluids that might contaminate the surrounding medium if the diaphragm ruptures. These conventional load cells were used by McGuigan and Valsangkar (2010) to measure earth pressure on buried culverts in centrifuge experiments (Figure 2.2).

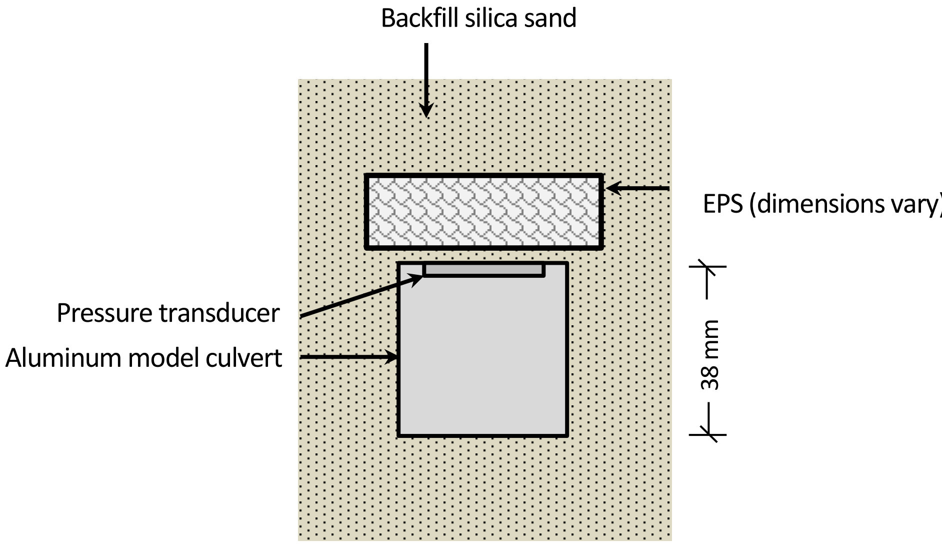

Figure 2.2 A schematic of the centrifuge experiment used to study induced trenching method (McGuigan and Valsangkar, 2010)

The Resonant-Wire Transducers: the resonant-wire pressure transducer was introduced in the late 1970s (Lazebnik et al., 1968 and Jennings and Burland, 1960). A wire is gripped by a static member at one end, and by the sensing diaphragm at the other as shown in Figure 2.3. An oscillator circuit causes the wire to oscillate at its resonant frequency. A change in pressure changes the wire tension, which in turn changes the resonant frequency of the wire. Since the change in frequency can be precisely detected, this type of transducer can be used for low differential pressure applications.

Cable

Transducer

Structure Wall

Mortar Pad

Lug

(http://www.geokon.com/content/datasheets/4800_Series_Earth_Pressure_Cells.pdf)

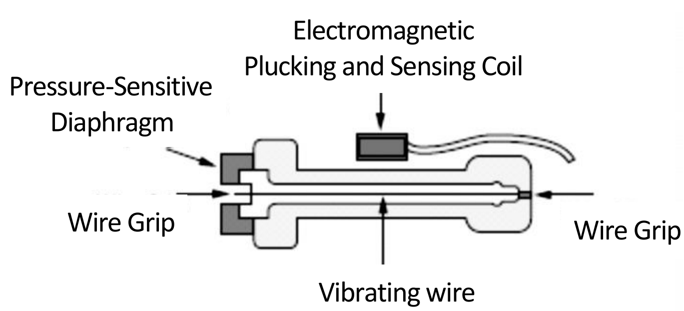

(http://www.omega.com/literature/transactions/volume3/pressure.html)

Figure 2.3 Side and front views of a vibrating wire load cell (Ahmed and Meguid, 2009)

Strain Gauge Sensors: One of the most commonly used pressure measuring tools is the strain gauge type load cells. They basically convert load into electrical signals. The strain gauges are bonded onto a structural member that will deform when load is applied as shown in Figure 2.4. In most cases, four strain gauges are used to obtain maximum sensitivity and temperature compensation. Lazebnik and Chernysheva (1968) highlighted that contact pressure cells need to have the same rigidity as that of the monitored structure (retaining wall, pipe, etc.). Lazebnik et al., (1973) conducted a comparison between different types of pressure cells made between the 1962 and 1971 and recommended a soil-cell stiffness ratio of 7 in order to reach a percentage error of less than 2%.

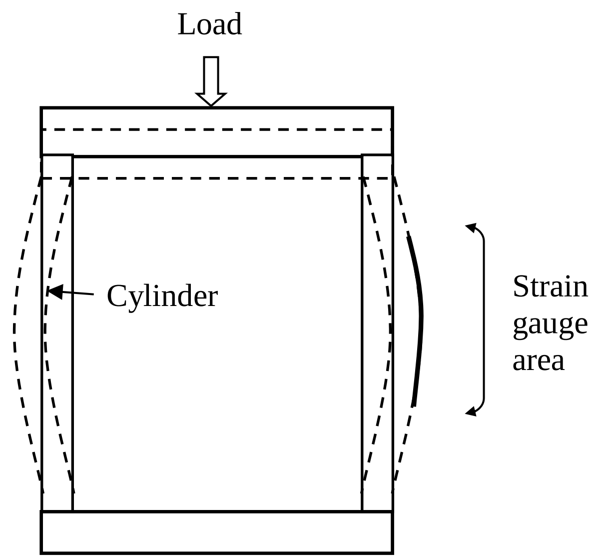

Figure 2.4 Cylindrical load cell with bonded strain gauges (Ahmed and Meguid, 2009)

Integrated strain gauge based load cells

Another technique for measuring contact soil pressures on burried pipes, shafts and tunnels was reported by Tobar and Meguid (2009). Sensitive load cells were integrated into the physical model being investigated as shown in Figure 2.5. The system has been used to measure earth pressure on different subsurface structures. It was further used to investigate erosion effects and deterioration of walls of buried structures and was satisfactory as well (Kamel and Meguid 2013).

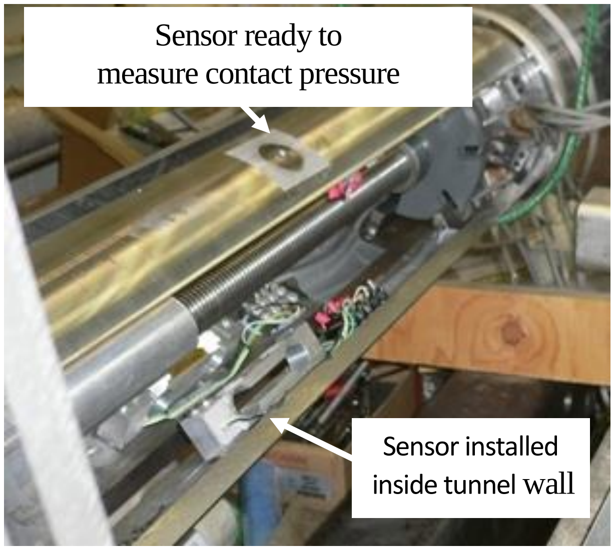

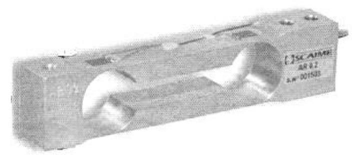

Load cell (Scaime)

Figure 2.5 Integrated strain gauge load cells to measure contact pressure on model tunnels (Tobar and Meguid, 2009)

Null Pressure Sensors: The concept of null pressure cells was introduced by Jennings and Burlan (1960). The diaphragm surface deformation under loading is consistently measured and a counter pressure is applied internally to the cell to bring the deflection back to zero. This applied pressure is equal to the actual earth pressure load. Margason and Irwin (1964) used the null pressure concept in earth pressure cells to measure soil pressure below road embankments. The cell was 7 inch in diameter and 1.125 inch in thickness. An electrical circuit was placed inside the fluid filled cell with diaphragm surface. Once the diaphragm displaces a distance of 0.0015 mm the circuit is closed and a signal is sent to increase fluid pressure until the diaphragm surface is back into position.

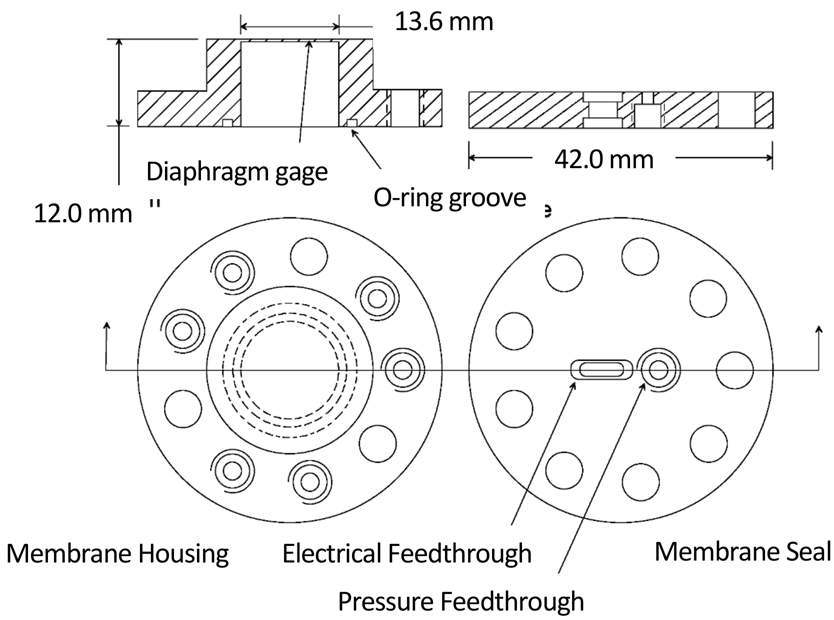

Figure 2.6 Null soil pressure sensor (Talesnick, 2005)

Talesnick (2005) developed a similar transducer based on the work of Deobelin (1990). The transducer (Figure 2.6) consists mainly of a steel chamber that is air pressurized with sensing elements that have bonded strain gauges. When the elements deform due to soil pressure the strain gauges would detect the membrane strain and the air pressure system would null the soil pressure and bring the membrane back to the original position. Talesnick et al., (2008) used the null pressure cells to measure contact pressure acting on buried structures. Talesnick et al., (2011) used null pressure sensors (2.3 cm in diameter and 0.7 mm in thickness) installed flushed with pipe surface to measure earth pressure on the pipe as shown in Figure 2.7.

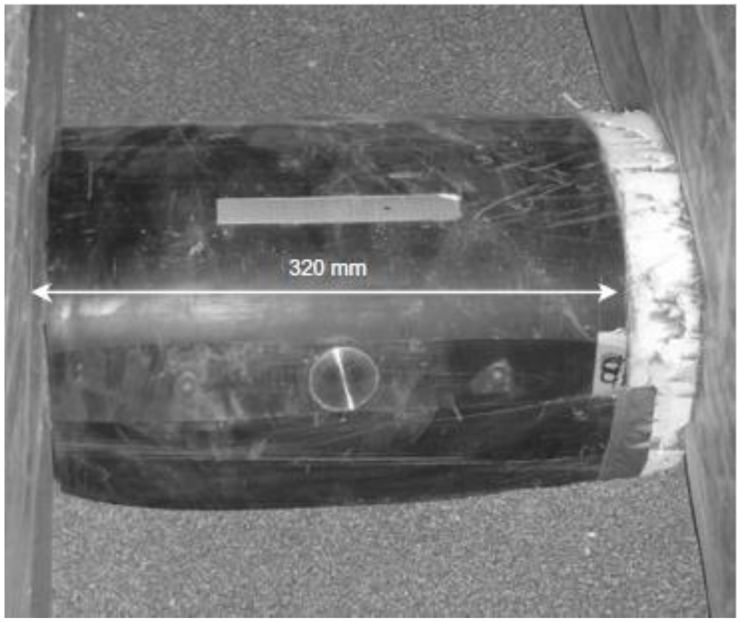

Figure 2.7 Instrumented pipe section in test cell (Talesnick et al., 2011)

2.4 Fiber optic sensors

The principle of operation of a fiber optic sensor (FOS) is having a sensing element that alters some parameters (intensity, wave length, polarization, phase, etc.) of an optical beam passing through it. This leads to a change in the characteristics of the optical signal received at the detector end. The application of optical fibers as a sensing tool started in the 70s (Lee, 2003). Fiber optic sensors have been used in medicine, navigation and water treatment applications.

The uses of FOSs in civil engineering include the monitoring of bridges, dams and tunnels (Bhalla et al., 2005 and Majumder et al., 2008). In geotechnical engineering FOSs are used to measure moisture content and chemical concentration in soils (Cosentino et al., 1995) and strains along buried pipelines (Ravet et al., 2006).

The three common types of FOPs are: Fabry-Pérot Interferometric Sensors (FPI), Fiber Bragg Grating Sensors (FBG), and Distributed Brillouin/Raman Scattering Sensors. FPI and FBG sensors are used in local strain measurement applications by civil engineers while the third is used mainly for long-term health monitoring of large structures (Inaudi and Glisic, 2007). The main difference between FPI and FBG is the technique used for altering the light properties. The FPI consists of two mirrors of reflectance separated by a gap that represents the gauge length (Figure 2.8).

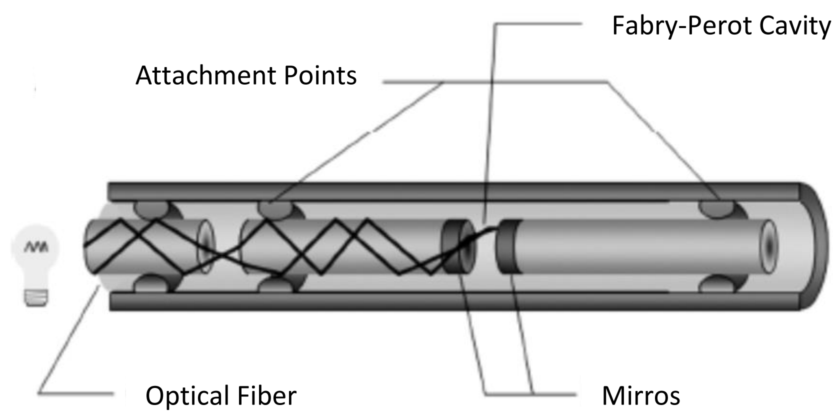

Figure 2.8 Fabry-Perot interferometer sensor (Inaudi and Glisic, 2007)

The Fiber Brag Grating sensor is manufactured by altering the optical fiber core through exposure to Ultraviolet (UV) light at certain locations. This causes a grating period to be formed. The input light passes through the fibers except for the component that has resonance with the grating period as shown in Figures 2.9 and 2.10.

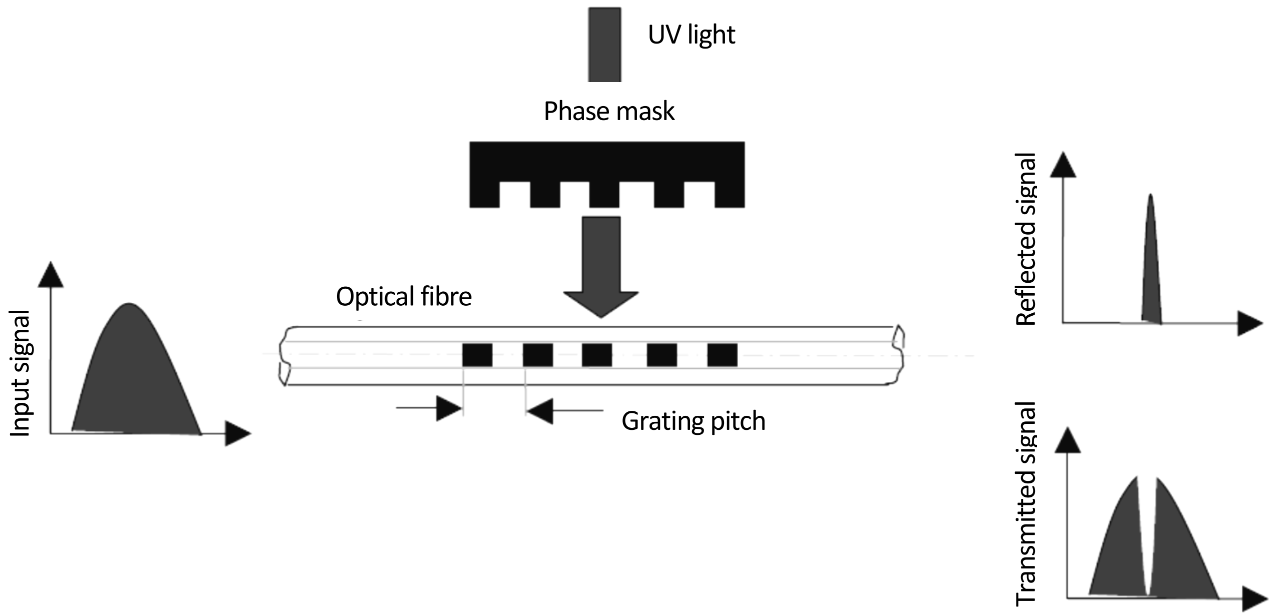

Figure 2.9 Fiber Bragg grating sensor (Bhalla et al., 2005)

Through a spectrum analyzer this wave can be detected. The grating period is the gauge length. When the gauge length changes due to straining of the grating pitch, the phase of the reflected wavelength shifts. The resonance value, $\boldsymbol{\lambda}_B$, for the Fiber Bragg Grating can be expressed by (White and Boltryk, 2007).

$$\lambda_B = 2\,\eta_{ref}\,\Lambda \tag{2.1}$$

Where $\boldsymbol{\eta}_{eff}$ is the refractive index of the fiber material and $\boldsymbol{\Lambda}$ is the grating pitch (see Figure 2.10).

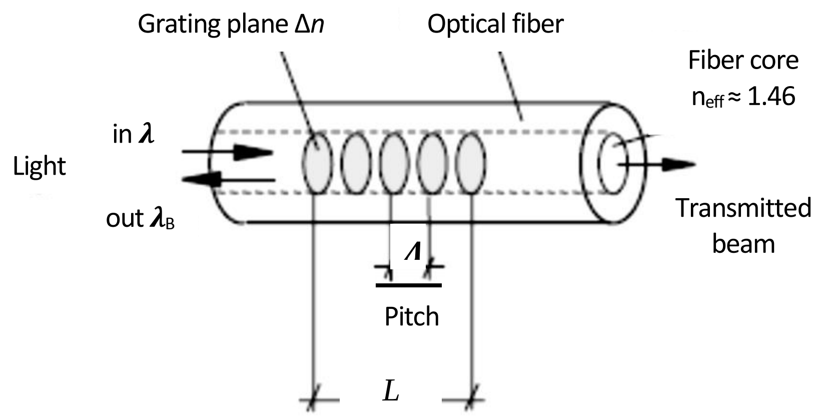

Figure 2.10 Fiber Brag grating principle (White and Boltryk, 2007)

An interesting example that demonstrates the application of FBG in contact pressure measurement is the work of Legge et al., (2006), where the Fiber Bragg grating stress cell was made by encapsulating the FBG sensor in a silicon casing. When the cell was exposed to a lateral pressure it experienced longitudinal strains. The silicon, having a high Poisson's ratio, enhances the longitudinal sensitivity of the sensor. The FBG cell solves several problems encountered by traditional load cells, such as sensitivity to water ingress, short life range and fragility.

FBG sensors allow for multiplexing which is having several sensors (gratings) over one optical fiber as shown in Figure 2.11. Each grating has its resonance value that reflects a specific wavelength among the light spectrum. This saves on the wiring time and additional installation of sensors.

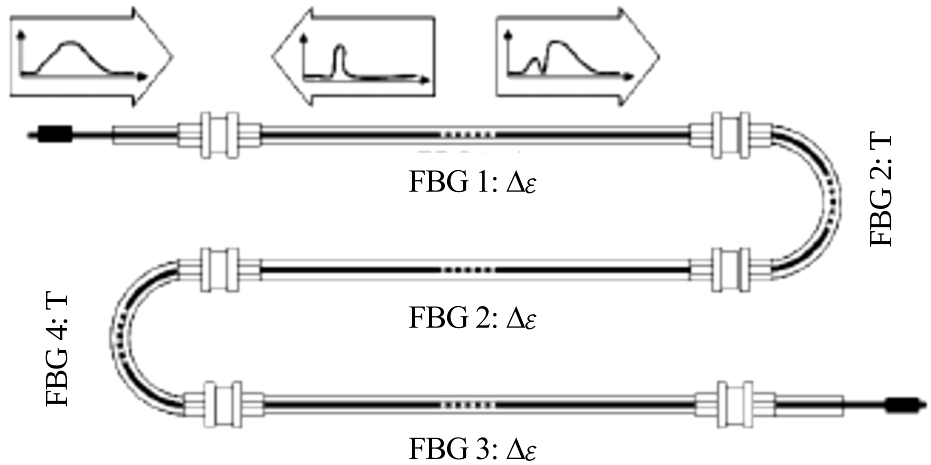

Figure 2.11 Multiplexing of FBG sensors (Inaudi and Glisic, 2007)

Dore et al., (2008) introduced fiber optic sensors that are capable of measuring horizontal strains at the interface between asphalt pavement and base layer through continuing on the work of Duplain and Van-Neste (2006). Duplain (2007) made further improvement to the previous patent by minimizing the dispersion effect of the measurand. This yielded less distorted readings by eliminating other physical changes, hence enhancing the sensor sensitivity.

2.5 Tactile Sensors

Adapted from the robotic industry, the basic principle of tactile sensors is the change of electrical resistance under pressure for a material placed between two electrodes or in touch with two electrodes placed at one side of the material (Weiss and Worn, 2005). Conductive elastomer cords or pads laid in a grid pattern are usually employed with the resistance measurements being taken at the points of intersection (sensels). Figure 2.12 shows a 3 x 3 array of resistive sensels (Girao et al., 2007).

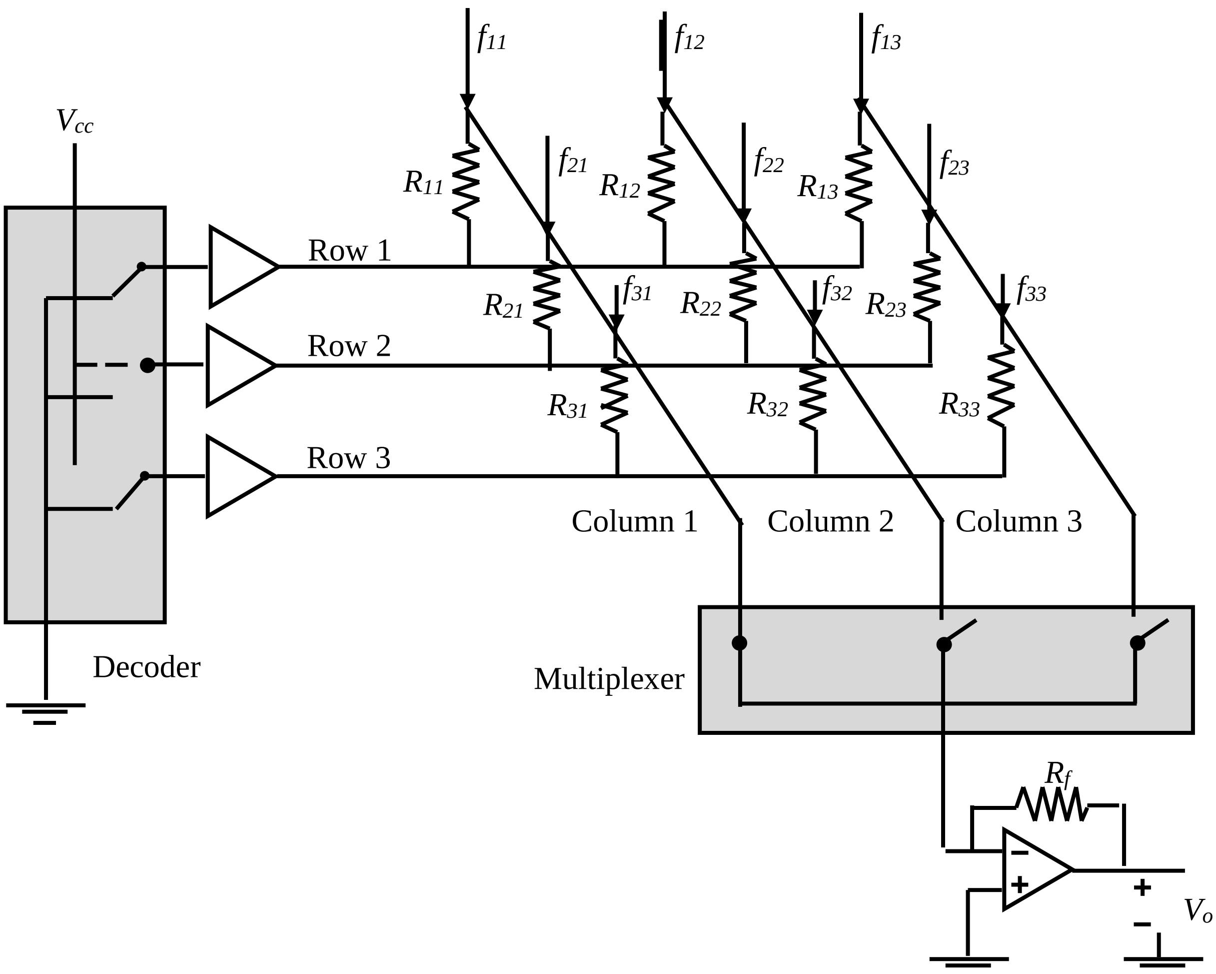

Figure 2.12 Resistive tactile transducer (Girao et al., 2007)

A standard tactile sensor typically consists of an array of force-sensitive cells embedded between two flexible polymeric sheets to measure only normal pressure distribution. Because of their limited thickness (usually less than 1 mm), tactile sensors possess favourable characteristics with respect to aspect ratio and stiffness over conventional load cells. In addition, the fact of being flexible enables shaping the sensing pads to cover curved surfaces, hence suitable for cylindrical shape structures (e.g. pipes shafts, or tunnel).

Although they were originally designed for robotics and dental applications, tactile pressure sensors have been used in geotechnical engineering applications to measure the distribution of normal stresses in granular soils. (Paikowsky, 1997-2006).

The first tactile sensor patent was credited to Krivopal (1989). Paikowsky and Hajduk (1997) and Paikowsky et al., (2006) used tactile sensor technology to measure pressure distribution under rigid footings supported by sandy soil. Results indicated an agreement between the measured pressures and the theoretical prediction using the Bearing Capacity theories. Springman et al., (2002) used tactile sensors in geotechnical centrifuge to measure the load distribution due to rock falls on protection structures. Tactile sensors have been used in several geotechnical applications since early 2000, they proved to be satisfactory even in centrifuge facilities and under impact loads as reported by Springman et al., (2002).

Tachi et al., (2006) managed to transform the pressure measured using tactile sensors into forces in three-dimensional space in an attempt to develop an optical tactile sensor capable of measuring both shear and normal forces. The process involves photographing sensels using CCD cameras. The sensels consisted of colored circular markers arranged in different layers forming a grid. Images were taken and analyzed using color coding technology.

Son and Parks (2007) used textile electrodes to form a cloth based tactile sensor. Several problems were encountered including the electrode wiring for large size grids (more than 10 by 20). To rectify the problem, an intermediate harness was introduced between the two layers that form the grid. All electrical connections were connected to the intermediate harness rather than directly to the electrodes.

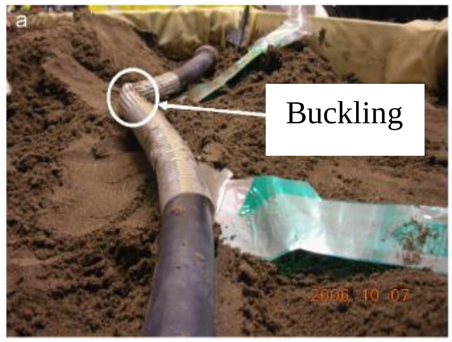

Figure 2.13 Tactile sensing sheets around deformed pipelines (Choo et al., 2007)

Choo et al., (2007) and Abdoun et al., (2009) measured the radial pressure acting on a pipeline using tactile sensing sheets as shown in Figure 2.13. O'Rourke et al., (2008) used tactile sensors to measure the lateral earth pressure on pipes (Figure 2.14) and recommended covering the sensors with two layers of Teflon to minimize shear stresses on the sensors.

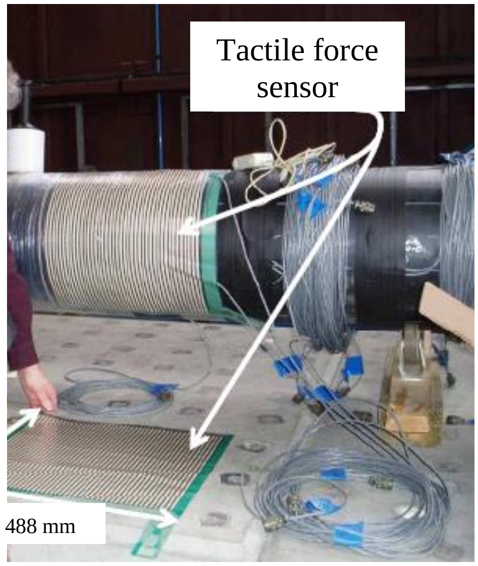

Figure 2.14 Tactile sheets around a pipe in the lab (O'Rourke et al., 2008)

Tactile sensors were used in trap door experiments (Rolwes, 2002) to simulate pressures on buried structures and record relative displacements in soil. The sensors were found to be challenging and capable of capturing either low or high pressures as a result of their sensitivity and degree of saturation. It was concluded that calibration could be challenging, and the generic calibration of the sensors may not be sufficient.

Tessari et al., (2010) recommended using double layer Teflon coatings to protect against shear stresses which tend to slide the two surfaces forming the pad. This is achieved through double coating by preventing transfer of forces parallel to the pad which would be dissipated by the smooth coating layers.

The inability to fully record stresses under seismic loading was reported by Olson et al., (2011) due to failure in capturing the full amplitude content at high frequencies, hence recommending them only for static loading scenarios.

2.5.1 Digitacts sensors

Tactile sensors employ different technologies. Mainly the Digitacts have been used in civil engineering applications due to its relative low cost. Figures 2.15 and and 2.16 show samples of such sensors. The other technology is the tactarray sensors (Figure 2.17) which are used in the research conducted in this thesis and further discussed in the next section in addition to comparison to other types of sensors available in the market.

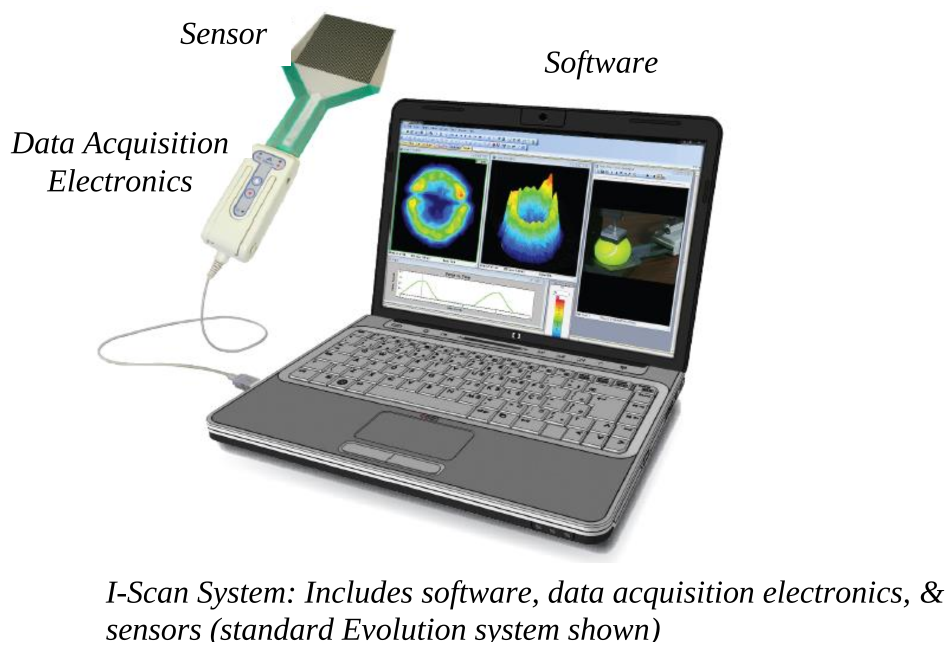

Figure 2.15 TekScan tactile sensors (https://www.tekscan.com/products-solutions/systems/i-scan-system)

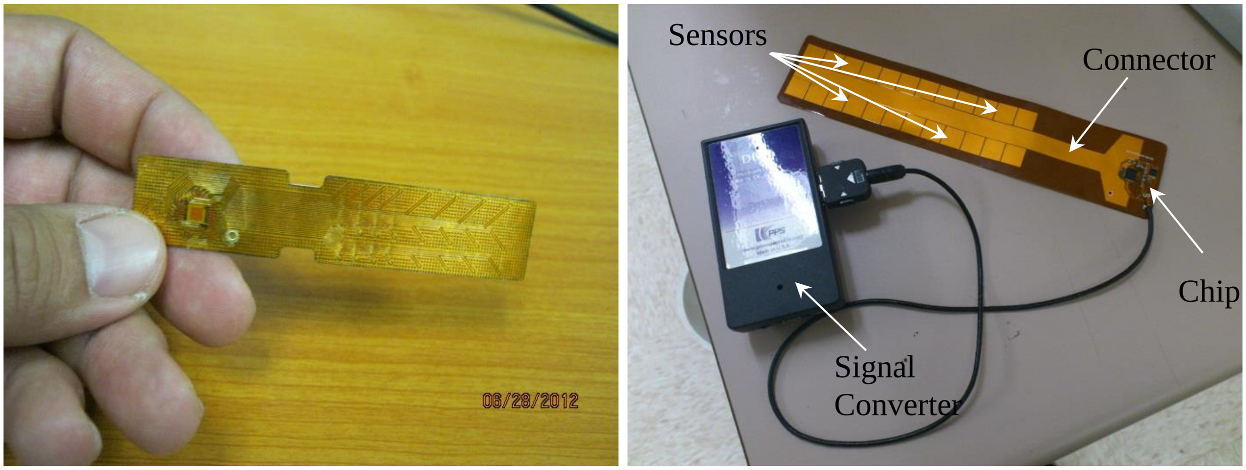

Figure 2.16 Digitacts tactile sensors

2.5.2 Capacitive Sensing Technology

TactArray distributed pressure measurement system (Pressure Profile Systems, Los Angeles, CA, USA) which was selected to be used in this study (Figure 2.17) consists essentially of two sets of orthogonal electrodes (plates) separated using flexible insulator that acts as a spring allowing for conformable and stretchable pad designs. When a normal load is applied on the sensors, it changes the distance between the electrodes resulting in a change in capacitance while applying a tangential force changes the effective area between the plates. The capacitive sensors are thus capable of detecting pressures by sensing the applied normal and tangential forces. Each sensing pad contains 255 square shaped sensors with pressure range from 0 to 140 kPa.

Tactarray sensors were found to provide repeatable data with higher accuracy. They are also durable for applications of buried structures as compared to other types of tactile sensors. They are more sensitive to lower pressure values as well. This is attributed to the capacitance measurement technology while other tactile sensors rely on resistive technology which measures resistance of a conductive material such as elastomer or ink between the orthogonal electrodes.

Figure 2.17 TactArray tactile sensors (PPS)

The problem with resistive tactile sensors is that the orthogonal electrodes contact each and then resistance is measured based on the contact area which increases as the pressure applied increases. This can lead to instability due to the continuous contact change that leads to rapid degradation of the resistive material. Consequently, the repeatability of results could be challenging. This has a direct impact on the accuracy of these types of tactile sensors.

Capacitive tactile sensors (Figure 2.19), on the contrary, maintain a single continuous state of no-contact between the orthogonal electrodes. The electrodes are separated by dielectric matrix acting as a spring as mentioned earlier in this section. The capacitor is formed at the overlap points of the electrodes and capacitance “C” is measured based on the distance “d” between the orthogonal electrodes at the overlap points where they (capacitance and distance) are inversely proportional (Equation 2.2). Table 2-1 shows a comparison between different types of tactile sensing technologies

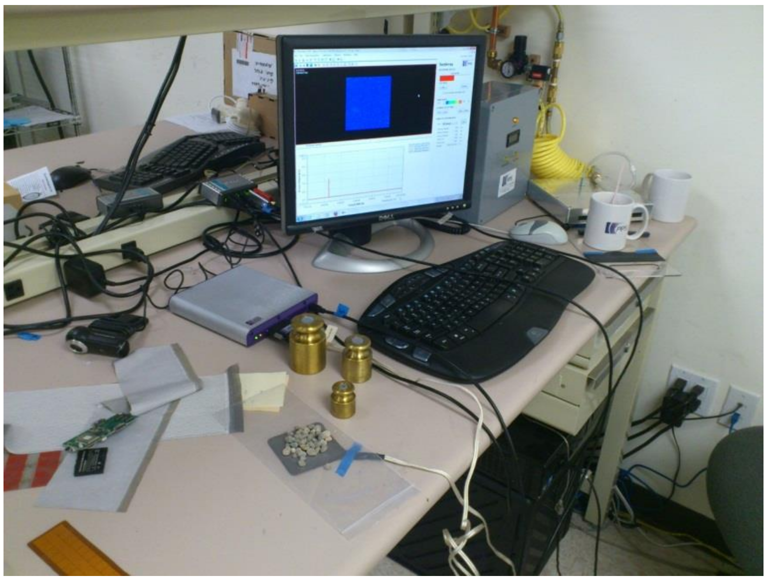

Figure 2.18 Testing the precision and repeatability of TactArray Sensors

$$C \alpha \frac{Area}{d} \qquad (2.\ 2)$$

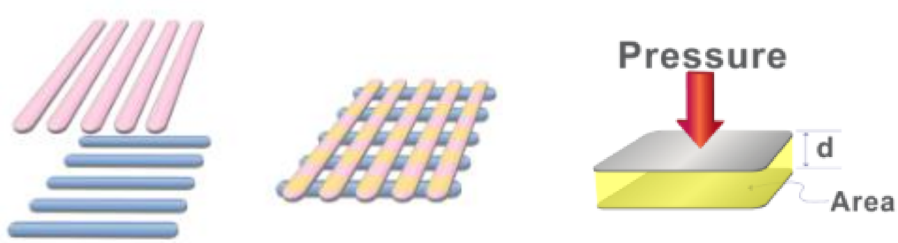

Figure 2.19 Capacitive technology based tactile sensors (PPS)

Table 2-1 Tactile sensors

Sensing Technologies	CAPACITIVE	RESISTIVE	PIEZOELECTRIC
Maximum Range	Good	Excellent	Fair
Sensitivity	Excellent	Poor	Fair
Minimum Element Size	Fair	Excellent	Poor
Repeatability	Excellent	Fair	Poor
Temperature Stability	Excellent	Fair	Poor
Design Flexibility	Excellent	Fair	Fair

2.5.3 Tactile Sensors Protection

Throughout this study, the sensors are protected from backfill abrasion by covering the instrumented pipe with a thin layer of stiff rubber sheet (1 mm in thickness) as shown in Figure 2.20. For PVC pipes, shim stocks made from the same pipe material are used to provide similar contact surface condition to the original pipe and to absorb the shear stresses developing at the soil-pipe interface

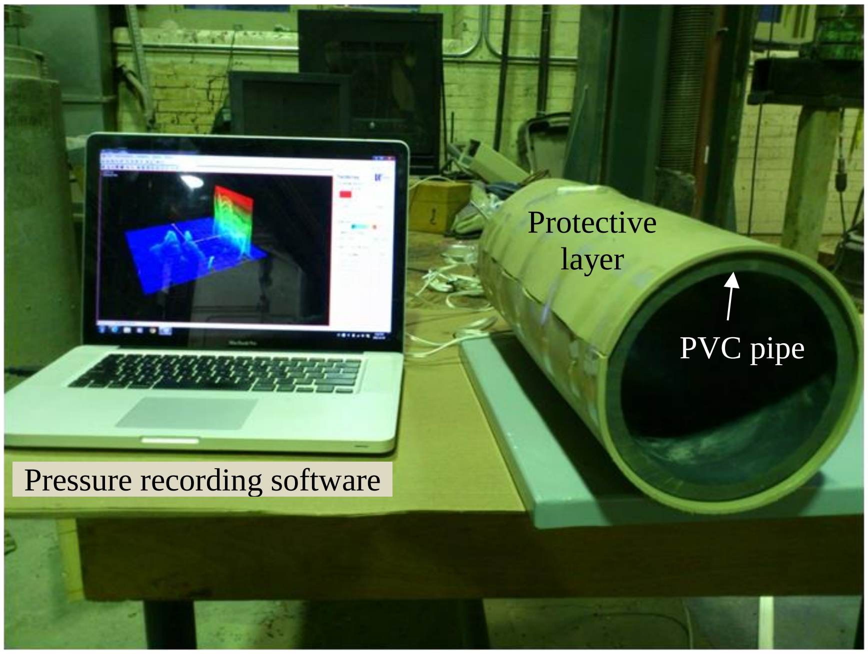

Figure 2.20 Instrumented cylindrical pipe

2.5.4 Validation of the sensing pads readings

A setup has been designed (Figure 2.21) by fabricating two different wooden frames, the first was designed such that the lower end of two opposing walls were cut with a half circular profile that fits over the instrumented pipe and the second was rectangular shaped walls for the box shaped culvert case. Different premeasured soil weights were placed and the recorded value was compared to the already measured.

The boxes are then filled with gravel of known weight (2000 grams) and the pressure distribution as well as the total weight were recorded by the data acquisition system connected to the sensors. The results showed pressure readings in both cases that are consistent with the load applied.

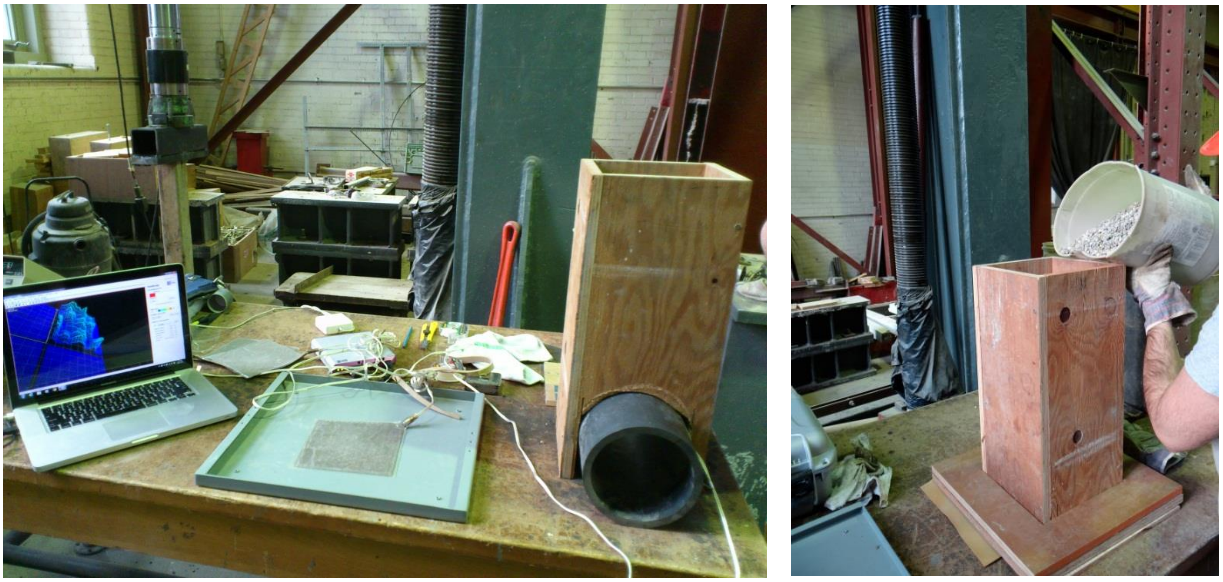

Figure 2.21 Verification of sensors accuracy and repetition in similar to experiment setup

Keeping in mind that the recorded readings did not change when the load was sustained for a duration of two hours. Test duration is about 30 minutes for the loading phase.

2.5.5 Effect of protection layers on pressure readings

A series of experiments was also conducted to study the effect of the protective layers on the measured pressure. A pneumatic loading system was used to apply vertical pressure directly over the sensing pad (Figure 2.22). The pressure was gradually increased up to a value comparable with that expected in the experiment. The response was compared before and after the addition of the protective layers

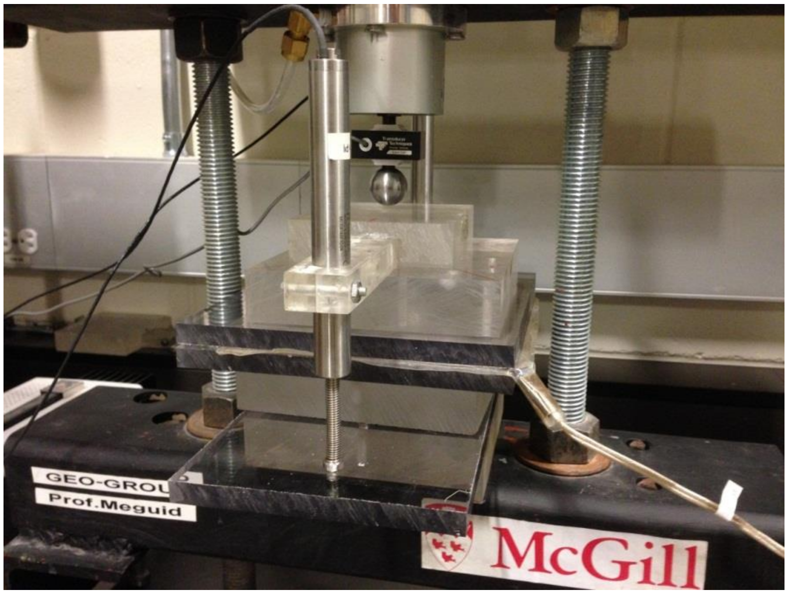

Figure 2.22 Effect of protective layers on the measured pressure

The results (Figure 2.23) show that scattered pressure readings recorded by the sensing pad due to a vertical compression of about 0.13 mm at an applied force of 900N (equivalent to 40 kPa). Insignificant increase in compression was recorded after the addition of the protective layer above the sensing pad. This indicates that the chosen protective material is stiff enough and does not cause additional compression under the loading level expected in the experiment.

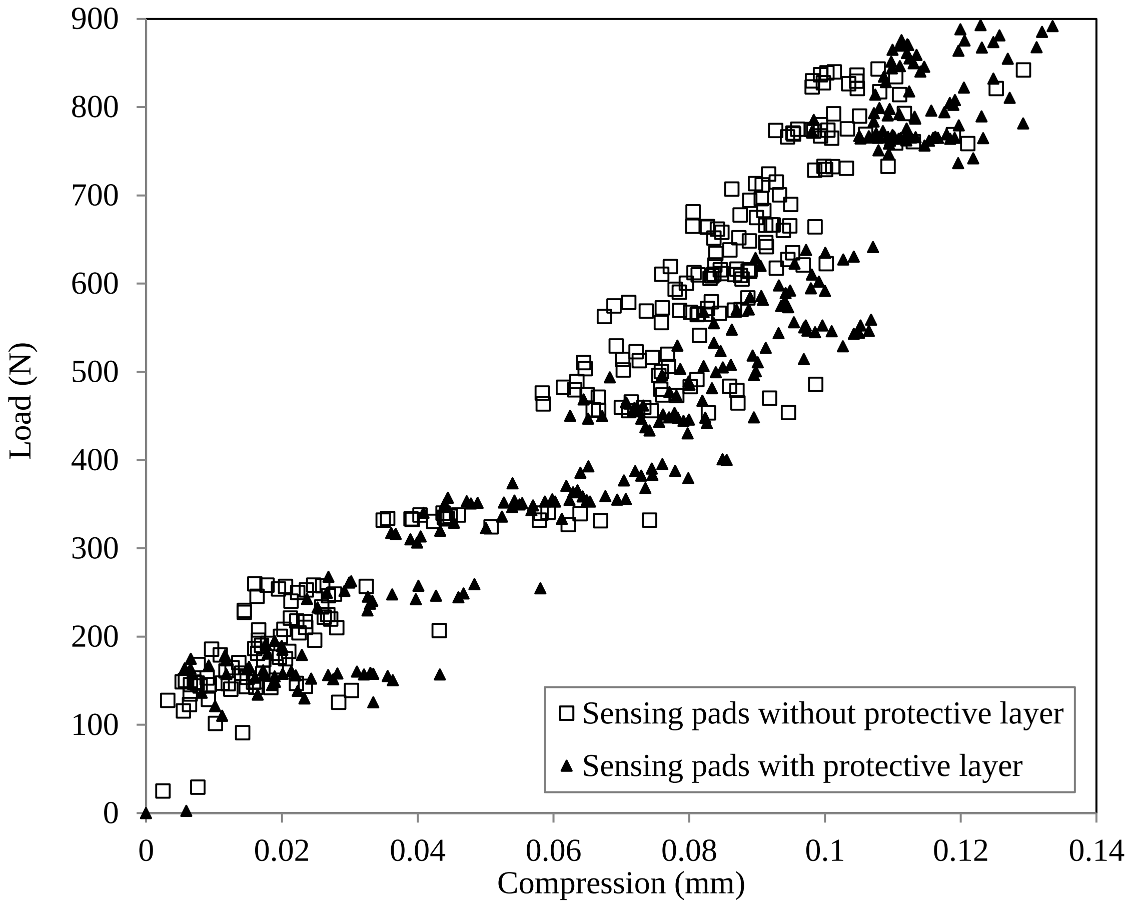

Figure 2.23 Results of investigation of protective layer effect

2.5.6 Advantages and Disadvantages

The most recognizable advantage of using tactile sensors for measuring soil pressure in geotechnical applications is the fact that each sensing pad contains multiple sensing points (sensels) which could reach up to a thousand points for 10cm wide pad (O'Rourke et al., 2008). This allows visualizing soil pressures across a given section. In addition, 3D images of the pressure distribution as can be seen in Figure 2.24 are produced over the monitored area with time.

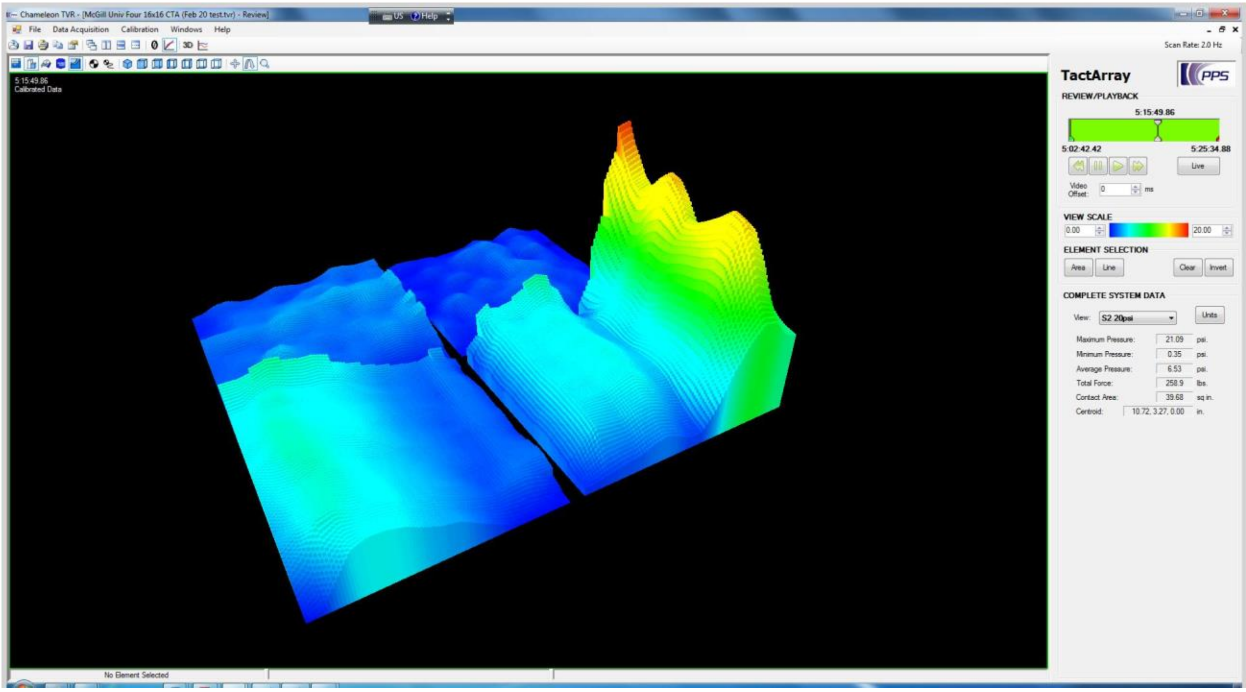

Figure 2.24 Sample Data showing 3D plot of pressure distribution captured by TactArray Tactile Sensors

The major disadvantage of tactile sensors is the extensive calibration required for each testing condition in order to obtain accurate results. The calibration process accounts for the hysteretic behaviour, loading rate, unloading and interface conditions. In general, tactile sensors are proven to be satisfactory for contact pressure measurement under static loading conditions.

2.6 Other Techniques

This section summarizes some of the recent developments reported by researchers to measure contact soil pressure for specific experiments. These include piezoresistive cells, normal and tangential earth pressure cells and mini sensors. A brief description of each is given below.

2.6.1 Piezoresistive cells:

These types of cells operate based on the fact that piezoelectric materials generate electric current of certain frequency when subjected to pressure. Examples of such materials are polyvinylidene fluoride (PVdF) and monocrystalline silicone. The piezoelectric material is usually laid in a grid format inside a flexible sensor. When this sensor is pressed, electric current is generated relative to the amount of pressure applied. As opposed to tactile sensors which are limited to static loading, piezoresistive sensors are suitable for pressure measurement under dynamic loads (Podoloff, RM. and Benjamin, M.., 1989).

Ilstad et al., (1994) measured contact soil pressures due to explosive loadings. A gauge has been developed (contact area of 1 m^2) using 9 separate sensors (0.2 x 0.2 m) placed between aluminum and steel plates. Further improvements were recommended to obtain a better calibration and improve the measured pressures.

2.6.2 Normal and tangential pressure cells:

Arnold et al., (2003) developed a load cell that is capable of measuring normal and tangential earth pressure simultaneously. The cell had 6 strain gauge based transducers arranged to form a statically determinant truss structure. Three of the transducers measure the vertical forces whereas the other three measure the horizontal forces. The system was used for investigating passive earth pressure on cantilever retaining walls.

2.7 Current and future developments

Earth pressure cells can be used to measure stresses within embankments, and contact pressures on retaining walls, tunnel linings and bridge abutments. Load cells can be of the mechanical, hydraulic, vibrating wire, or electrical-resistant strain gauge type. They measure strains or displacements under the applied loads that are translated into loads through calibration. The pressure cells, properly installed in appropriate locations, can give good data on the stress distribution between a buried structure and the surrounding ground at specific locations. They should be installed in orthogonal sets of at least three for confirming that adequate stress levels are being achieved.

Over the past two decades, several developments have been made in the area of pressure sensors employing fiber-optics, tactile sheets and piezoresistive materials. Fiber-optic transducers bring to the measurement systems many of the advantages that optical-fiber technology has brought to communications systems. The very high bandwidth of optical fibers allows them to convey a large amount of measurand information through a single fiber; because optical fiber is a dielectric, it is not subject to interference from electromagnetic waves that might be present in the sensing environment. In addition, fiber-optic sensors can function under adverse conditions of temperature, and toxic or corrosive atmospheres that can erode metal sensors. Adapted from the robotic industry, tactile sensors are devices which measure the parameters of a contact between the sensor and an object. The basic principle of this type of sensor is the measurement of the resistance of a conductive elastomer material or foam between two points.

A summary of the main types of sensors used in geotechnical engineering practice along with the advantages and disadvantages of each type is given in Table 2-2, while Table 2-3 presents a list of applications that utilized different contact pressure measurement techniques in geotechnical engineering.

With the advances in technology more patents and techniques will be introduced which are expected to broaden the application fields and enhance the accuracy of pressure measurement sensors. It should be noted that the present review is not intended to provide extensive coverage of all existing pressure measurement devices used in civil engineering; it rather provides a review of the different available techniques used to measure contact pressure between surface or subsurface structure and the surrounding ground to help select the best technique for each researcher based upon feasibility, expertise, price and accuracy.

Table 2-2 Comparison between selected contact pressure measurement techniques

TECHNIQUE	ADVANTAGES	DISADVANTAGES
Conventional techniques	• Investigated over 70 years • All technical problems are known • Various suppliers available • General Familiarity	• Problems of strain gages • Geometry problems: aspect ratio, arching, point loading, lateral stress rotation • Single pressure value
Flexible tactile sensors	• Stress distribution over an area rather than a single pressure value • Visualizing soil pressure distribution in 3D • Very thin and flexible • Different sizes and shapes	• Qualitative measurements • Extensive calibration at each sensel if quantitative data required • Creep, shear stress, water ingress and insensitive to low stresses
Fiber optic sensors	• No electric current related problems • Water resistant system • Remote sensing (several kilometres) • Multiplexing (several sensors with one wire)	• Short gage length (about 25 mm) • Temperature sensitivity • Relatively new

2.8 Summary and Conclusions

In conclusion, a wide range of earth pressure cells is available for the measurement of contact pressure on buried structures. Most of the available earth pressure cells are rigid in nature and therefore are considered suitable for measuring earth pressure at the interface between a structure and the surrounding ground. Minimum movement of the cell surface should be allowed during loading to avoid significant relaxation of stresses and consequently deviation from the actual pressure. Among the above reviewed load cells, the null pressure sensors are able to minimize cell deflection and therefore can provide the best performance among the above reviewed load cells. A major limitation of the load cells is the need for installing several cells at different locations to capture the pressure distribution across a given surface. In addition and due to the rigidity of the load cells, they are not suitable for pressure measurement on flexible structures.

Tactile sensors (capacitive technology based) were selected for the experimental work conducted in this study mainly due to their negligible stiffness and providing a pressure distribution on the rigid surface rather than a point reading which could be affected by a concentration of pressure or soil arching especially when large soil particles are used.

The TactArray sensors were custom made to suit the laboratory environment as they pressed by granular material. Test duration was chosen to limit the creep effects.

Table 2-3 Selected applications of different contact pressure measurement cells

SENSOR TYPE	REPORTED APPLICATIONS
Null Pressure Sensors	Stresses on Buried structures in controlled pressure chambers (Talesnick et al., 2008).
Fiber Optic Sensors	One-dimensional stress in sand (Legge et al., 2006).
Tactile Sensors	Pressure distribution under rigid footings on sand (Paikowsky S.G., 1997, Paikowsky et al., 2006). Load distribution due to rock fall on protection structures (Springman et al., 2002). Earth pressure acting on buried pipes (Choo et al., 2007, O'Rourke et al., 2008, Weidlich et al., 2008 and Abdoun et al., 2009).
Piezoresistive cells	Contact pressure due to explosive loadings (Ilstad et al., 1994).
Normal and tangential pressure cells	Passive pressure mobilization on cantilever retaining walls (Arnold et al., 2003).
Soil pressure mini-sensor	Contact pressure at low range with high accuracy (Xiao and Xiaoke 2005).
Integrated strain gauge based load cells	Earth pressure acting on subsurface structures such as tunnels and shafts (Tobar and Meguid 2009).

Chapter 3

Experimental investigation of the effect of geogrid inclusion on the earth pressure acting on buried pipes*

3.1 Abstract

Understanding earth pressure distribution on buried structures is essential for the analysis and design of pipes, tunnels and vertical shafts. In this chapter an experimental investigation that has been conducted to measure the contact pressure distribution on rigid pipes overlain by a geogrid sheet is presented. Tactile sensing technology that can follow the cylindrical shape of the pipe and continuously capture the pressure distribution acting on the pipe is utilized. The physical model involves a buried pipe installed in granular material and subjected to strip surface loading. The effect of introducing a geogrid reinforcement layer above the pipe on the contact pressure distribution is examined. Results showed that introducing a geogrid layer above the buried pipe can reduce earth pressures transferred to the pipe wall and that such effect increases as more surface load is applied.

3.1 Introduction

It has been proven that the installation of a geogrid layer under a footing can have a positive effect on the bearing capacity and load-settlement response of the footing (Das, 1994). This is attributed to the confining effect and the interaction mechanism between the geogrid and the surrounding soil as shown in Figure 3.1.

*A version of this chapter has been published in Soils and Foundations, Volume 55, Issue 3, June 2015, Pages 588–599

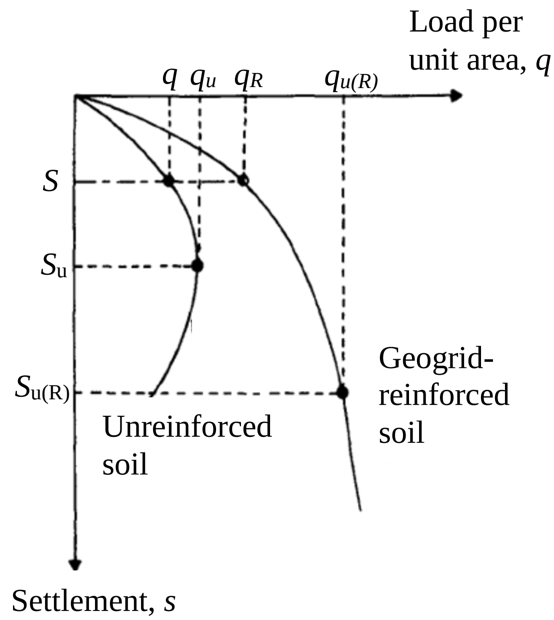

Figure 3.1 The load-displacement curves for unreinforced sand and geogrid-reinforced sand supporting a strip foundation (Das, 1993)

Measuring earth pressure acting on buried structures has been used in practice to monitor the performance of subsurface structures including foundations, culverts, buried pipes, retaining walls and tunnel linings. Pneumatic, hydraulic, vibrating wire, or strain gauge based devices are among the commonly used earth pressure measurement techniques for large scale projects where mainly rigid load cells are installed at selected locations against the walls of the structure as discussed in Chapter 2. It has been concluded that rigid cells typically read stresses that are either lower or higher relative to actual soil stresses depending on the cell stiffness, size, aspect ratio and cell placement procedures (Selig, 1964; Kohl et al., 1989; Talesnick et al., 2011).

Custom-made tactile pressure sensors (discussed in Chapter 2) are suitable to measure pressure distribution on cylindrical shaped structures. The sensors generally consist of two sets of orthogonal electrodes (plates) separated using flexible insulator that acts as a spring allowing for conformable and stretchable pad designs.

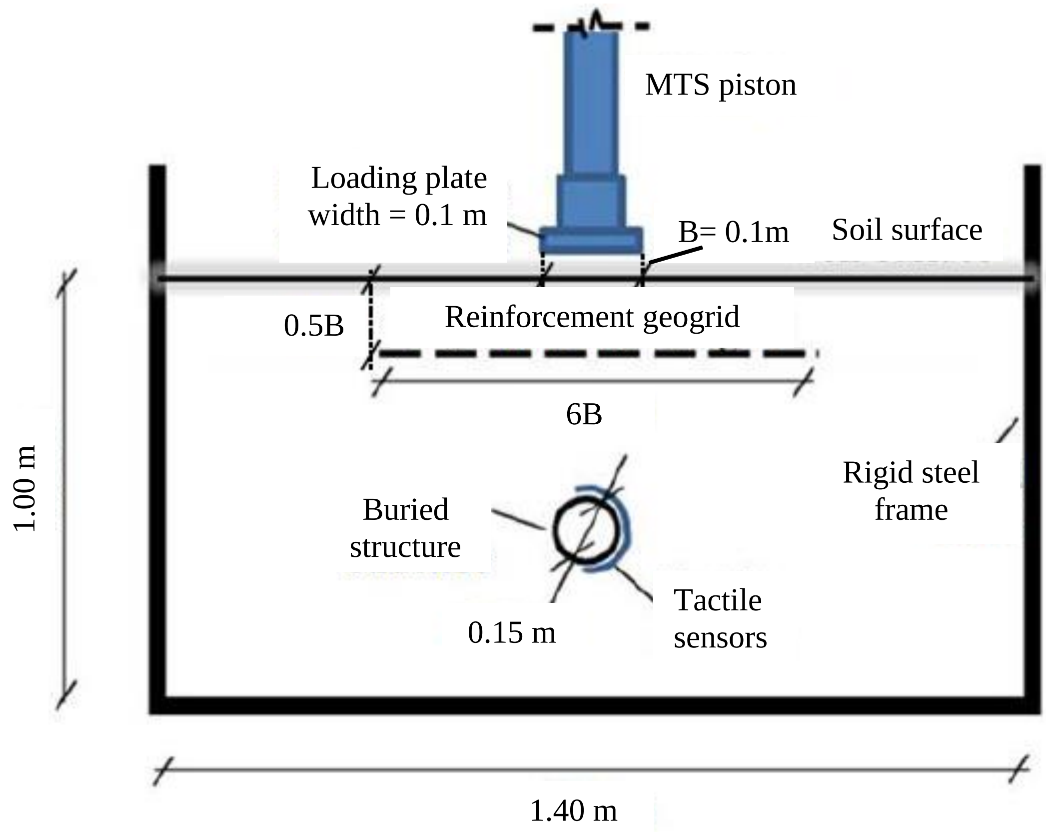

Figure 3.2 Schematic of the test chamber and the buried pipe

The experimental setup comprises a rigid pipe that is instrumented with tactile sensors and buried in granular material while a vertical strip load is applied through an MTS machine parallel to the centreline of the pipe. The effect of placing a geogrid reinforcement layer on the radial earth pressure distribution is then examined. Figure 3.2 shows a schematic of the experimental setup. A brief review of some of the relevant studies is provided below.

3.1.1 Footings on reinforced soils

The use of geosynthetics as a soil reinforcing material has proven successful over the years for different geotechnical applications. The presence of Geogrid was found to provide the interlocking action with the soil particles through the apertures generating both frictional and bearing resistances thus increasing soil confinement. The use of geogrid reinforcement under surface loading generally improves the soil bearing capacity and the load settlement response as reported by several researchers (Baus and Wang, 1983, Guido et al., 1987, Das et al., 1994 and Shin et al., 2002, Alamshahi and Hatal, 2009).

Guido et al., (1985) investigated experimentally the effect of geogrid reinforcement on the bearing capacity and settlement in dense sand carrying square footings. The role of various parameters, including the reinforcement depth, width and number of layers was investigated.

A significant improvement in the bearing capacity was measured when 3 geogrid layers were placed within a depth (d) equal to the width B of the footing. Khing et al., (1993) studied experimentally the response of two layered soils with geogrid reinforcement at the interface. It was recommended that a geogrid length of 6 times the foundation width located at a depth of 2/3 the foundation width is needed for the best performance. Omar et al., (1993) investigated the ultimate bearing capacity of foundations placed over geogrid reinforced sand using a geogrid length of 8B at a depth of 2B for both strip and square footings.

Das and Omar (1994) concluded that for small scale tests as the foundation width increases the improvement in bearing capacity due to geogrid placement in sand decreases until a foundation width of B=130mm the bearing capacity reaches a constant value when other geogrid related dimensional parameters are kept constant while relative density of compaction of sand is changed . Das and Khing (1994) found that introducing a void in cohesive soil supporting a strip footing causes a reduction in bearing capacity and an increase in settlement. It was highlighted that if the induced void is located at a depth greater than or equal to 2.5B the increase in bearing capacity due to the presence of the geogrid above the void is about 25%.

Bearing capacity of strip foundations above geogrid reinforced sand was further investigated by Shin et al., (2002). The effect of placing several geogrid layers is examined on the bearing capacity and settlement. A critical geogrid embedment depth was found to be about twice the width of the foundation.

Table 3-1 presents a summary of selected studies related to footings over geogrid reinforced soils. A list of relevant parameters for optimized performance based on previous studies are shown in Table 3-2.

Another geogrid application is related to erosion protection under surface loading (Ahmed and Meguid, 2009). It was observed that the presence of geogrid reduces settlement resulting from volume loss in the foundation soil and protects against sudden bearing capacity failure.

DeMerchant et al., (2002) analyzed geogrid effect in replacement fill material such as flyash while (Chaudhary, 2010) used expanded shale light weight aggregate. The performance of Stiff Geogrid (BX 1200) was compared to the less stiff (BX 1100). It was found that the BX 1100, consistently, provides more increase in the bearing capacity of the reinforced fill. They attributed this behaviour to the fact that the lower stiffness geogrid elongates as the surface load is applied thus interacting and interlocking with the soil particles. While the stiff geogrid stays as a rigid layer over which soil particles would slide before interlocking action develops.

BCR (bearing capacity ratio) = $\frac{\text{Bearing Capacity}_{\text{reinforced}}}{\text{Bearing Capacity}_{\text{non reinforced}}}$

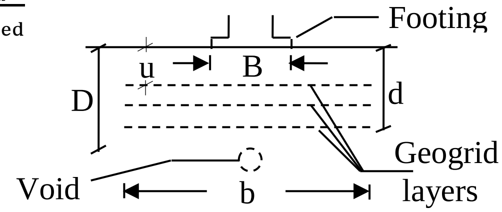

Table 3-1 Footings on soils with reinforcement and/or induced voids

Author and year	**Soil type**	**Geosynthetic type and location**	**Observations**
		Experimental work on <u>reinforced</u> soil with induced <u>void</u>	
Das and Khing **(1994)**	Strong Sand over weak clay	Geogrid SS0 Single layer at interface	d/B_{cr}=2.5 BCR = 1.25
Alawaji **(2001)**	Sand over collapsible soil	Geogrid biaxial SS2 Single at interface	u/Diameter=0.1 $D_{gegorid}$/Diameter=0.4, BCR=3
		Experimental work on <u>reinforced</u> soil <u>without induced void</u>	
Akinmusuru and kinbolade ***(1981)***	Sand	Rope fibers 1 to 3 layers	BCR = 3 , u/B = 0.5 Optimum no. = 3
Guido et al., ***(1986)***	Sand	Geogrid SS1 biaxial Geotextile 3401 Multiple Layers	BCR=3 u/B_{cr} = 1 b/B=2
Guido et al., ***(1987)***	Sand	Geogrid SS1, SS2, SS3 (biaxial) Multiple layers	BCR = 2 to 3 u/B_{opt} = 0.67
Hirokawa and Miyazaki ***(1992)***	Sand	Geogrid biaxial SS2, Single Layer	u/B_{opt} = 1 b/B = 3
Omar et al., ***(1993)***	Sand	Geogrid SS0 Multiple Layers	(Str / Sqr) d/B_{cr}: Str 2, Sqr 1.4 b/B_{cr}: Str 8, Sqr 4.5
Khing et al., ***(1994)***	Strong Sand over weak clay	Geogrid SS0, SS1 Single layer at interface	Optimum height of Sand H/B = 2/3, BCR=1.25, b/B=6
Das et al., ***(1994)***	Sand or clay	Biaxial Geogrid SS0 Multiple Layer	(sand / clay) BCR: sand 1.4, clay 4 b/B_{cr}: sand 5, clay 8 u/B_{cr}: sand 0.3, clay 0.4
Adams and Collins ***(1997)***	Sand	Biaxial Geogrid Multiple layers	BCR = 1.6 to 2.5 b/B_{cr}=0.25
Shin and Das ***(2000)***	Sand	Geogrid SS0 Multiple layers	BCR = 2.4, b/B=8 BCR=2.43BCR`-1.43

Shin et al., (***2002***)	Sand	Biaxial Geogrid SS1 Multiple Layer	BCR_s<BCR_u
Patra, et al., (***2006***)	Sand	Biaxial Geogrid SS1	$q_{uR(e)}=q_{uR}*[1-R_{KR}]$
Latha and Somwnshi (***2009***)	Sand	Biaxial and Uniaxial Geogrid, Multiple layer	BCR=1.8-2.5 $d_{cr/B}$=2 b/B=4

Table 3-2 Recommended parameters for geogrid reinforcement

u/B	Range from 0.25 to 0.4	Notice that settlement is twice the unreinforced case. Thus checking for BCR_s is crucial
N	6	
b/B	6	
d/B	2.25	
BCR_s = 0.7 BCR_u , BCR_u = 2 , BCR_s = 1.5		

Ghazafi and Lavasan (2008) tested the effect of using geogrid as a reinforcement under multiple footings on granular soils with interfering zones and highlighted that the increase in bearing capacity is up to 2 times the increase for an isolated footing over similar reinforced soil due to development of an arch between footings that forms a larger and stronger overall unit.

3.1.2 Buried structures in geosynthetic reinforced soil

Corey et al., (2014) presented laboratory results of a high-density polyethylene pipe buried at shallow depth and subjected to static loads with and without geogrid. Contact pressure and deflection of the flexible pipe were recorded as a result of the geogrid reinforcement. The geogrid caused a reduction in the stresses transferred to the pipe crown by 10%.

Sanan (1980) investigated soil-geofabric-culvert interaction for flexible pipes of relatively shallow depths ranging from 0.5D to 2D using finite element analysis. The emplacement of the geofabric was found to develop tensile resistance leading to a reduction in earth pressures transferred to the buried structure.

Yamamuto and Kusuda (2001) used aluminum cylindrical rods of constant length to model the soil medium while the reinforcement material was a sheet of paper to which the aluminum rods above and below are glued to provide frictional resistance. The aluminum rods are favoured as they do not need boundary walls to hold them when stacked forming a totally free boundary environment. Image processing was used to monitor the rod movements and rotations as failure progresses (Figure 3.3). They recommended using double layer reinforcements for optimum strength. They also noticed that increasing reinforcement width particles motion tend to spread horizontally instead of vertically.

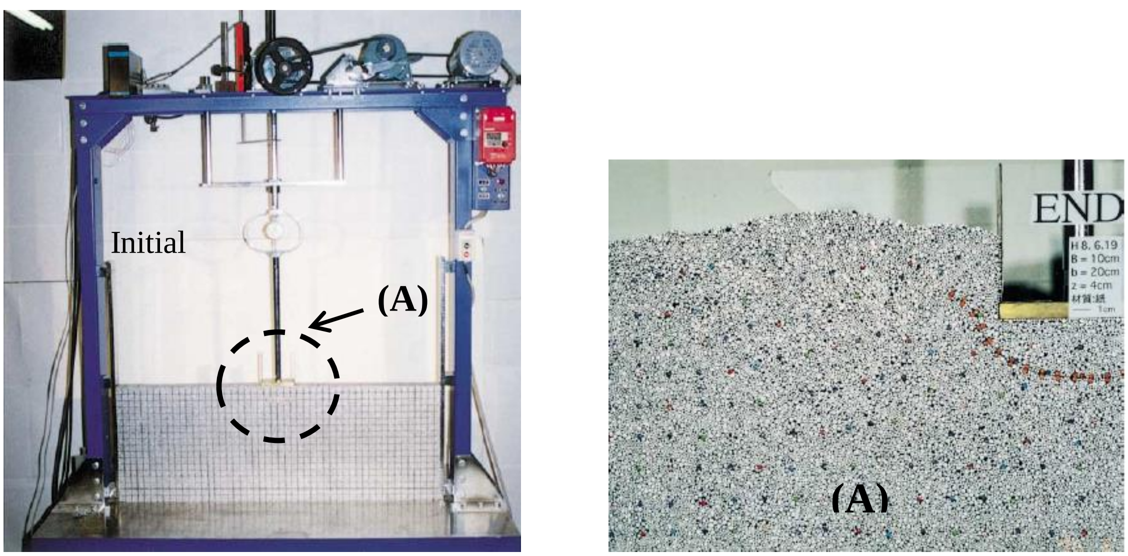

Figure 3.3. Test apparatus using aluminum rods stacked as soil medium (Yamamoto and Kusuda, 2001)

In (2002) Yamamuto and Otani showed how the reinforcing material spreads the load over a wider and deeper zone as can be seen Figure 3.4

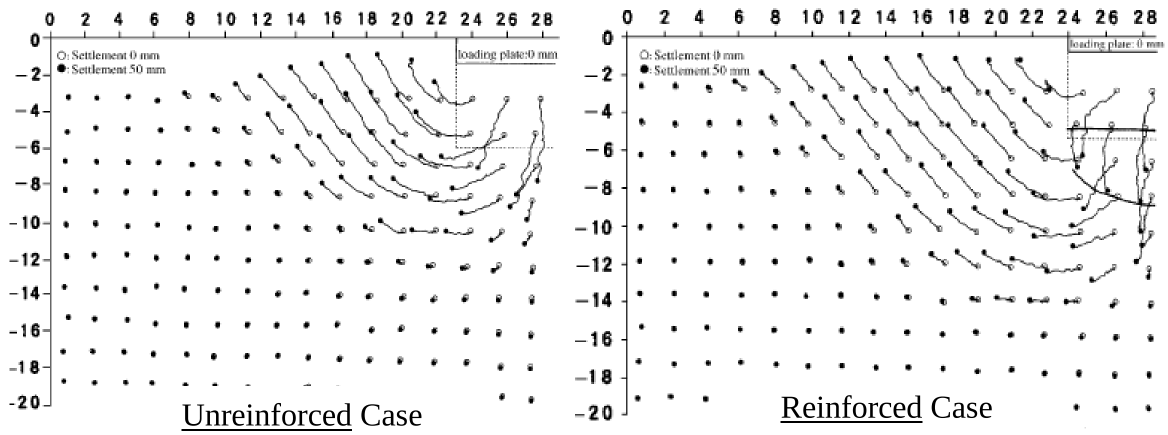

Figure 3.4 Translation and rotation of aluminum rods (Yamamoto and Ottani, 2002)

3.1.3 Scale effects

Although using small scale (1g) tests is effective, the main challenge in 1g experiments is the scale effects. DeMerchant et al., (2002) and Chaudhary (2010) noted that at relatively low stress levels the angle of friction developed is usually higher which means that bearing capacity of a reduced scale footing under 1g conditions tends to be higher compared to actual prototype.

Das et al., (1998) highlighted that the reinforcement used in reduced scale experiments is generally full scale resulting in a mismatch in geometry and more importantly stiffness between the model and prototype response. It was recommended that a weaker geogrid be used in small scale tests. Yamamuto and Kusuda (2001) attributed the discrepancy between full scale footings behavior and model tests to the coefficient of maximum bearing capacity ($N_\gamma = 2q / \gamma B$) which is significantly decreases when the width increases.

The objective of this experimental study is to understand the different interaction mechanisms arising due to implementing geogrid material over buried structures by measuring the changes in contact pressure distribution developing as a result of the reinforcement layer.

3.2 Experimental Setup

The experimental setup consists of an instrumented buried pipe embedded in a strong box. The pipe is instrumented using tactile sensing pads wrapped around its outer perimeter covering the area near the middle third of the pipe length. Granular soil is used as backfill material. A universal MTS testing machine with a capacity of 2650 kN is used to apply the strip loading (see Figure 3.5). A detailed description of the experimental setup components individually is provided below.

3.2.1 Test Chamber

Figure 3.5 Details of the experimental setup

In Figure 3.2. the dimensions of the test chamber (1.4 m x 1.0 m x 0.45 m) are selected such that they represent two-dimensional loading condition. The rigid walls are placed far from the pipe to minimize boundary effects. The distance from the outer perimeter of the pipe to the side walls of the tank is 0.65 m. All steel wall surfaces were painted with epoxy coating and covered with double greased plastic sheets to minimize friction with the backfill material.

3.2.2 Instrumented pipe

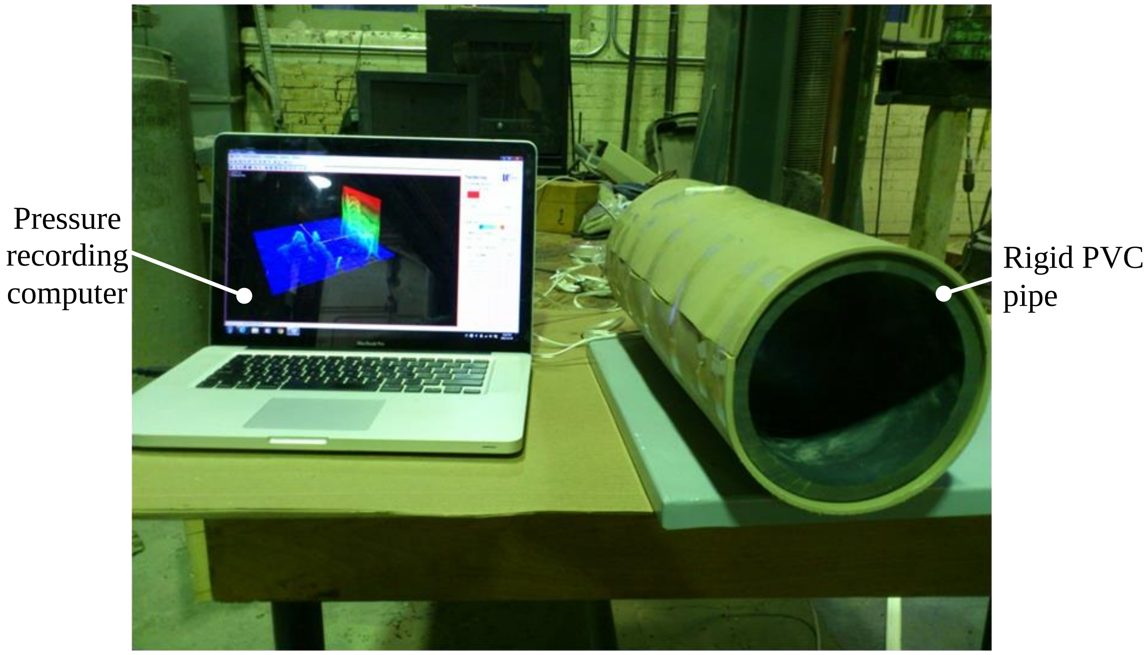

Figure 3.6 Instrumented pipe with protective layers

A rigid PVC pipe with 15 cm outer diameter and 1cm in wall thickness is used in this study. The pipe crown is placed 0.45 m below the soil surface and instrumented using two custom made pads of TactArray sensors placed directly on the outer surface of the pipe. Each sensing pad contains 255 square shaped sensors with pressure range from 0 to 140 kPa. The sensors are protected from backfill abrasion by covering the instrumented pipe using two thin layers (1 mm in thickness each) of rubber and PVC which provides similar contact surface condition to the original pipe (Figure 3.6). Two LVDTs are installed orthogonally inside the pipe to monitor diameter change during loading.

3.2.3 TactArray sensors

The custom made sensors consist of two pads containing two sets of orthogonal electrodes (plates) separated using flexible insulator that acts as a spring allowing for conformable and stretchable pad designs. When a normal load is applied on the sensors, it changes the distance between the electrodes resulting in a change in capacitance while applying a tangential force changes the effective area between the plates. The capacitive sensors are thus capable of detecting pressures by sensing the applied normal and tangential forces. To protect the sensors from sharp points and abrasive material, shim stocks made from the same pipe material are used. The shim stocks also absorb the shear stresses developing at the soil-pipe interface. The details of the contact pressure measurement technique are discussed in Chapter 2.

3.2.4 Backfill soil

Dry sandy gravel soil with average unit weight of 16.28 kN/m^3 is used as backfill material. The friction angle of the backfill soil determined using direct shear tests is found to be 47^o. The grain size distribution of the soil is shown in Figure 3.7.

The soil was placed and tamped in thick layers (10 cm each) to form a dense base bedding layer below the pipe. The instrumented pipe was then placed over a thin sand layer (1 cm) to improve the contact between the soils and the pipe. Sand is also placed around the outer pipe surface using a thin vertical wall placed 1 cm far from the pipe side. The placement continued until a 1 cm layer of sand covered the pipe crown. The gravel backfill is then placed around the pipe.

Backfill placement continued in layers over and around the pipe up to the target soil height of 1.0 m. Table 3-3 represents the soil properties.

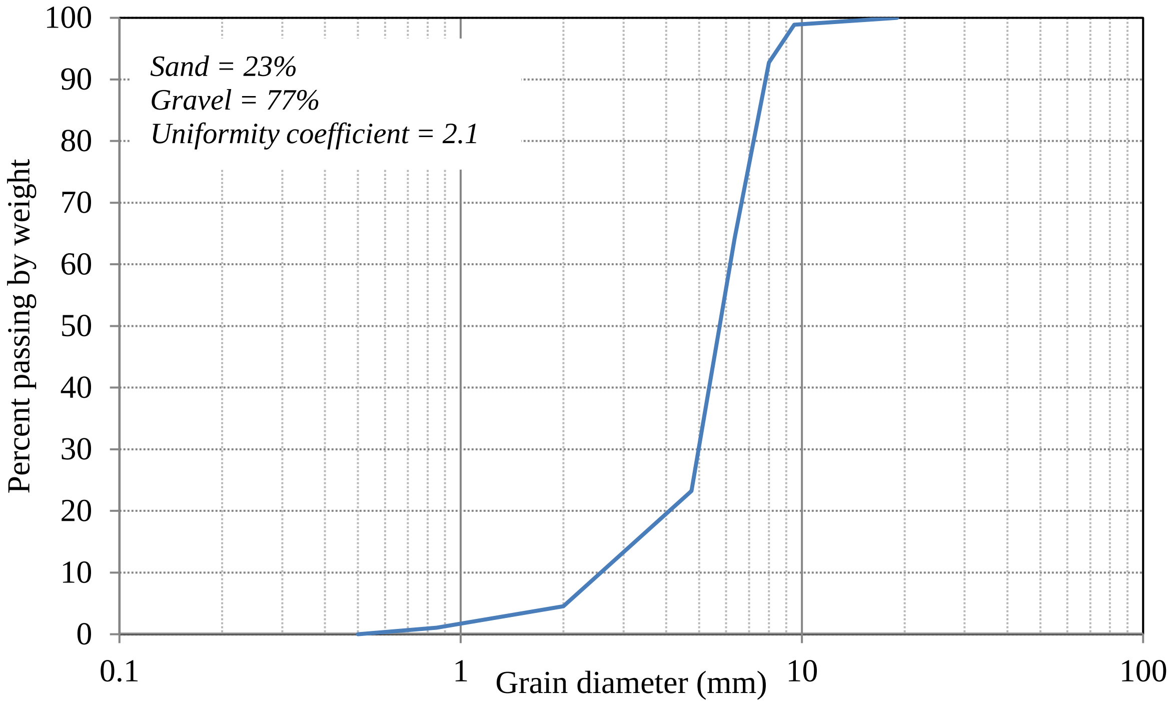

Figure 3.7 Particle size distribution of the backfill material

Table 3-3 Properties of the backfill material

Property	Value
Specific gravity	2.65
Coefficient of uniformity (C_u)	2.4
Coefficient of curvature (C_c)	1.6
Minimum dry unit weight (γ_{min})	15.1 kN/m^3
Maximum dry unit weight (γ_{max})	17.3 kN/m^3
Experimental unit weight (γ_d)	16.3 kN/m^3
Internal friction angle (ϕ)	47^o
Cohesion (c)	0

3.3 Testing procedure

A soil placement procedure has been established and used consistently in all tests to ensure consistent initial conditions. A total of four experiments was conducted including two benchmark tests with only the instrumented pipe inside the backfill and the other two include one layer of biaxial geogrid. Geogrid type BX1100 (polypropylene material and tensile modulus of 205 kN/m at 2% strain) with dimensions 0.4 m x 0.6 m is placed at a depth of 5 cm below the sand surface. For all tests, the placement of the backfill continued up to a distance 0.45 m above the crown.

The radial earth pressure distributions on the pipe were measured using the tactile sensors installed around its circumference throughout the experiment. Surface load was then applied using a rectangular steel plate (45 cm long x 10 cm wide) attached to the actuator of the MTS machine and placed above the pipe centerline. The load was gradually applied for five minutes under displacement control scheme with a constant displacement rate of 1.3 mm/min. The test would be stopped when either a surface displacement of 6.5 mm is reached (serviceability failure) or the pressures on the tactile sensors exceeded their allowable capacity. After the completion of each test, the tank was emptied using a vacuum machine connected to a collection barrel. The pipe was then retrieved and the setup was prepared for the next test. A sample of the radial pressure distribution recorded using the data acquisition software during one of the tests is shown in Figure 3.8.

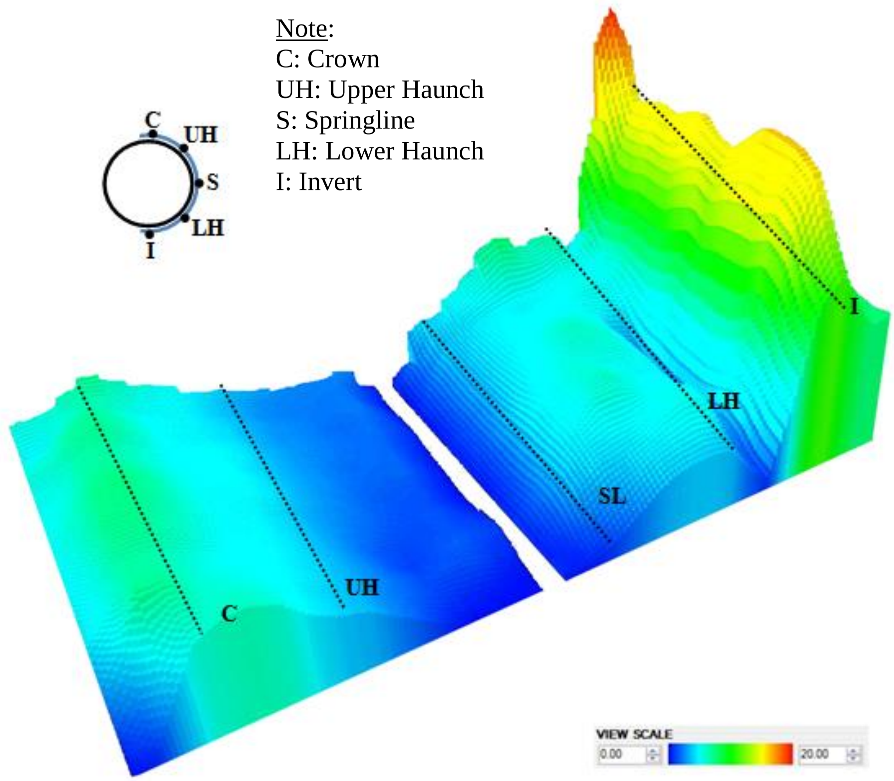

Figure 3.8 A snapshot of the measured earth pressure distribution around the pipe

3.4 Results and Discussions

3.4.1 Load-displacement relationship

Figure 3.9 shows the relationships between the applied footing pressure and surface displacement with and without geogrid reinforcement. It is noted that due to the allowable pressure of the tactile sensors (20 psi or 140 kPa), the tests were stopped before the footing pressure reached the ultimate bearing capacity in both cases. However for a given surface movement, the load the foundation can carry was found to increase with the use of geogrid reinforcement. The data was used to validate a finite-discrete element model developed by others in the research group (Ahmed et al., 2015).

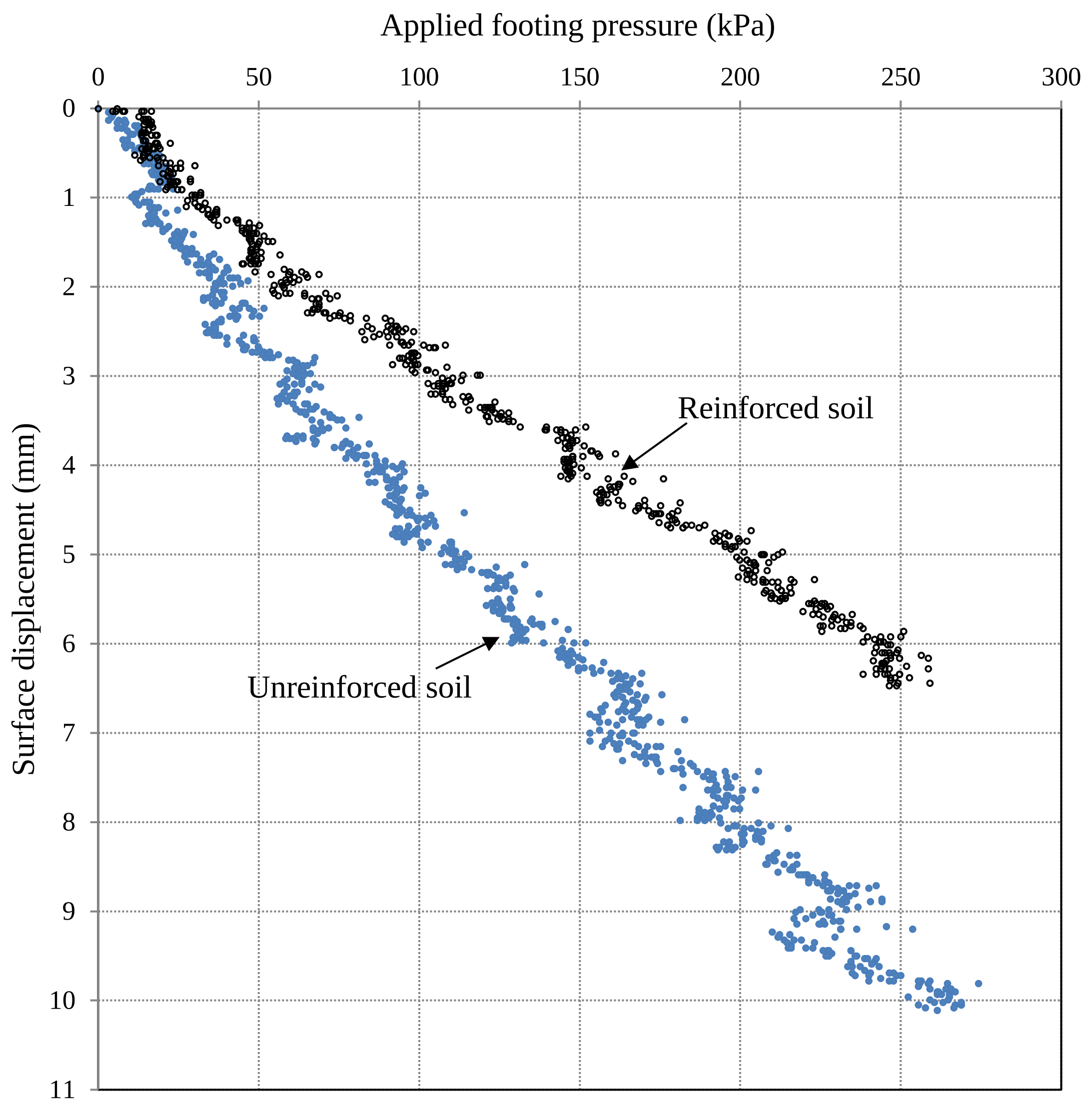

Figure 3.9 Load-displacement relationship due to footing load over reinforced and unreinforced soil

3.4.2 Initial pressure distributions on the pipe

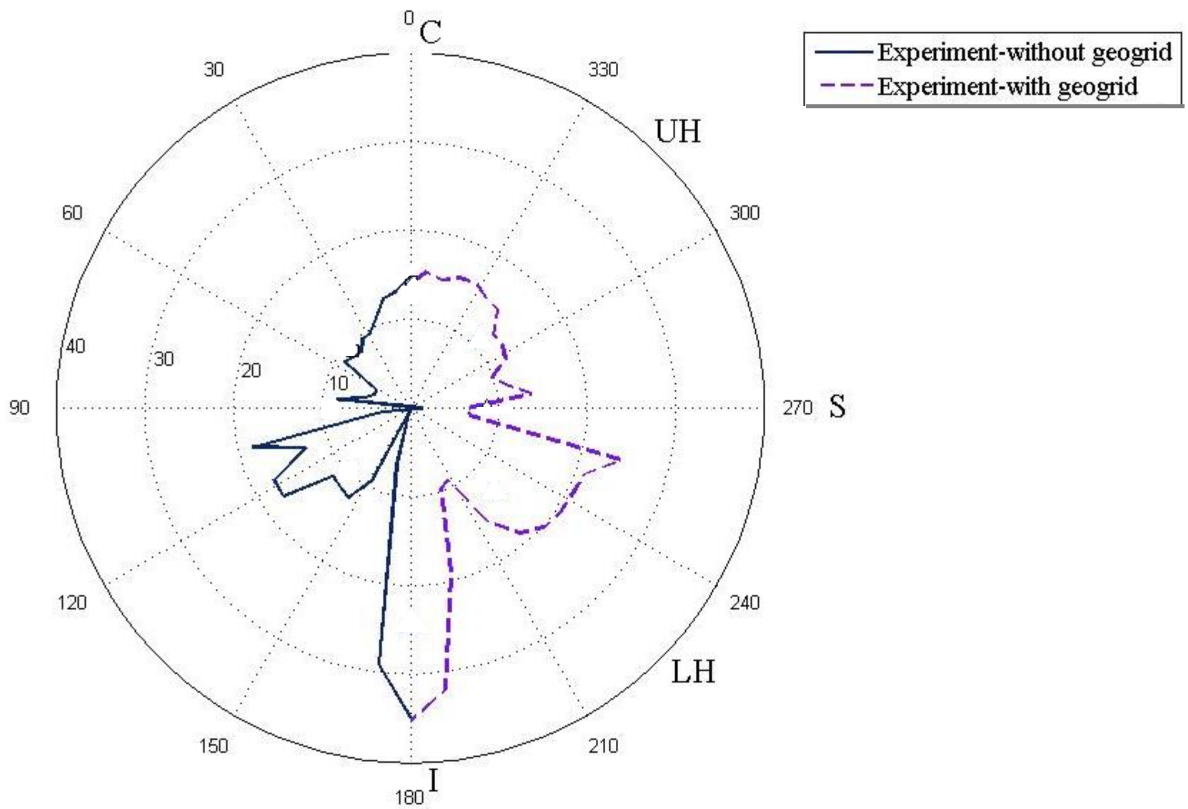

Figure 3.10 Initial pressure distribution on the pipe (units kPa)

The calculated initial pressures acting on the pipe are shown in Figure 3.10. For comparison purposes, the pressure distributions for the cases of unreinforced and reinforced soils are presented on the opposite sides of polar chart. The use of tactile sensors allowed for the pressure distribution on the pipe to be continuously measured. The difference in initial pressure between the unreinforced and reinforced tests can be explained by the possible variation in tamping forces during the soil placement process. The sensitivity of tactile sensors allowed for such pressure difference to be recorded. The largest radial pressure values were observed at the pipe invert.

3.4.3 Pressures on the pipe due to the applied footing load

The changes in radial pressure acting on the pipe during the loading process are analyzed and compared with the measured values. Four locations have been chosen to investigate the pressure changes including the crown, the upper haunch, the lower haunch and the invert of the pipe. The springline of the pipe was not selected for the analysis. The changes in pressure at the crown, upper haunch, lower haunch and invert are shown in Figures 3.11, 3.12, 3.13 and 3.14, respectively. In each figure, the normalized radial pressure is presented against the surface displacement below the footing for the unreinforced and reinforced cases.

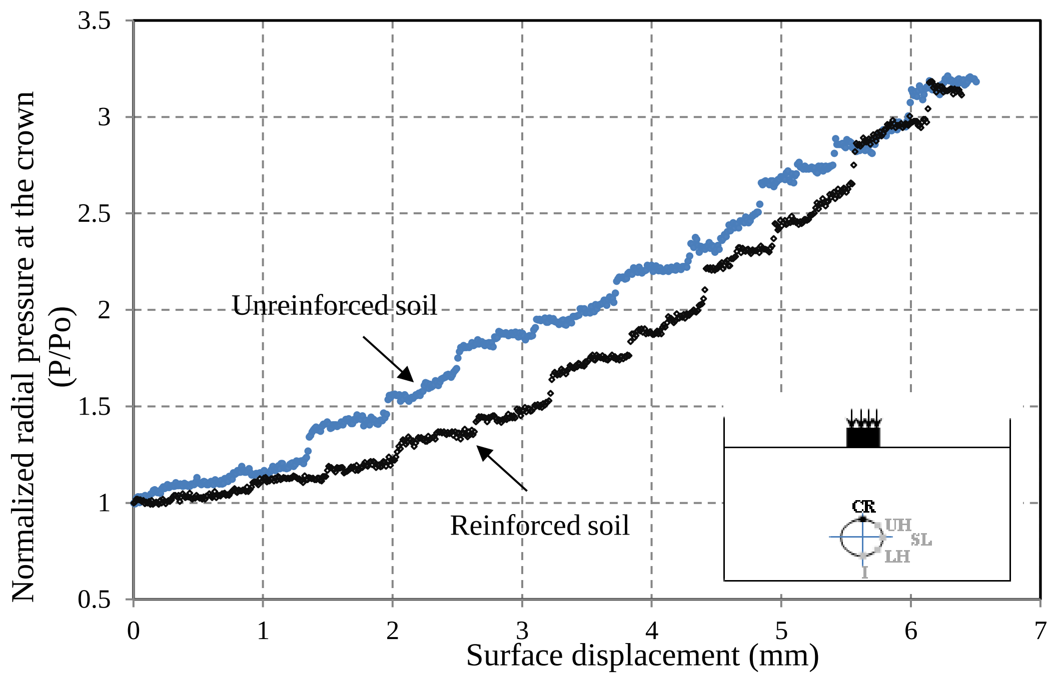

Figure 3.11 Changes in radial pressure at the crown

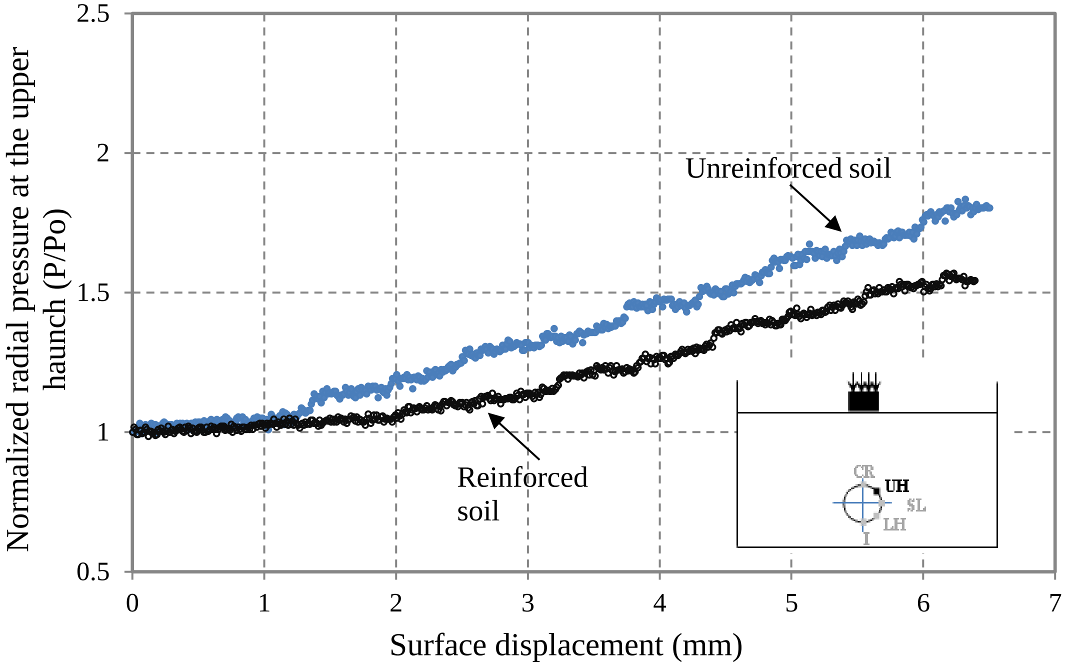

Figure 3.12 Changes in radial pressure at the upper haunch

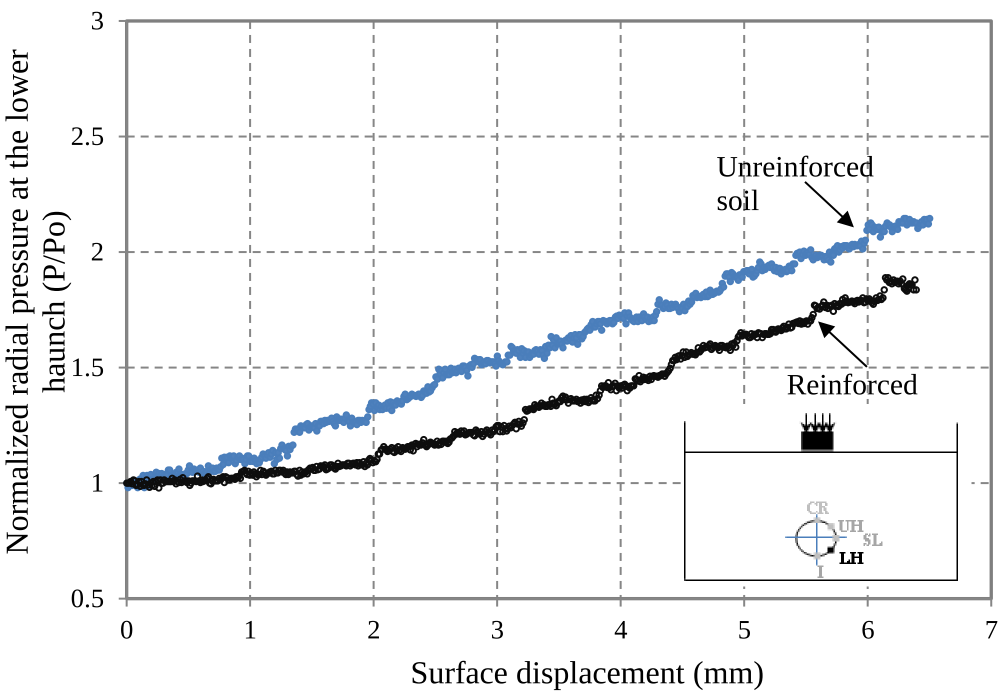

Figure 3.13 Changes in radial pressure at the lower haunch

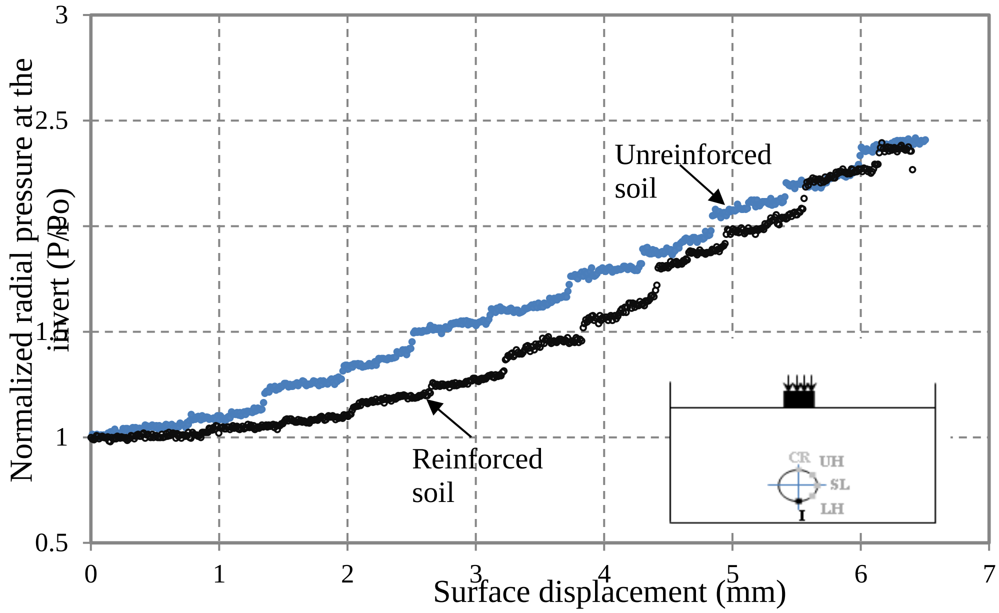

Figure 3.14 Changes in radial pressure at the invert

It can be seen from the above figures that the radial pressure around the pipe generally increased with the increase in footing pressure. In the case of geogrid reinforcement, the increase in pressure at a certain location was smaller compared to the unreinforced case. This can be explained by the fact that part of the applied load is transferred laterally through the geogrid. This indicates the effectiveness of the geogrid in reducing the effect of surface loading on a buried pipe.

It is worth noting that, in the previous figures (3.11 to 3.14) the maximum settlement reached is 6.5 mm for all tests which is attributed to reaching the pressure capacity of the sensing pads. The extended numerical analysis conducted using FE-DE method (Ahmed et al., 2015) allowed for the application of surface displacement of about 20 mm which confirmed the observed response.

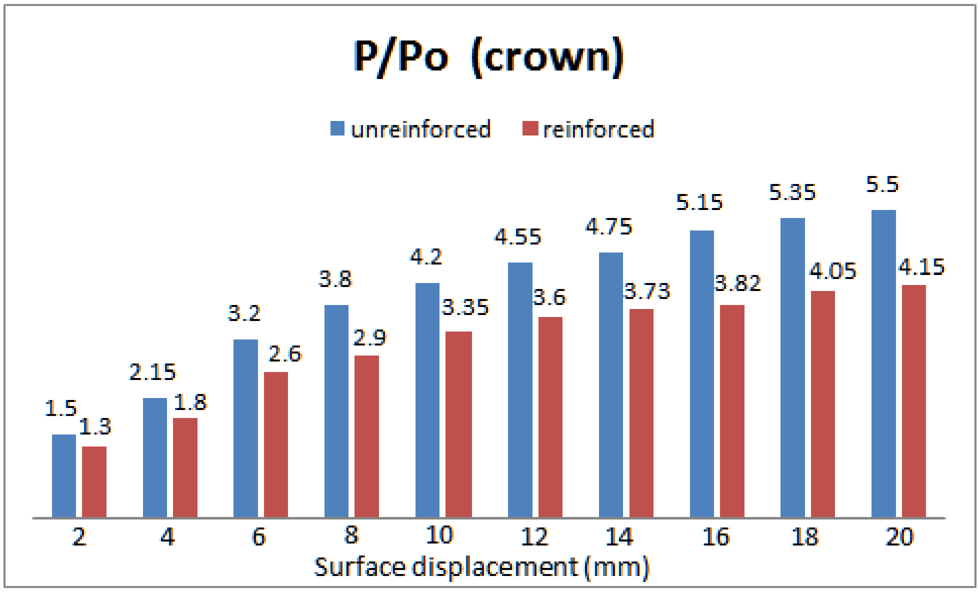

Figure 3.15 Augmented role of geogrid in reducing crown contact pressure at higher surface loads

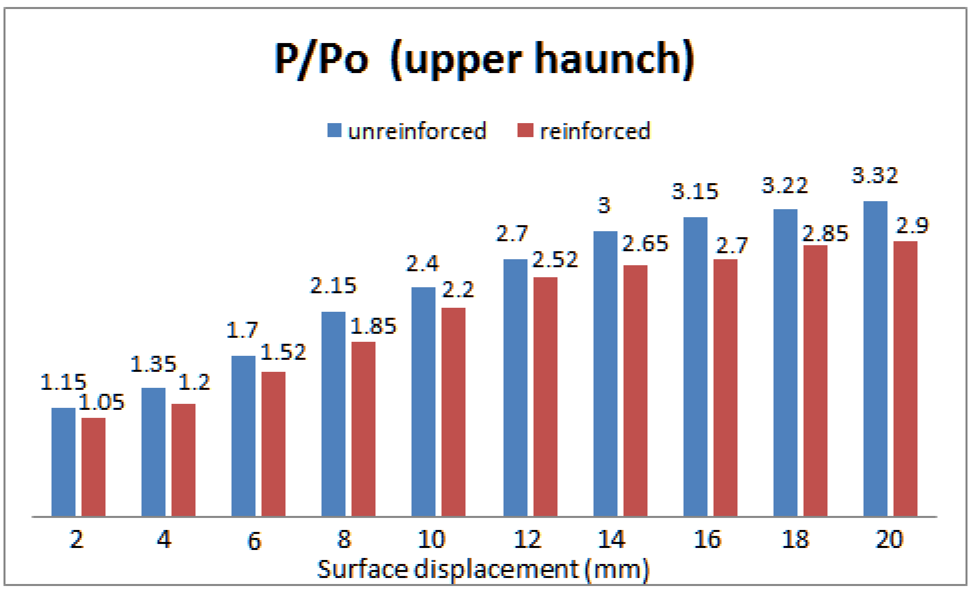

Figure.3.16 Augmented role of geogrid in reducing upper haunch contact pressure at higher surface loads

A total of 25% reduction in contact pressure occurred at the crown (Figure 3.15) while at the upper haunch the change was found to be about 13% (Figure 3.16). It was found that the effect of the geogrid in reducing the earth pressure on the buried pipe increased as the vertical displacement of the geogrid increased. This is attributed to the increased interaction between the geogrid and the surrounding backfill material and the mobilization of more friction increasing the interlocking effect, hence less pressure is transmitted to the pipe.

3.5 Summary and Conclusions

This study investigated the earth pressure distribution on buried pipes using laboratory experiments conducted on 15 cm pipe placed in granular backfill material and subjected to strip surface loading. The contact pressure distribution on a rigid pipe was measured using the tactile sensing technology. Contact pressure was measured using tactile sensors to provide a continuous pressure profile around the pipe. The effect of installing a layer of geogrid reinforcement near the surface on the radial pressure distribution was examined.

Radial pressure acting on the pipe generally increased with the increase in applied footing load. With the introduction of geogrid reinforcement, the radial earth pressure acting on the pipe was found to be smaller than that of unreinforced case. It was also found that the effectiveness of the geogrid reinforcement increased with the increase in surface loading.

This study revealed that geogrid reinforcement requires sufficient surface movement to mobilize the interlocking effect. If the backfill soil is densely compacted and the buried pipe is not deformable, the effect of the geogrid may not be significant. On the other hand, if the backfill is allowed to settle sufficiently to activate the geogrid, load will be redistributed resulting in a pressure reduction on the pipe.

Chapter 4

Investigating the role of EPS geofoam in reducing earth load on buried pipes subjected to static and cyclic loading*

4.1 Abstract

In the previous chapter, geogrid was used to reinforce the backfill soil above buried pipes resulting in a reduction in pressure being transferred to the walls of the pipe. In this Chapter, the effect of placing a compressible material (EPS geofoam) immediately above buried structures in reducing the earth load on the pipe walls is examined. The laboratory setup developed in Chapter 2 has been utilized where blocks of EPS geofoam of different densities are placed within the backfill material above the buried pipe (see Figure 4.1). A series of experiments has been conducted by applying a strip load parallel to the pipe axis under both static and cyclic conditions.

The earth pressure distribution acting on the pipe is measured using tactile sensing technology to obtain the contact pressure distribution on the pipe. Results revealed that the presence of EPS geofoam layer above the pipe can have a significant impact on the earth pressure distribution around the pipe. For the investigated EPS material type, geometry, and location with respect to the pipe, the radial pressure was found to significantly decrease at certain locations particularly at the pipe crown. This investigation concluded that the inclusion of EPS blocks above rigid pipes can limit the adverse effect of cyclic loading resulting in steady initial contact pressure after removal of surface pressure.

*A version of this chapter has been published in 66th Canadian Geotechnical Conference (GeoMontreal).

4.2 Introduction

Canadian municipalities will be investing billions of dollars in the next few years to build new culverts and buried pipes for water and wastewater lines. Loads on these buried conduits have been shown to be dependent upon installation conditions. Pipe installations are called trench installations when the pipe is located completely below the natural ground surface. Frictional forces between the sides of the trench and the backfill material help to support the weight of the soil overlying the pipe.

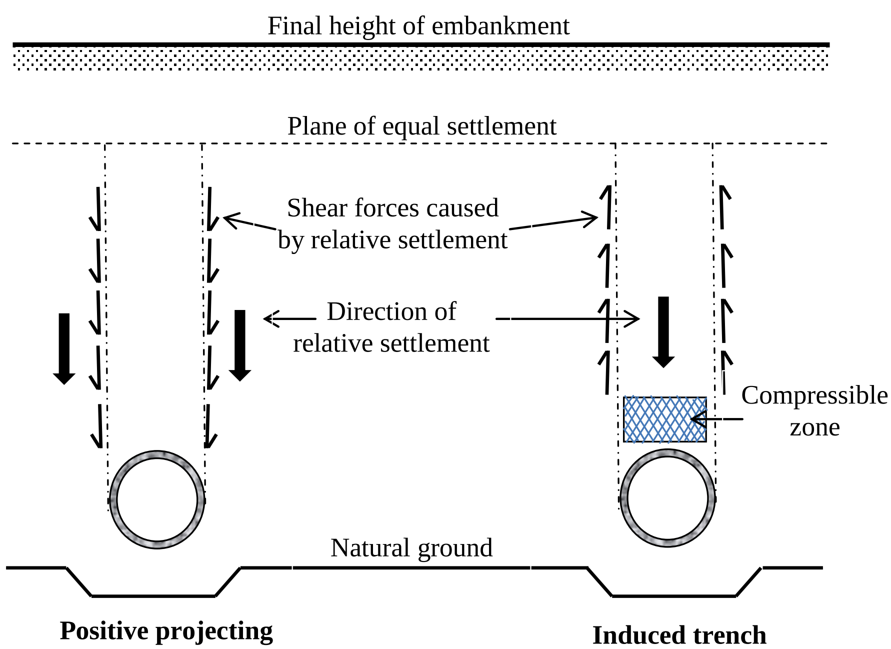

Figure 4.1 Positive projecting versus induced trench installations

On the other hand pipe installations are called embankment installation when soil is placed in layers above the natural ground. In order to reduce the vertical earth pressure on rigid pipes, the induced trench method has been developed where a compressible layer is placed above the pipe to simulate trench installation soil structure interaction effect. Induced trenching technique (also known as imperfect ditch) has been investigated over the past century.

As opposed to the conventional (positive projecting) approach where buried structures are placed under high embankments, induced trench method results in a downward movement of the soil prism located above the structure with respect to the surrounding backfill. This leads to the mobilization of upward shear stresses as shown in Figure 4.1 resulting in a reduction in the pressure transferred to the buried conduit.

Despite the known advantages of the induced trench method, the American Concrete Pipe Association (ACPA, 2000) removed the induced trench technique from the Design Manual in 2000 (McAffee and Valsangkar, 2008). This was attributed to the uncertainty regarding the sustainability of the load reduction achieved using the induced trenching method. On the other hand, ACPA (2000) has improved and updated the design and analysis tools for positive projecting technique by adopting standard installations direct design (SIDD) and using a finite element computer program (e.g. soil-pipe interaction design and analysis, SPIDA).

4.3 Literature review

Larsen (1962) is one of the first researchers who studied the induced trench design of culverts. This was achieved using baled straw as compressible material and comparing the measured pressures with similar culverts built using the positive projecting method. The layer of baled straw was placed directly on the pipe such that the central prism of soil above the conduit would settle more than the adjacent soil. Favorable results were obtained for the two investigated concrete pipes with diameters of 1.37m and 1.68m supporting 11.6m to 20m of fill height.

Lefebvre et al., (1975) used induced trenching to construct a 15.5 m span flexible culvert with backfill of 13.4 m in height. The structure, shown in Figure 4.2, was spanning over the Vieux Comptoir River, 800 km North of Montreal. Positive arching (induced trenching) was achieved by providing a compressible zone within the footing. The stresses measured at the crown showed a drop of 75 % in overburden pressure allowing for a thin steel membrane roof to be used resulting in a cost effective design.

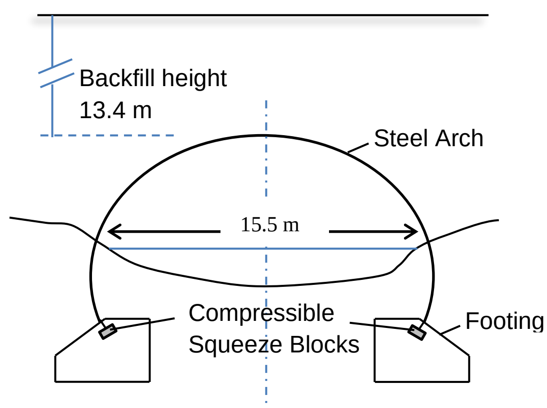

Figure 4.2 Culvert at Vieux Comptoir (Lefebvre et al., 1975)

Sladen and Oswell (1988) used induced trenching for an existing sewer line in a valley in Calgary that needed to be buried due to a change in land use. Taylor (1973) and Sheer and Willet (1969) monitored two pipeline projects to understand the long-term performance of induced trenching construction. Vaslestad et al., (1993) investigated the effectiveness of the induced trenching achieved using EPS geofoam layer placed above rigid culverts (1.6m diameter and 15m high). Four full scale experiments were conducted on culverts constructed between 1988 and 1992 in Norway (three in cohesionless soils and one in clay). The reduction in vertical stresses recorded at the crown was in the range of 50% to 75% of the overburden pressure.

McAffee and Valsangkar (2008) reported both centrifuge and full scale experimental investigations of 0.9 m diameter pipe installed under 2 m of backfill material with compressible zone made using sawdust material. A reduction of 75% in vertical pressure was recorded. It was also concluded that in imperfect trench construction lateral pressure may increase and may, in certain cases, exceed the vertical stresses.

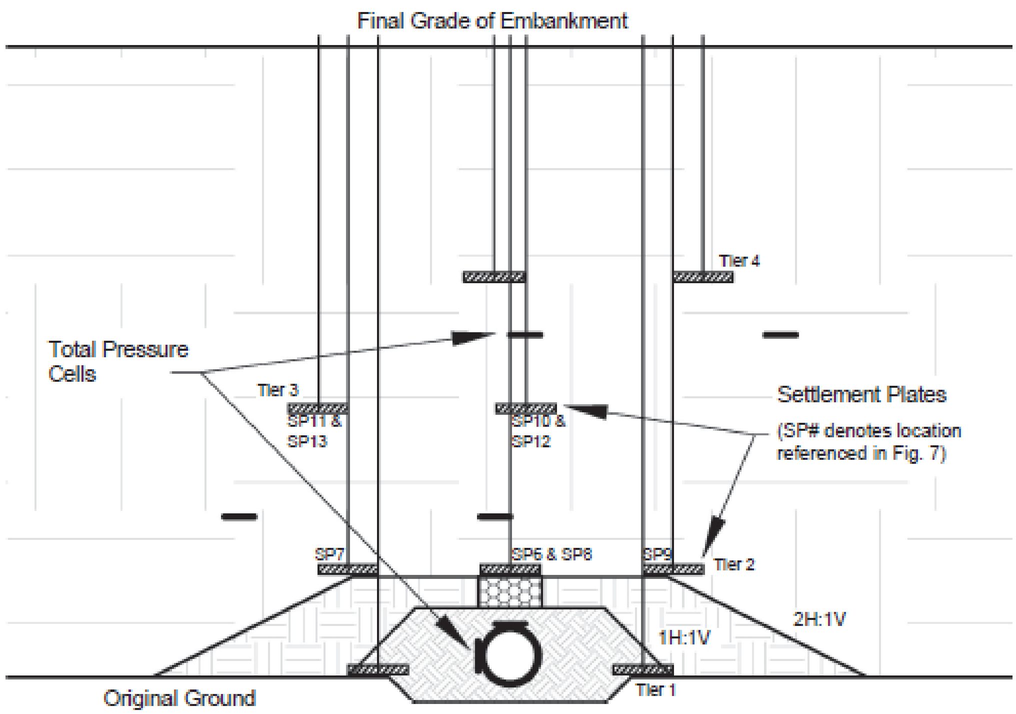

Figure 4.3 Induced trench test (McAffee and Valsankar, 2008)

The above research concluded that conventional (positive projecting) method of pipe installation under embankment can result in an increase in contact pressure at the crown of the pipe by 25% to 50% of the theoretical overburden pressure. It has also been agreed that induced trenching causes a significant reduction in pressure of up to 80% at the pipe crown with possible increase in lateral pressure near the pipe springline.

The experiments conducted on circular pipes generally rely on measuring contact pressures using conventional load cells placed at selected locations. The additional stiffness introduced by the load cell may result in arching effects and possibly overestimation of measured pressure (Ahmed and Meguid, 2009). The case of shallow embankments where the live loads result in cyclic contact pressure on the burried structure was not sufficiently investigated in previous studies.

4.4 Objectives

The objective of the study is to investigate the soil-structure interaction for a buried pipe installed using the induced trench method and subjected to static as well as cyclic loading. Contact pressure was measured using tactile sensing technology. This allows for continuous pressure profile to be captured during the loading and unloading processes.

4.5 Experimental Setup

Figure 4.4 Experimental setup

The experimental setup consists of an instrumented buried pipe embedded in granular material placed in a test chamber. The pipe is instrumented using tactile sensing pads wrapped around its outer perimeter covering the area near the middle third of the pipe length. Granular soil is used as the backfill material. A universal MTS testing machine with a capacity of 2,650 kN is used to apply the strip loading (see Figure 4.4). A more detailed description of each element is provided in the previous Chapter (section 3.4).

As discussed above, for the induced trench to take place a compressible material has to be placed on top of the culvert (Figure 4.5). EPS22 geofoam blocks density 21.6 kg/m^3 of 0.25 m in width, 0.42 m in length and 0.05m in thickness were used as the compressible material (see Table 4-1).

Table 4-1: Properties of GeoSpec EPS 22 geofoam (Plasti-Fab Ltd)

Material Property	Test Method	Units	GeoSpec Type Designations
Product Density	ASTM C303	kg/m^3 (pcf)	21.6 (1.35)
Compressive Resistance Minimum @ 1% Deformation	D1621	kPa (psi)	50 (7.3)
Compressive Resistance Minimum @ 5% Deformation		kPa (psi)	115 (16.7)
Compressive Resistance Minimum @ 10% Deformation		kPa (psi)	135 (19.6)
Flexural Strength Minimum	ASTM C203	kPa (psi)	240 (35)

4.6 Methodology

The buried pipe was subjected to surface strip load parallel to the pipe axis. The load was applied using an MTS machine controlled via data acquisition system.

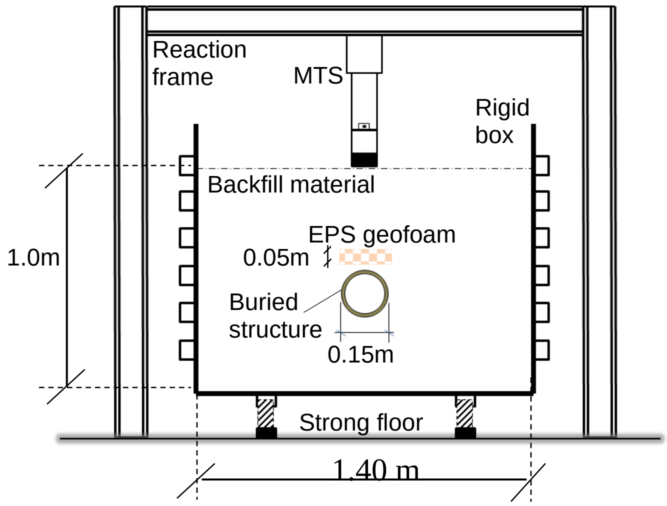

Figure 4.5 Schematic of the test setup

To choose a suitable backfill height above the pipe, tests were conducted using three different cover (H) to diameter (D) ratios, namely 3, 2.5 and 2. The geofoam block was retrieved after each test and the change in height was recorded. A soil height of 2D was found to provide a balance between the measurable compression of the geofoam and the soil volume to be used in the experiments. The compression experienced by the tested geofoam block (for H/D = 2) is shown in Figure 4.6.

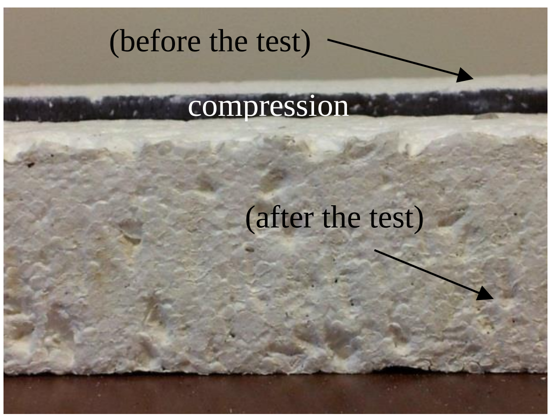

Figure 4.6 Compression of a geofoam block due to induced trench installation

4.6.1 Placement procedure

A soil placement procedure has been developed to ensure consistent initial conditions. The pipe is installed over a compacted bedding material and the backfill is placed and tamped in layers over and around the pipe. A total of four experiments were conducted, two benchmark tests with only the instrumented pipe inside the backfill and the other two include EPS geofoam placed at a distance of 1.25 cm (half inch) above the pipe crown. For all tests, the placement of the backfill continued up to a height of two times the pipe diameter above the crown.

Earth pressure distributions were measured and compared in both cases using the tactile sensors. Surface load is then applied using a rectangular steel plate (45 cm long x 10 cm wide) attached to the actuator of the MTS machine. After the completion of each test, the tank was emptied using a vacuum machine connected to a collection barrel. The pipe was then retrieved and the setup was prepared for the next test. The load was gradually applied under displacement control through the rectangular plate with a constant displacement rate of 1.3 mm/min to simulate static loading conditions as recommended by Das et al., (1994).

4.6.2 Load application

The test procedure is illustrated schematically in Figure 4.7. Position A shows the tank after placing the various elements described in section 3, The tank is then placed under the MTS machine as shown in position B. The MTS hydraulic jack is lowered until it comes in contact with the backfill (position C). The loading and unloading (alternating between position B & C repeatedly) process started and earth pressure is recorded using the data acquisition system.

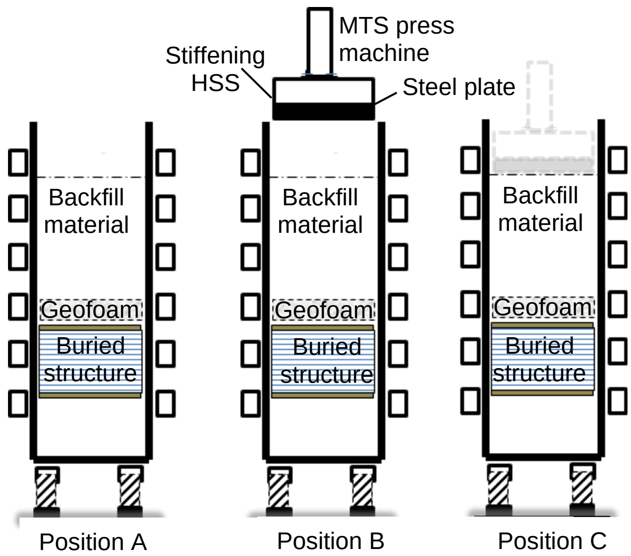

Figure 4.7 Testing procedure

4.7 Measured Earth Pressure Distributions

In this section, the recorded contact pressure readings are compared for the benchmark case (no geofoam) and for the case where an EPS Geofoam layer is installed above the pipe. The loading versus time history is found in Appendix.

4.7.1 Initial Radial Pressure on the Pipe

Snapshots of the three-dimensional earth pressure distributions before surface loading is applied for the two investigated cases (with and without geofoam) are shown in Figures 4.8 and 4.9. It is worth noting that the recorded pressures were taken using two adjacent sensing pads meeting near the springline of the pipe. In the first case, Figure 4.8, the measured pressures at the crown, springline and invert were found to be 12, 8, and 40 kPa respectively.

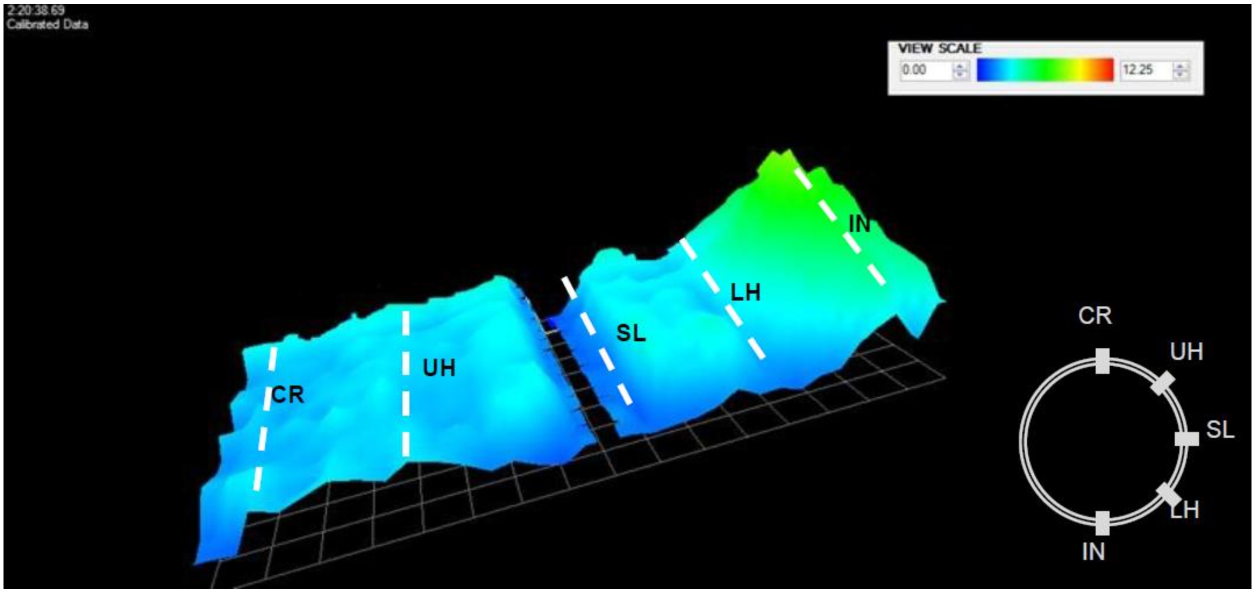

Figure 4.8 Initial earth pressure distribution (without geofoam)

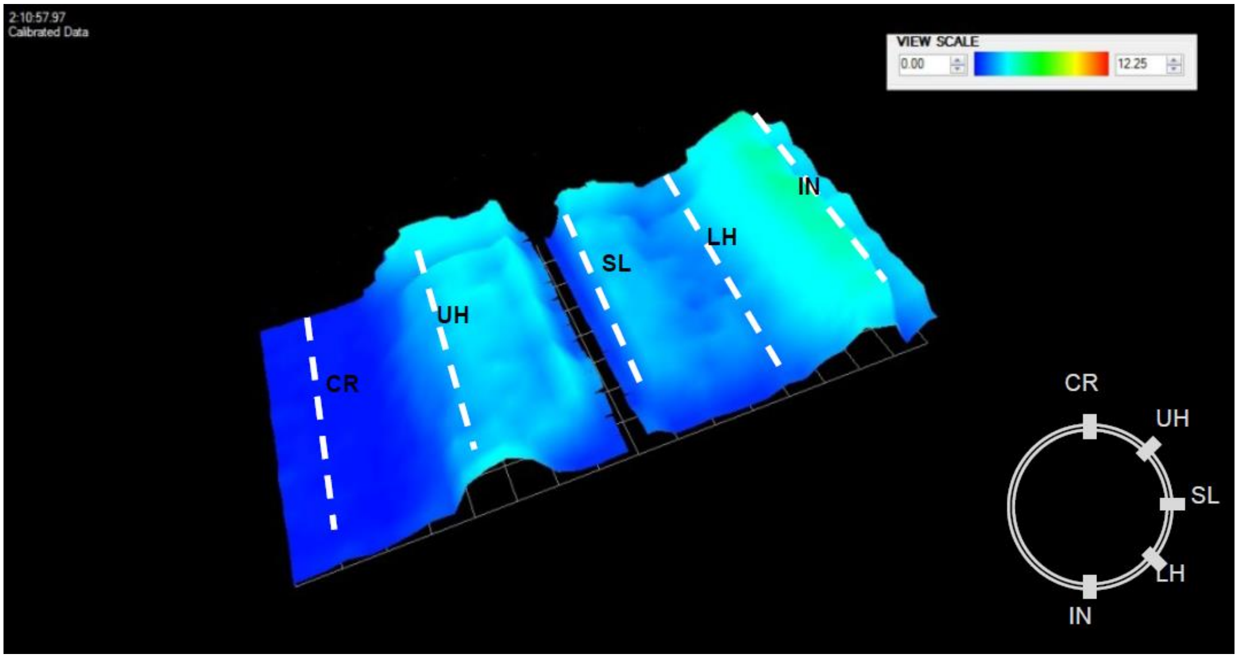

Figure 4.9 Snapshot of the earth pressure around the pipe after geofoam installation

These measured pressures in Figure 4.8 are consistent with the negative arching that develops due to the installation of a rigid pipe using the embankment construction method over compacted bedding_material. The results are also consistent with Hoeg's theoretical solution that predicts a radial pressure of 10.5 kPa at the crown.

$$\sigma_r = \frac{1}{2}p\left\{(1+k)\left[1-a_1\left(\frac{R}{r}\right)^2\right]-(1-k)\left[1-3a_2\left(\frac{R}{r}\right)^4-4a_3\left(\frac{R}{r}\right)^2\right]cos2\theta\right\} \tag{4.1}$$

The constants are defined by the following equations for the fully bonded interface case

$$a_1 = \frac{(1-2v)(C-1)}{(1-2v)C+1} \tag{4.2}$$

$$a_2 = \frac{(1-2v)(1-C)F-\frac{1}{2}(1-2v)^2C+2}{[(3-2v)+(1-2v)C]F+\left(\frac{5}{2}-8v+6v^2\right)C+6-8v} \tag{4.3}$$

$$a_3 = \frac{[1+(1-2v)C]F-\frac{1}{2}(1-2v)C-2}{[(3-2v)+(1-2v)C]F+\left(\frac{5}{2}-8v+6v^2\right)C+6-8v} \tag{4.4}$$

ν = The medium Poisson's ratio;

k = The lateral pressure factor;

R = The pipe radius;

r = The distance from the pipe center to the medium soil element;

C = The Compressibility ratio; and

F = The Flexibility ratio.

Where C and F are the stiffness ratios parameters to express the relative stiffness between the conduit and the soil calculated as follows

$$C = compressibility\ ratio = \left(\frac{1}{2}\right)\frac{1}{1-v}\frac{M^*}{\frac{E_C}{1-v_C^2}}\left(\frac{D}{t}\right) \tag{4.5}$$

$$F = flexibility\ ratio = \left(\frac{1}{4}\right)\frac{1-2v}{1-v}\frac{M^*}{\frac{E_C}{1-v_C^2}}\left(\frac{D}{t}\right)^3 \tag{4.6}$$

in which:

M* = The constrained modulus;

Ec = The conduit Young's Modulus;

D = Pipe diameter;

t = Pipe wall thickness; and

ν_c = The conduit Poisson's ratio.

Figure 4.9 shows the distribution of the contact pressure for the case of geofoam block installed above the pipe. As can be seen in the figure the presence of the geofoam layer was found to cause re-distribution of the earth pressures acting on the pipe with significant reduction in pressure at the crown and the lower half of the pipe circumference.

The pressures measured at a cross section near the middle of the pipe are shown in Figure 4.10. Results show that the measured initial earth pressure varies around the pipe circumference. The pressure at the invert was found to be sensitive to the compaction of the bedding layer, with maximum pressure value of 40 kPa at the crown. After the installation of the geofoam, the initial pressure at both the crown and invert locations decreased by about 10 kPa. This presents a reduction of more than 90% at the crown and about 25% at the invert.

It has been noted that the difference in pressure at the crown and invert (about 28 kPa) is equivalent to the contact pressure measured due to the self-weight of the pipe (in air). This observation is true for both initial and maximum loading conditions and confirms that, despite the sensitivity of the pressure distribution to the pipe placement procedure, the sensors are able to read the net pressure induced by the backfill material with reasonable accuracy. The measured responses at different locations on the pipe due to cyclic loading are summarized below.

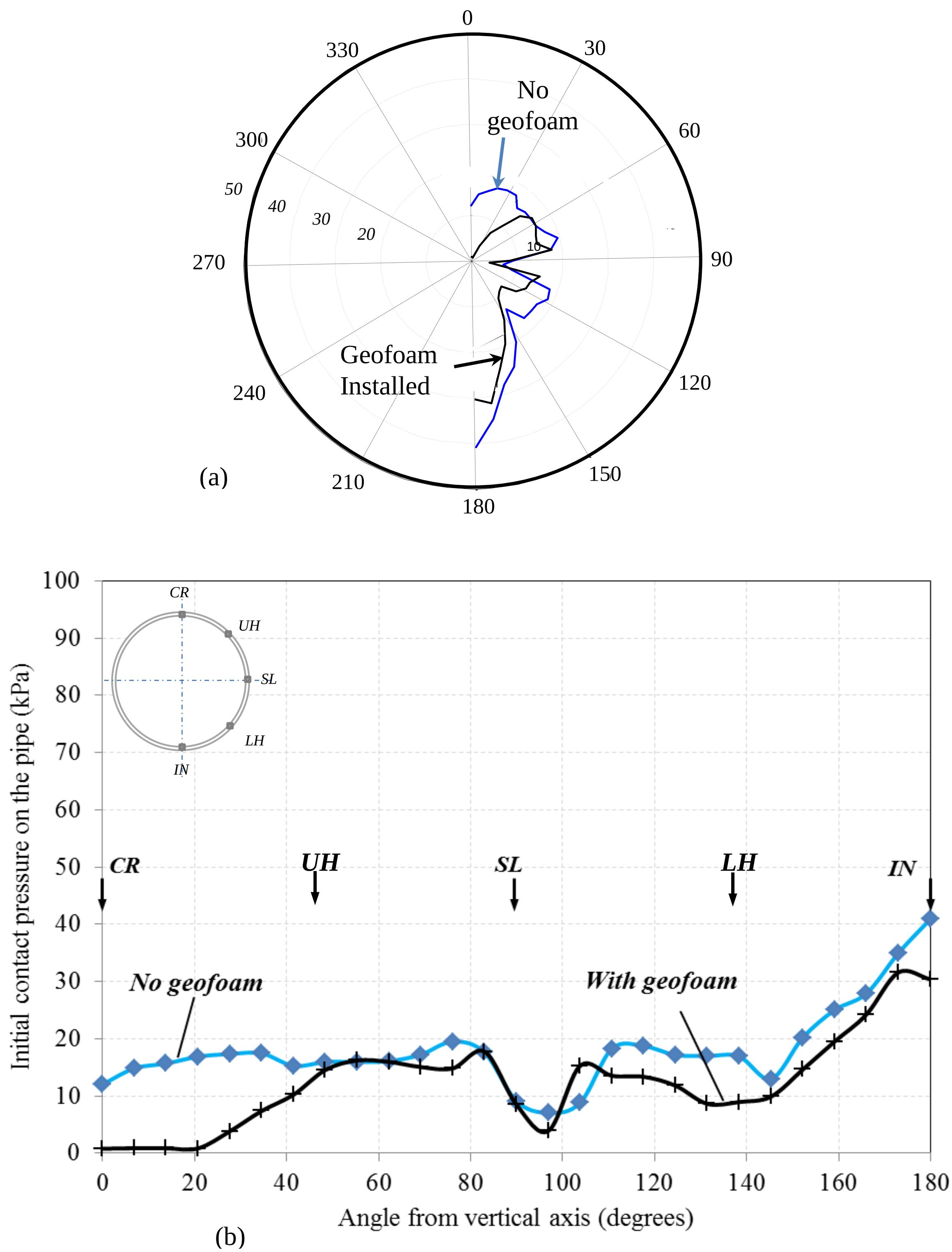

Figure 4.10 Initial earth pressure distribution on the pipe

4.7.2 At the crown:

Before the geofoam is introduced, the initial radial pressure at the crown was found to increase from 12 kPa to 85 kPa when the surface pressure increased from 0 to about 200 kPa as illustrated in Figure 4.11. After the first loading cycle is completed and the surface load is removed, the soil compression has led to an increase in radial pressure on the pipe from 12 kPa to 25 kPa. On reloading, the pressure increased from 25 kPa to 85 kPa at a slightly smaller rate.

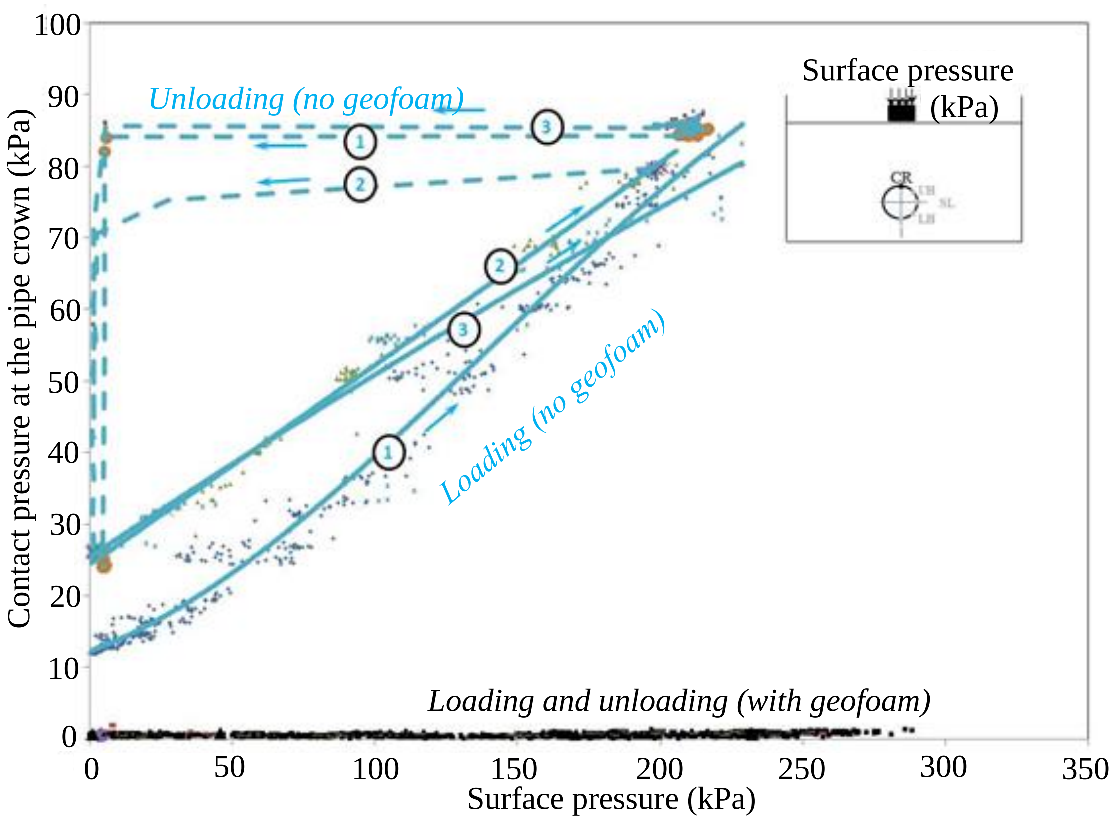

Figure 4.11 Changes in earth pressures under cyclic loading (at the crown)

After the geofoam is introduced, the initial radial pressure was significantly small (about 2 kPa). During the first loading cycle, the pipe did not experience an increase in pressure from the initial value. Unloading and reloading did not create additional stresses in the pipe and the recorded radial pressure did not increase above 2 kPa.

Under cyclic loading, an increase in residual pressure upon unloading was observed in the tests without geofoam (positive projecting installation). After the first cycle the residual pressure (pressure after complete removal of surface load, i.e. airbag deflated) changed from 12 kPa (initial condition) to 25 kPa (contact pressure before reapplying the surface load for the second cycle). This was not the case for the induced trench condition when the geofoam was installed as the pressure was negligible.

4.7.3 At 45 degrees (upper haunch):

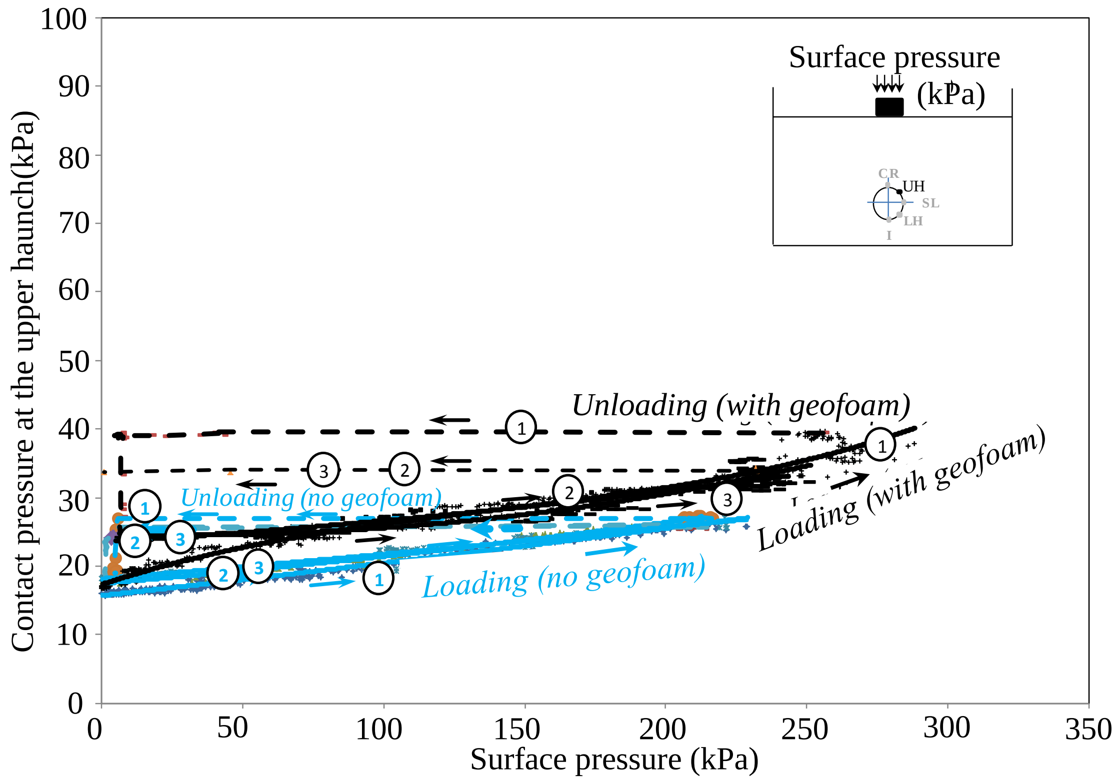

Figure 4.12 Changes in earth pressures under cyclic loading (at the upper haunch)

Figure 4.12 shows that for the case of positive projecting (no geofoam), radial pressure at the upper haunch location increases from 16 to 24 kPa as the applied surface load increases from zero to 200 kPa. For the case of induced trenching (with geofoam) the pressure, although started at a similar value of 17 kPa, it reached 40 kPa when the surface load was 200 kPa which represents about 67 % increase in pressure. Vaslestad (1993) highlighted that induced trenching may result in an increase in lateral earth pressure due to the load re-distribution within the soil but did not provide an estimated value of such increase neither showed a specific location at which it occurs.

Under cyclic loading, an increase in residual pressure was observed in the tests involving geofoam. After the first cycle the residual pressure (pressure after complete removal of surface load, i.e. airbag deflated) changed from 17 kPa (initial condition) to 24 kPa (contact pressure before reapplying the surface load for the second cycle). In addition, under maximum surface load the contact pressure at the upper haunch dropped from 40 kPa to 34 kPa.

4.7.4 At 90 degrees (springline):

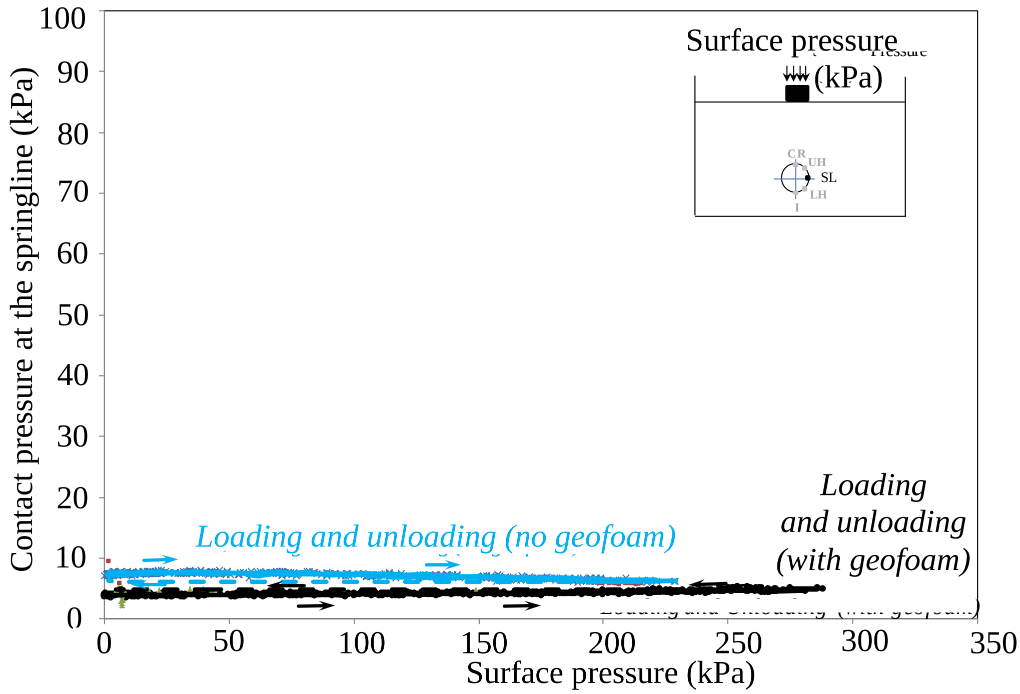

Figure 4.13 Changes in earth pressures under cyclic loading (at the springline)

The recorded data (Figure 4.13) at the springline showed generally low pressure values (less than 8 kPa) and the presence of geofoam was found to reduce the contact pressure by about 25%. It was observed that cyclic loading did not have a significant effect on the recorded pressures.

4.7.5 At 135 degrees (lower haunch):

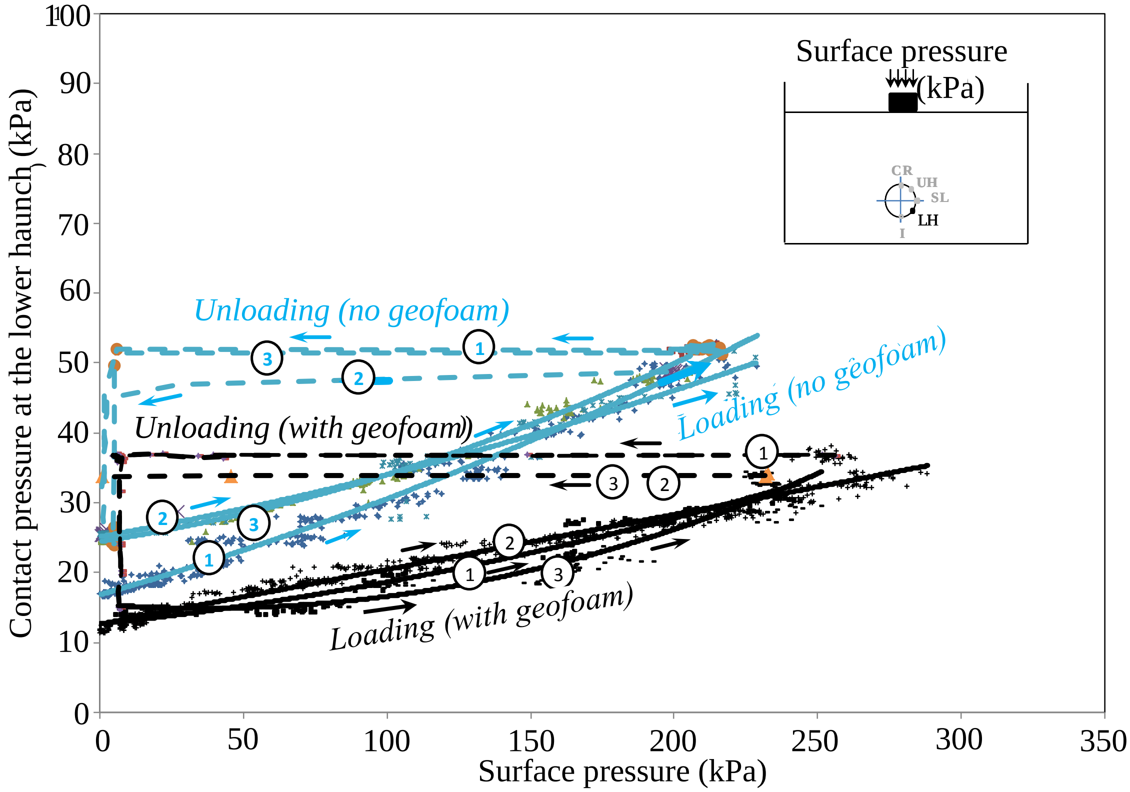

Figure 4.14 Earth pressures in cyclic loading (lower haunch)

The initial pressure for the case of no geofoam started from about 16 kPa and increased to 50 kPa as the surface pressure increased to 200 kPa. Upon unloading, the initial pressure returned to 26 kPa with a residual value of about 10 kPa as shown in Figure 4.14. The presence of geofoam reduced the initial pressure to 12 kPa, with maximum pressure of 37 kPa when the surface load reached 200 kPa, and no residual pressure following each cycle. The presence of the geofoam was found to reduce the radial pressure at 135° location by about 25% following the completion of the repeated load cycles.

4.7.6 At 180 degrees (Invert):

The recorded pressure at the invert is similar to that at 45° with about 15% increase in pressure after the geofoam placement. It should be noted that at this location, significant residual pressure was measured. Following the first cycle, the pressure increased from 40 kPa to 82 kPa in the cases with and without geofoam.

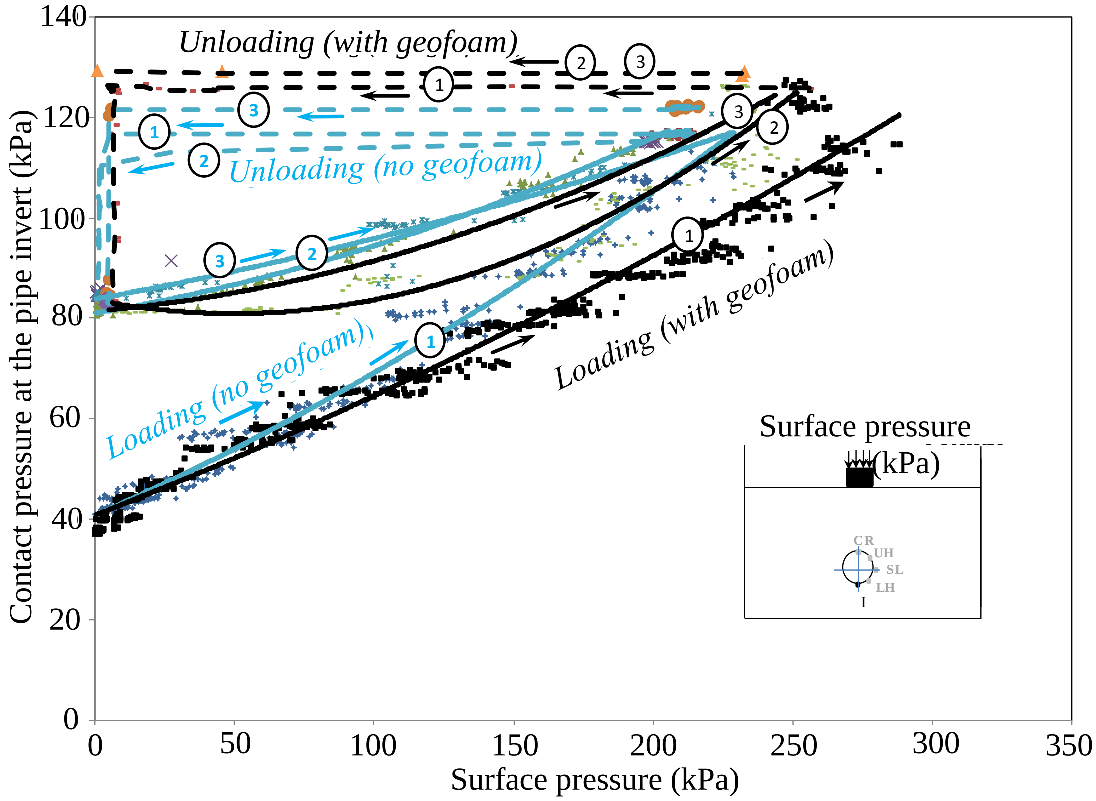

Figure 4.15 Earth pressures in cyclic loading (invert)

4.8 Summary and Conclusions

This study examined the effect of installing EPS geofoam blocks on the earth pressure distribution on buried pipes installed using the embankment construction technique. A physical model was designed and built to allow for a granular backfill material to be contained in a rigid box and for a surface pressure to be applied using an MTS press machine. A rigid PVC pipe was instrumented using conformable TactArray pressure sensors wrapped around the outer perimeter and installed within the backfill material. To examine the effect of introducing a geofoam layer above the pipe on the radial pressure induced by surface loading, a relatively shallow burial depth of two times the pipe diameter above the crown was chosen in this study. This depth is considered appropriate and ensures that sufficient load is transferred to the pipe during the loading and unloading process during which induced trenching is in effect.

Two sets of experiments were conducted- the first included two benchmark tests with no compressible layer and the second included two tests with a geofoam layer installed above the pipe. For the investigated geofoam density, geometry and backfill material type, the presence of geofoam resulted in a significant reduction in radial earth pressure on the pipe at the crown.

The upper haunch showed a significant increase in contact pressure due to the positive arching developing in the soil. In the previous research projects such effect was not quantified or detected. Such influence is recorded along the full circumference of the buried structure and shows that the drop in contact pressure is not necessarily in all locations or uniform as it changes and at the zone between 30 and 40 is actually offset by the increase in soil pressure due to diversion of the prism weight. Thus it has to be taken into consideration when designing buried structures constructed using the induced trench technique. A summary of the measured pressure changes are given in Table 4-2 below.

It can be concluded from this study that using geofoam inclusion as a compressible material above buried pipes is beneficial and can lead to a substantial reduction in earth pressure on the pipe. The most significant load reduction was found to happen at the crown. This is attributed to the soil arching leading to the distribution of earth pressure away from the crown.

Table 4-2 Measured pressure changes after Geofoam Installation

Location	% Change in radial pressure	% Change in residual pressure after unloading
CR (0^o)	-90%	No residual pressures
UH (45^o)	+67%	-15%
SL (90^o)	-35%	No residual pressures
LH (135^o)	-24%	No residual pressures
IN (180^o)	+15%	+100%

This experimental study suggests that geofoam inclusion can significantly enhance the response of buried pipes particularly for shallow buried structures under repeatable loading.

Chapter 5

Contact pressure distribution on buried box sections installed with geofoam inclusion

5.1 Abstract

An experimental study to evaluate the role of EPS geofoam inclusion on the distribution of contact pressure acting on box-shaped conduits under deep embankments is presented in this Chapter. The experiments are conducted using the test chamber described in chapters 3 and 4. Tactile sensors are used to measure contact pressures allowing for the 3D pressure distribution on the box walls to be measured. The second part of this study aims at exploring the effect of geofoam density on the overall response of the system. Two different EPS densities were used (Geospec 22 kg/m^3 and Geospec 15 kg/m^3) and two layouts of the compressible material around the buried box (top only or top & sides) were examined. A comparison of the measured response with some of the available theoretical solutions used for the design of buried structures is made.

A total of 12 tests were conducted as part of this study. The surface pressure was applied using pressurized air bag to simulate an embankment of up to 8.5 m in height under a controlled environment. The introduction of EPS geofoam above the buried box caused a pressure reduction at the top and bottom of the box with a slight increase in pressure on the side walls. A reduction of up to 70% in contact pressure was measured when induced trenching technique is used with Geospec 15 kg/m^3 installed above the conduit.

5.2 Introduction and literature review

Induced trench technique of pipe installation (imperfect ditch) has been studied by researchers for several decades with a track record of reasonable performance in the past 20 years (Spangler and Handy, 1973). As discussed in Chapter 4, the conventional method of installing buried conduits under an embankment is called positive projecting where the pipe represents a stiff object in the ground resulting in an increase in earth load on the pipe. Induced trenching, on the other hand, is a soil arching mechanism that develops due to the presence of a compressible material above the buried structure leading to the mobilization of upward shear stresses along its boundaries causing a reduction in earth pressure on the structure (see Figure 5.1).

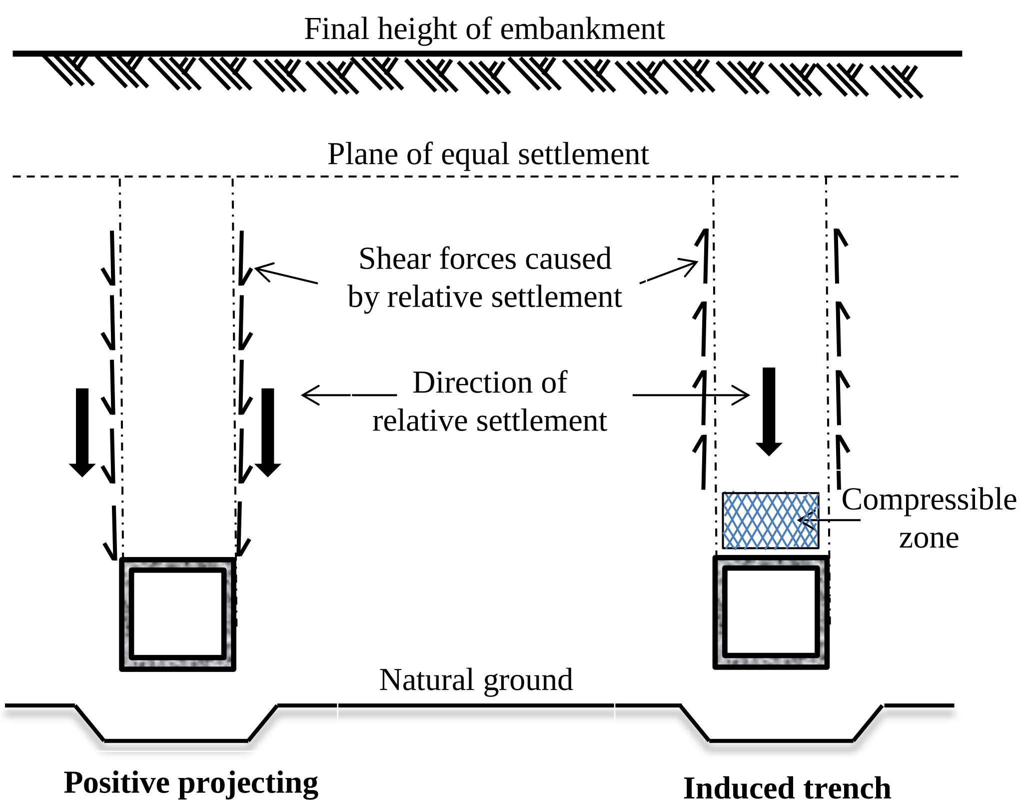

Figure 5.1 Problem Description

The objective of this Chapter is to experimentally investigate the contact pressure distribution on a buried box structure installed using the induced trench method in a small scale setup and investigating the roles of geofoam density and layout on the earth loads acting on the structure.

5.2.1 Marston-Spangler theory

The concept of induced trench was first introduced by Marston and Anderson (1913) who coined the term that refers to the placement of a compressible material above a buried conduit to reduce earth loads. The experimental work of Marston (1922; 1930), Spangler (1950) and Spangler and Handy (1973) has led to the development of the induced trench procedure to determine the earth load on deeply buried pipes under deep embankments known as the “Marston-Spangler” theory.

Sladen and Oswell (1988), Scarino (2003) and Taylor (2003) criticized the theory claiming that it is generic and empirical in nature and lacks criteria for selecting the geometry, location and mechanical properties of the compressible material a. McAffee and Valsangkar (2008) attributed the success of Marston-Spangler theory to the fact that it provides conservative results. It is worth noting that the theory was developed for circular cross-sections with earth load calculated at the pipe crown.

5.2.2 Previous experimental work

In Chapter 4, some of the earliest induced trench studies were summarized. Spangler (1958), Larsen (1962) and Lefebvre et al. (1976) used full scale experiments with various compressible materials and results showed an up to 80% reduction in contact pressure at the crown of large diameter pipes of circular cross sections as was mentioned earlier.

It has been agreed that positive projecting technique increases the earth load by 25% to 50% of the theoretical overburden pressure. Conversely induced trenching lead to a reduction in earth load of up to 75% at the crown (or upper wall) and up to 40% increase in lateral earth pressure.

One of the earliest studies to investigate box culverts installed using induced trench method was that of Floyd and Clark (1979) to measure the response of a 2.13 x 2.13 m reinforced concrete barrel resting on bedrock under a 30m high sand embankment. The compressible material used was loose straw and compressible soil mix. They used both strain gauges for measuring stresses and a system of rods and plates for measuring settlement. Water ingress and vandalism lead to damage of the measuring tools hence failed to present results due to unreliable data. Vaslestad (1993) reported a reduction of about 63% in earth pressure for cohesive soils due to the placement of the compressible material which was geofoam above a 2.0mx2.0m box culvert underneath 10m high silty clay soil.

McAfee and Valsangkar (2008) conducted centrifuge experiments to study the effect of induced trenching on 38 mm x 38 mm box culverts subjected to 30g simulating a soil height of 10 m. A reduction in earth pressure of 79% on the top slab compared to positive projecting. A summary of the relevant literature and the investigated parameters including compressible material stiffness, E, width, w, height, h, and location relative to the conduit width, B and height, H is given in Table 5-1.

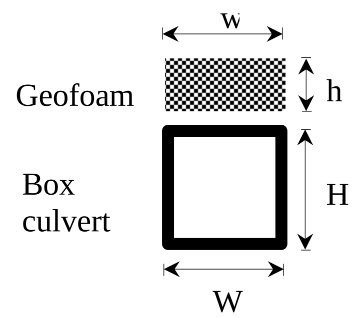

Table 5-1 Parametric studies in the literature for box culverts

Authors	Optimum parameters			Methodology		Reduction compared to overburden (for top slab) and other remarks
	w/B	h/H	E	Exp.	Numerical	
Vaslestad (1993)	1	0.78		Full Scale	CANDE	• 63% • successful full scale. • case of cohesive soil.
Okabayashi (1994)	1	0.167		Centrifuge		• 65% • best location is right above the box. • width effect is minimal.
Borque (2002)	1 1.2	0.66		Centrifuge	FLAC	• 30% • twin box culverts.
Mcleod (2003)	1	1		Centrifuge (un-yielding)	FLAC	• 80% • moderate increase on lateral. • increase of width has no effect
McAffee (2005)	1	0.5		Centrifuge	FLAC	• 53% • tried double layer geofoam, got same result.
Kim&Yoo (2005)	1.5	1.5	•		ABAQUS ISBILD (yielding and un-yielding)	• 60% • increasing width has no effect • compaction has no effect • increasing stiffness lowers reduction by same percent. • placed geofoam directly on top of culvert. • noticed down drag forces.

Yoo et al., (2005)	1	0.25	•		ABAQUS NASTRN (yielding and un-yielding)	• 50% • bedding and sidefill treatment are more important than foundation • placed compressible material on top and sides to reduce drag down forces
Kang et al. (2008)	1	0.25	•		ABAQUS MSC/NASTRAN (yielding and un-yielding	• studied new geofoam layout (top + sides) which led to 50% extra reduction for bottom slab. • width has limited effect • quantified drag down forces effect up to 80%
Vaslestad 2009	1	0.78			PLAXIS 2D	• 73% • 15 year monitoring proved successful
McGuigan and McAfee (2010)	1.2	0.5	•	Centrifuge (yielding)	FLAC	• 78% • Quantified drag down forces experimentally effect up to 60%.

5.2.3 Drag down forces on box sections

Kim and Yoo (2005) used finite element analysis to compare embankment, trench and induced trench installations for box culverts. For best results, they suggested placing the compressible material directly above the culvert. Kang (2007) investigated numerically the effect of placing geofoam blocks around circular culverts. An improvement in load reduction was calculated at the crown, invert and lower haunch.

Kang et al., (2008) found that placing geofoam on the side walls of box culverts helps reduce the pressure on the bottom slab due to reducing the sidewall shear. They also highlighted the presence of the drag down forces on the side walls of the box culvert that may cause an increase in contact earth pressure on the lower slab. Similar observation was made by Katona (1982), Tadros et al. (1989) and Yoo et al. (2005).

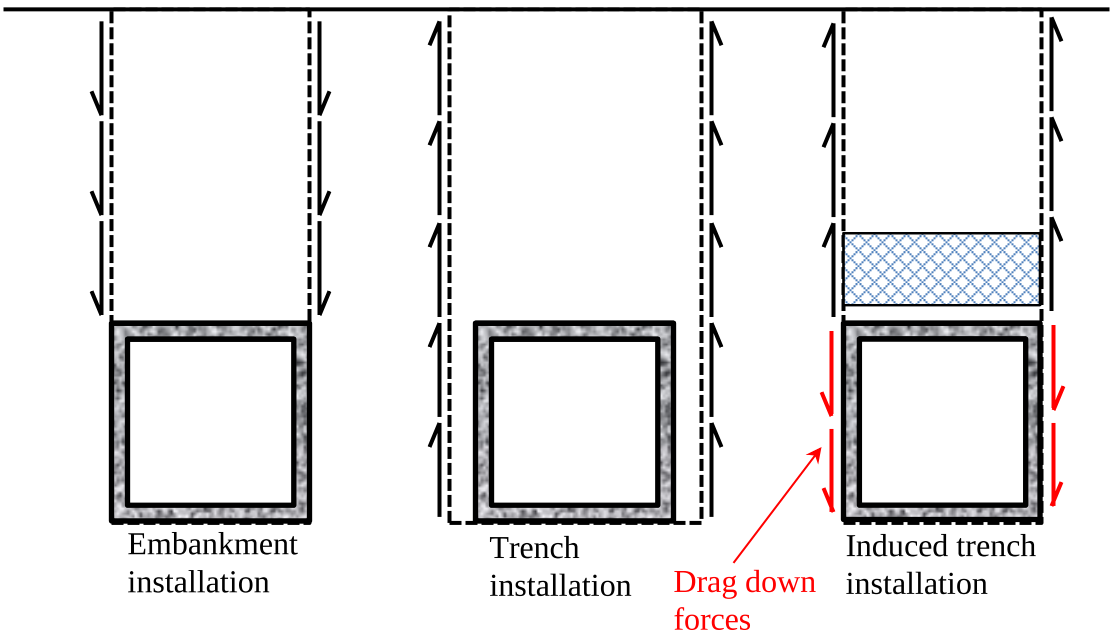

Figure 5.2 A schematic of the box culvert installation methods

McGuigan and McAffee (2010) used combined centrifuge testing and numerical modeling to investigate the drag forces for embankment and induced trench installation for box culverts. Contact pressures recorded at the lower slab were found to be about 59% more than the top slab after adding the weight of the culvert for both yielding and unyielding bedding conditions. However, no significant drag effect was found for embankment installations without compressible material (less than 10% increase).

5.3 Objectives

This study aims at investigating the soil arching around a box culvert built using embankment installation technique. Contact pressure profiles were measured continuously around the structure using TactArray flexible sensors. Two different geofoam densities (EPS-22 and EPS-15) are used in this study and the associated drag forces are estimated for each case.

5.4 Experimental Setup

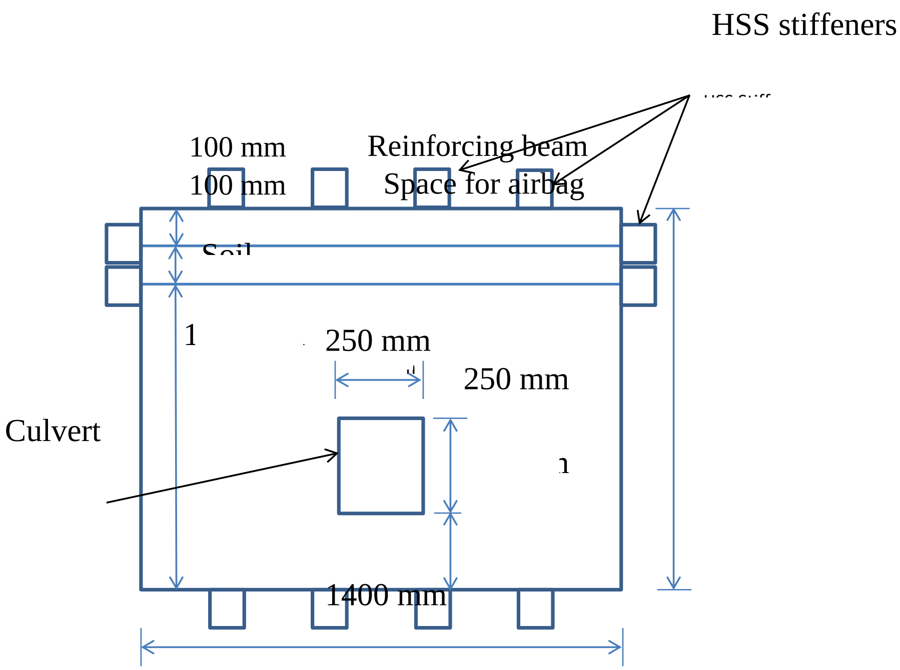

Figure 5.3 Schematic showing dimensions of setup

The experimental setup is schematically shown in Figure 5.3. It consists of an instrumented rigid steel box with square cross section embedded in a test chamber. Various elements of the setup are exhibited in Figure 5.4. The culvert is instrumented using tactile sensors wrapped around its outer middle third section. Granular soil is used as backfill material. The loading was applied using the inflatable airbag placed on top of the backfill as shown schematically in the side view in Figure 5.4.

As the airbag is inflated and restrained by the cover, the air pressure pushes downwards applying a distributed load over the entire backfill surface simulating a much higher backfill load. The airbag was inflated up to 20 psi (138 kPa) which is equivalent to an overburden pressure of about 8.5 m high backfill. A detailed description of the setup components is given in the next sections followed by a summary of the experimental procedure.

5.4.1 Test chamber

The chamber dimensions (1.4 x 1.2 x 0.45 m) are selected such that they represent two-dimensional loading condition. The rigid walls are placed far enough from the buried box to minimize boundary effects (distance from the wall of the buried structure to the side wall of the tank is 0.625 m which is more than twice the box width). All steel wall surfaces were painted with epoxy coating to minimize friction with the backfill material.

In addition a double layer of plastic sheets (2 mm thick) was placed on the back and front of the strong box. The layer in contact with the box was fixed while the layer in direct contact with the soil was free providing a smooth sliding surface, and hence minimizing friction effects.

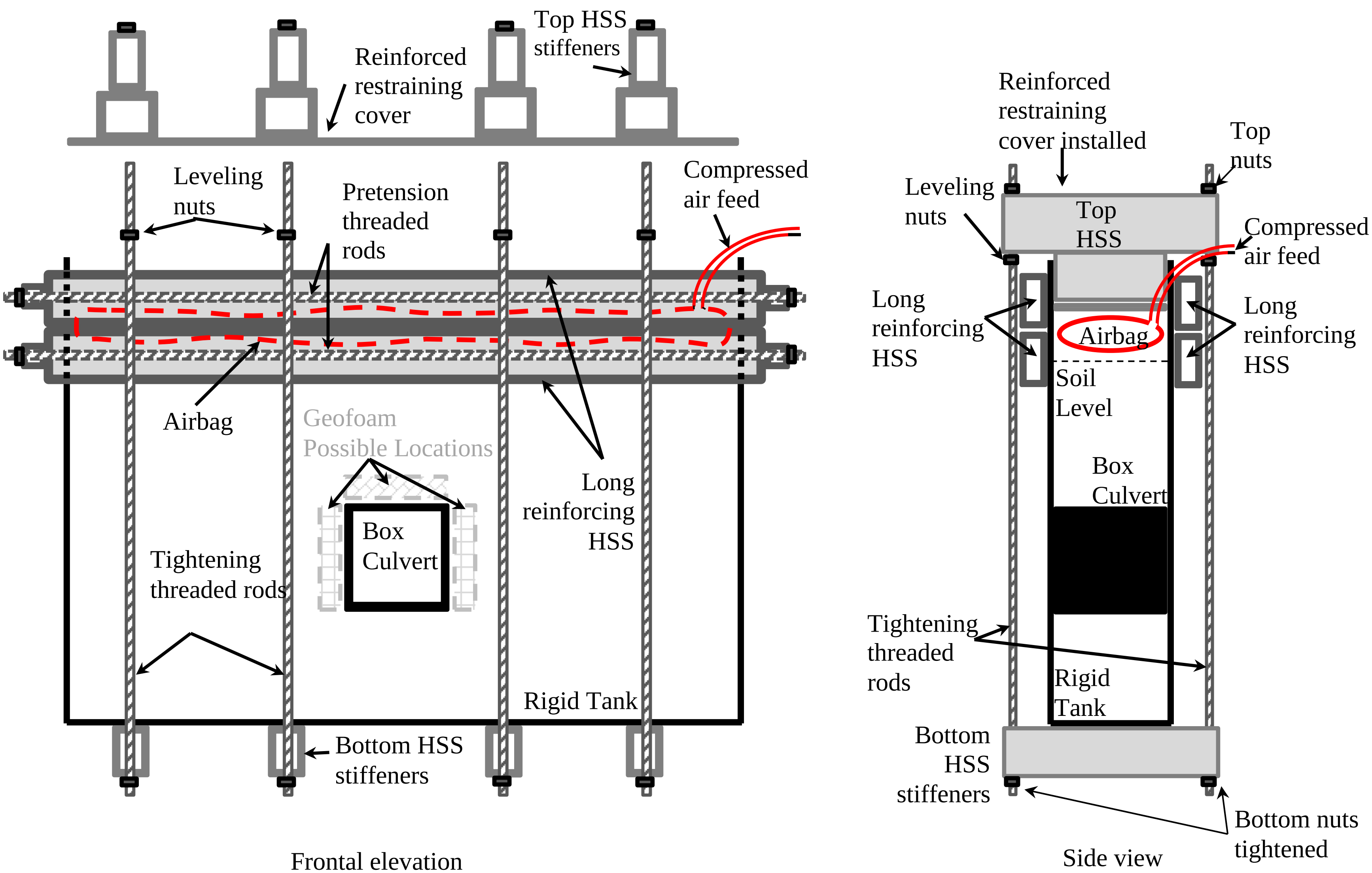

Figure 5.4 Detailed schematic of setup

Due to the pressure imposed by the airbag, an additional reinforcement was designed to confine the setup in both the lateral and vertical directions. Lateral confinement was provided using four 6-inch reinforcing HSS steel beams (two at the front and two at the back) and four 4-inch HSS steel beams (two on each side) in the area where the airbag is located as shown in Figure 5.5. In addition, pretension threaded rods help keep the steel beams tight in place to minimize deformation as a result of the applied air pressure

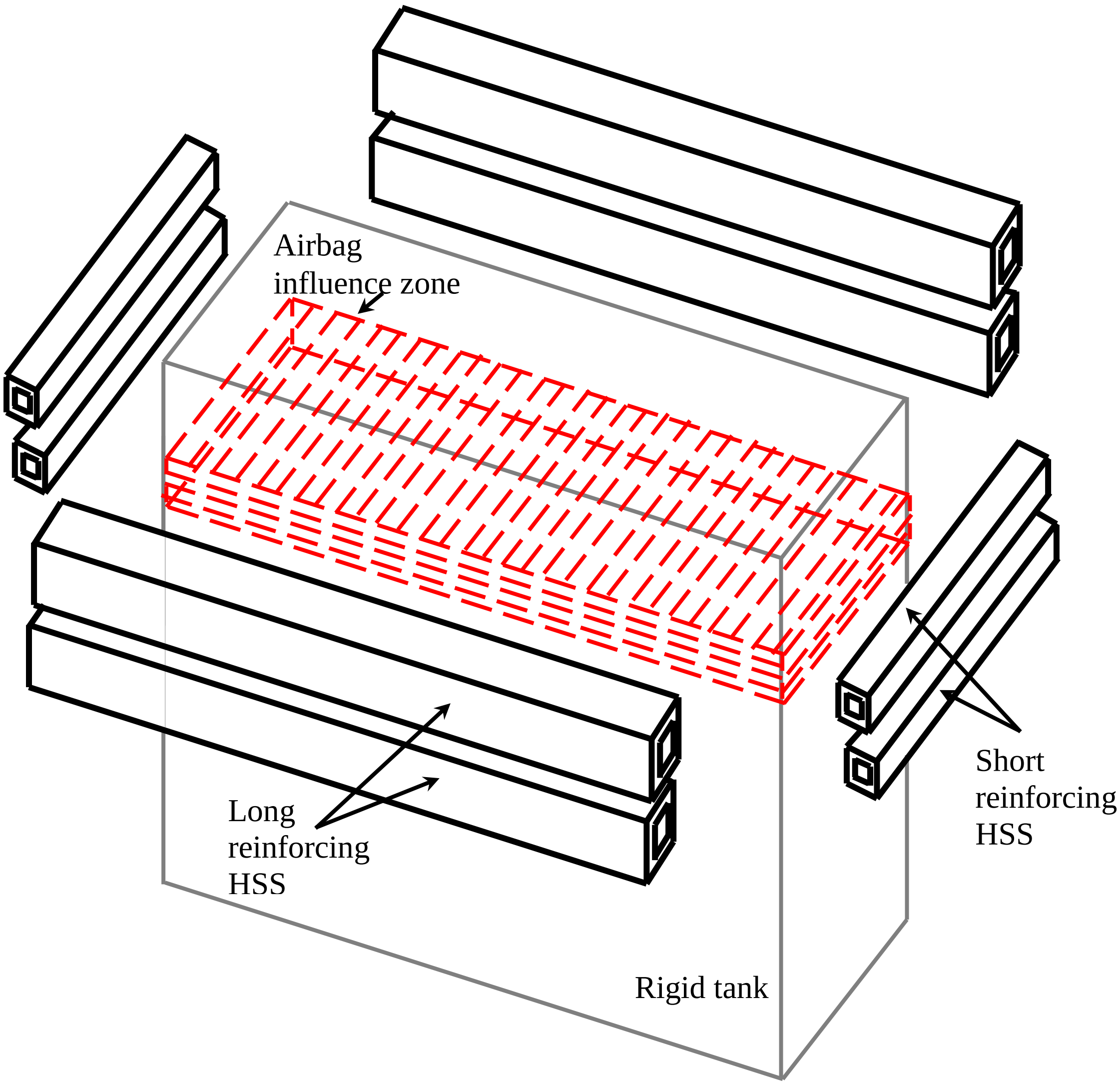

Figure 5.5 Lateral confining system

To create a constrained space for the airbag, a reinforced cover plate connected to a reaction frame is used throughout the experiments. The cover (Figure 5.6) consists of a thick metal plate with the exact dimensions of the inside of the chamber, welded to the top HSS Stiffeners to prevent it from buckling under high pressures. The reaction system is connected to the bottom of the chamber through eight threaded rods 1 inch in diameter and fastened to top and bottom HSS sections as depicted in Figure 5.7.

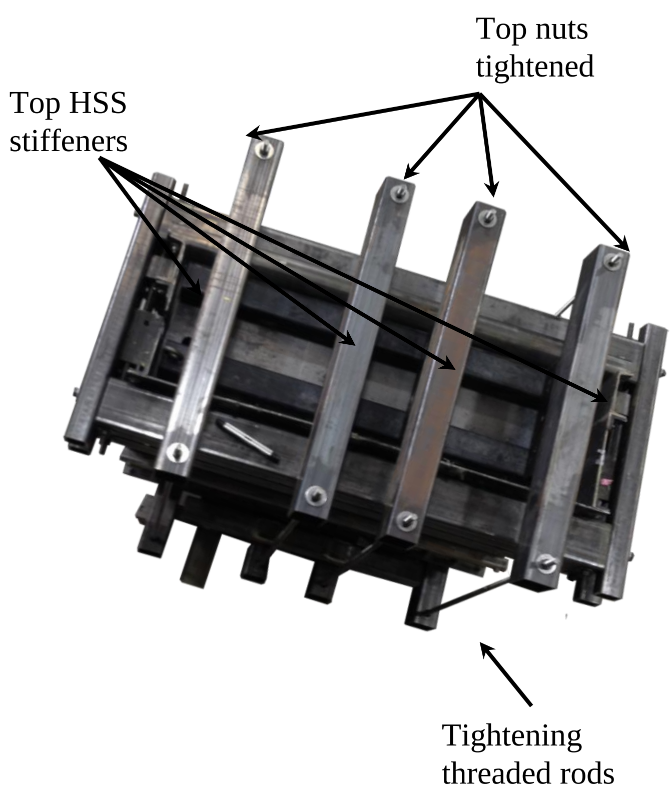

Figure 5.6 Test chamber top view (showing reinforced restraining cover)

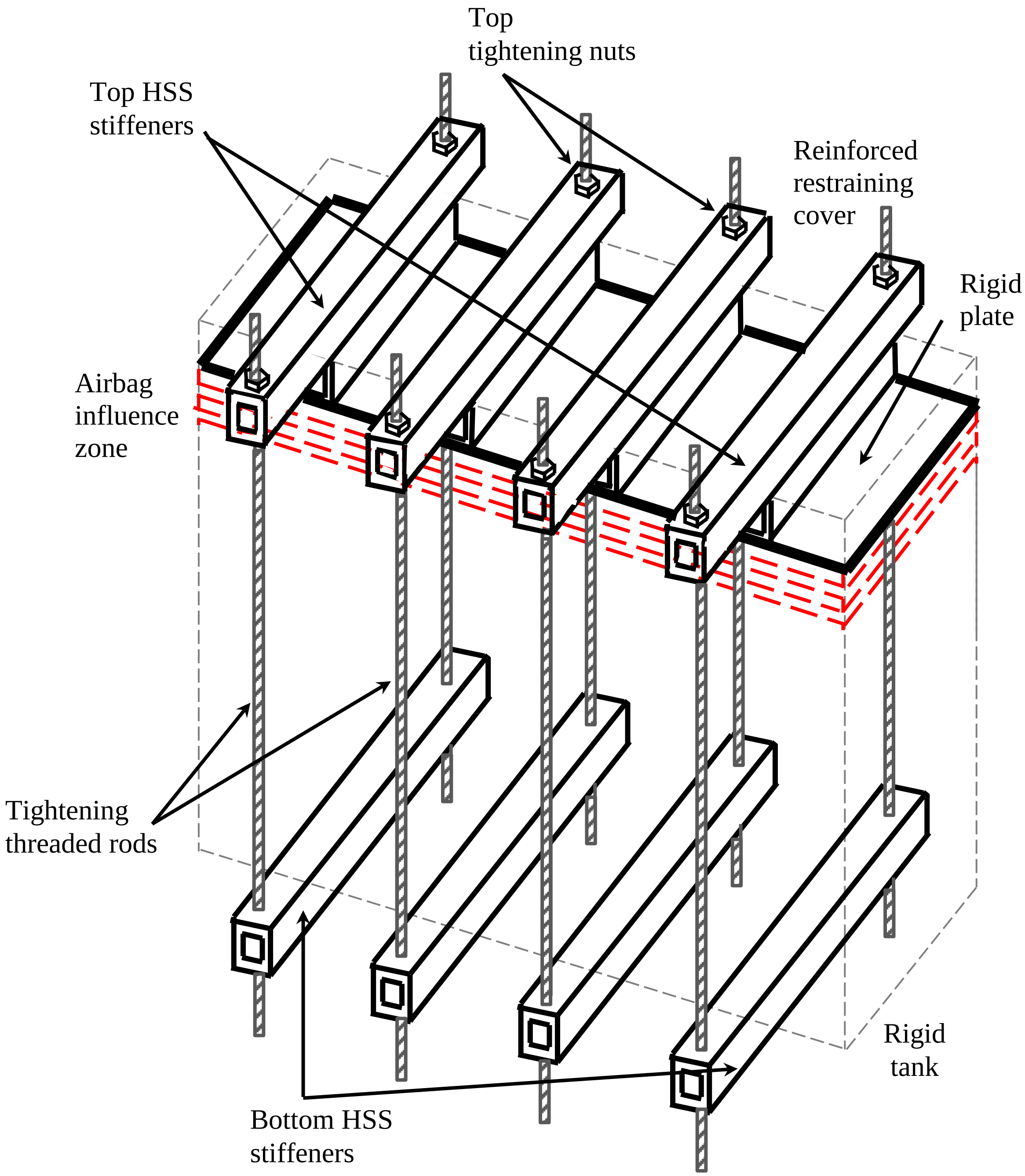

Figure 5.7 Vertical restraining system

Figure 5.8 shows the assembled chamber in its final form after being strengthened to accommodate the expected level of the applied load. Movements of the front and back sides of the chamber are monitored using a multileveled dial gauge station (Figure 5.9). A maximum outward movement of 2 mm at the front side was measured at a maximum applied pressure of 20 psi, therefore, a third HSS beam was added to further reinforce the walls in this area. The movement was monitored again using 6 dial gauges (4 at the front side and two at the back side) showed no deformation at this stage.

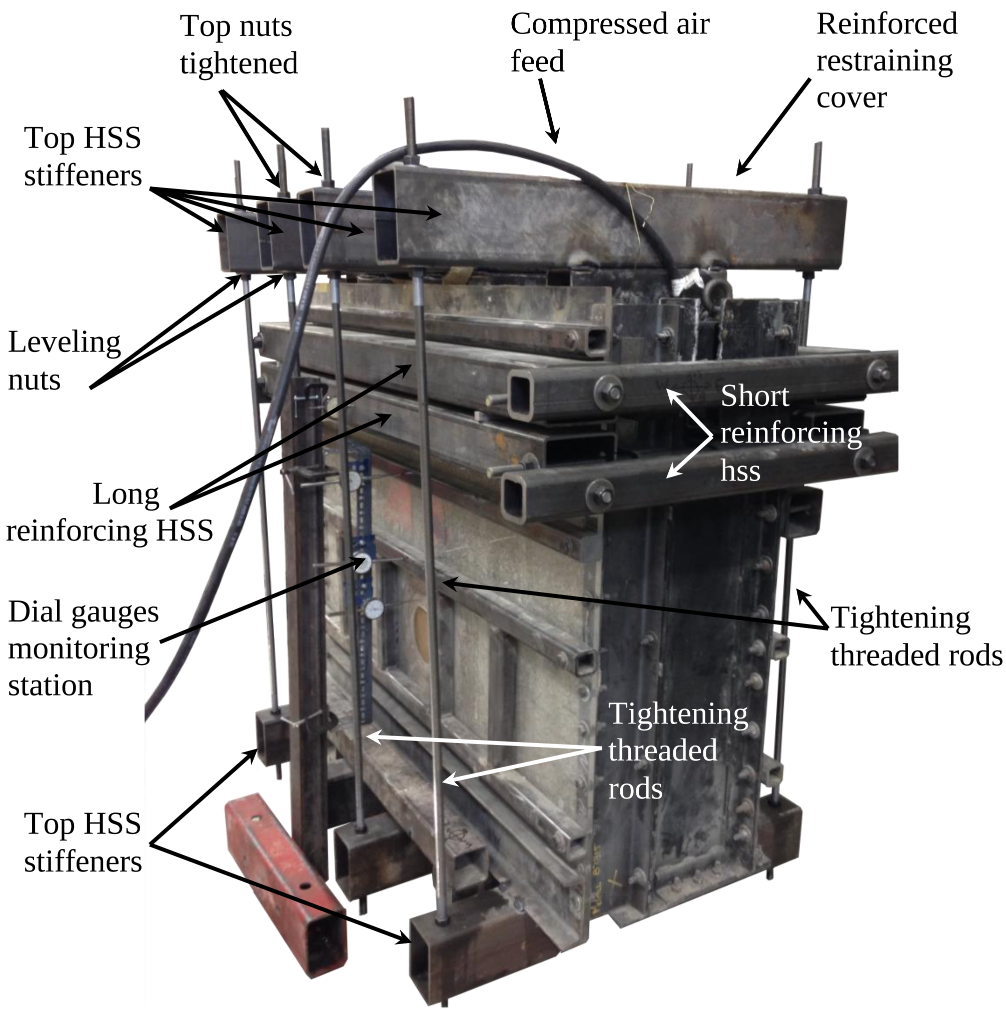

Figure 5.8 Assembled test chamber

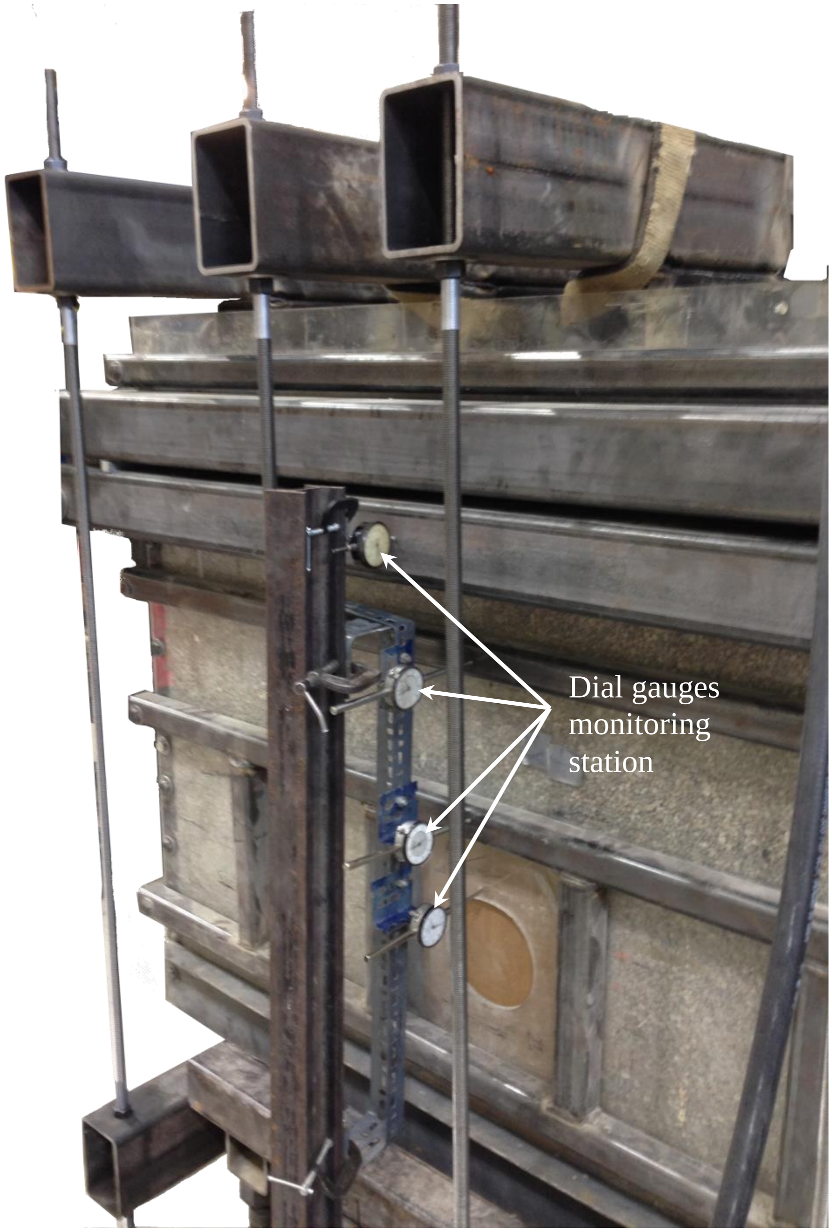

Figure 5.9 Dial Gauges for monitoring bulging during loading

5.4.2 Air pressure system

Figure 5.10 shows the air pressure system that consists of the air bag, air pressure control unit and compressed air feed hose. The airbag can be inflated up to 30 psi (207 kPa) in air before rupture. A thin layer of rubber sheet is placed between the soil and the air bag to prevent puncturing due to the possible presence of gravel particles with sharp edges. The reinforced restraining cover is then placed and fastened as illustrated in Figure 5.8. The hose supplying the air is attached to the airbag valve outside the tank and the air control system is connected to air pressure supply. The loading process begins by applying air pressure in 1 psi (6.9 kPa) increments every minute up to 20 psi (140 kPa). The air pressure system had an emergency button to stop the test in case of airbag failure. The space created for the airbag is smaller than the inflated volume to distribute the air pressure onto the soil surface evenly.

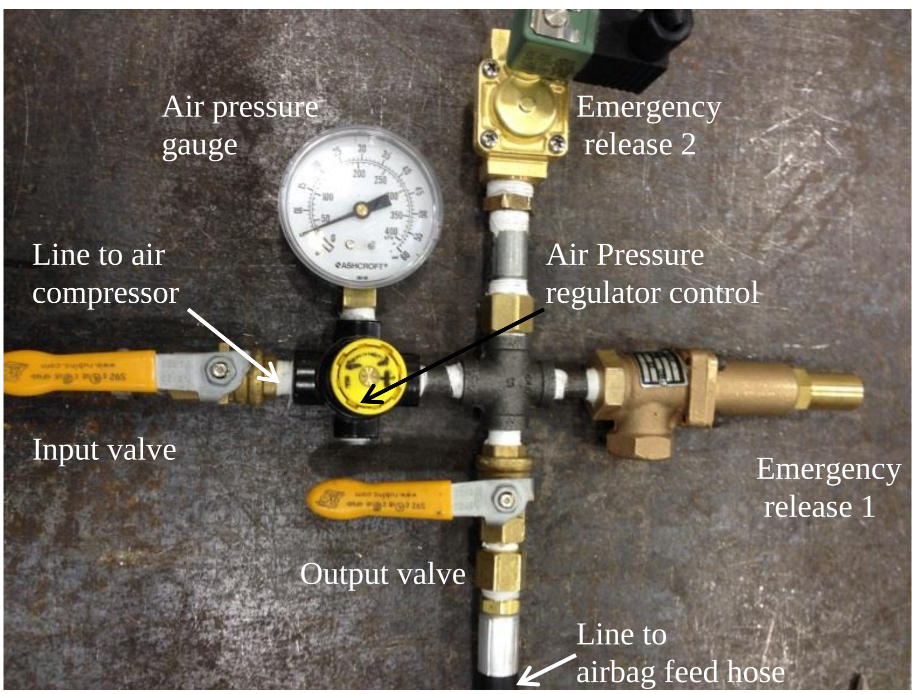

Figure 5.10 Air pressure system

5.4.3 Instrumented buried box

A rigid steel box section with dimensions 0.25 x 0.25 x 0.435 m and 1 cm in wall thickness is used in this study. The top wall is located 0.5 m below the soil surface. It is instrumented using TactArray sensing pads (S1, S2, S4) placed directly on its outer perimeter at the top, side and bottom walls, respectively, as shown in Figure 5.11. Each sensing pad contains 255 square shaped sensors with pressure range from 0 to 140 kPa for the top (S1) and side (S2) pads and from 0 to 350 kPa for the bottom pad (S4). The sensors are protected from backfill abrasion by wrapping the box in a thin layer (1 mm) of rubber overlain by a PVC sheet (Figure 5.12a)

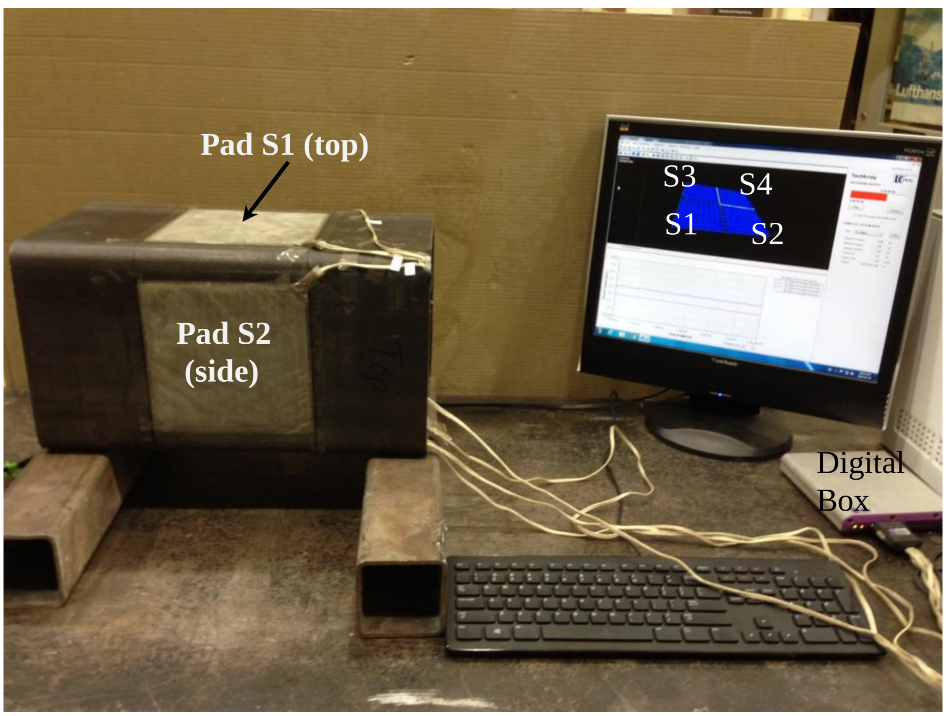

Figure 5.11 Instrumentation of the buried structure

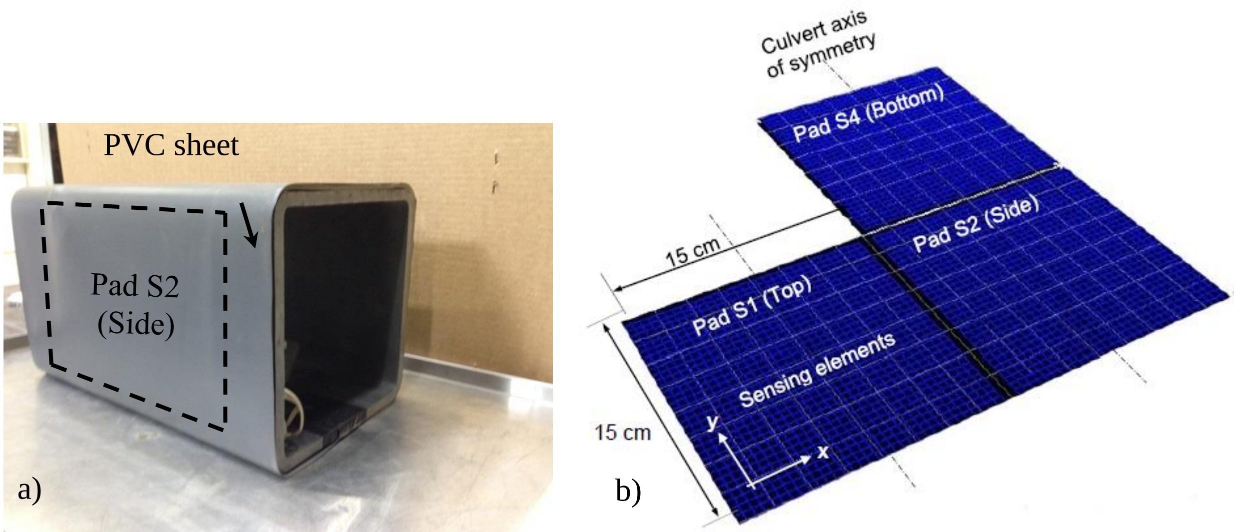

Figure 5.12 (a) instrumented box wrapped in protective layer (b) tactile sensor pads orientation on the box

5.4.4 TactArray sensors

The pressure sensors used for this project consist of three sensing pads (S1, S2 and S4) as shown in Figure 5.12b. When a normal load is applied to the capacitive sensors, it changes the distance between the electrodes resulting in a change in capacitance that is translated into an output signal recorded by the data acquisition system.

In addition to the manufacturer calibration, the reading of the sensing pads are also calibrated before commencing the experiments. Each of the used pads is attached to the upper side of the steel box and a precise amount of soil of known weight is then placed over the pad using a guide tower. Sensor reading is then compared with the applied pressure. Additional weights were added to check the reading at higher pressure. The maximum difference between the applied and recorded readings was found to be less than 10%. Additional details about the sensing pads are provided in section 2.4 of Chapter 2.

5.4.5 Backfill soil

The backfill material used in the previous chapters, dry sandy gravel with average unit weight of 16.28 kN/m^3, is used in this study. The friction angle of the backfill soil determined using direct shear tests is found to be 47^o.

5.4.6 Geofoam

A compressible material is installed either on top (Figure 5.13) or on top and sides (Figure 5.14). The geofoam block is 43 cm in length, 25 in width and 5 cm in thickness. Two types of geofoam are used based on the material density, namely, EPS15 and EPS22. The material properties are provided in Table 5-2.

Table 5-2 Geofoam physical properties

EPS geofoam properties			
EPS material type	density (kg/m^3)	E (MPa)	(ν) Poisson's ratio
EPS-22	21.6	6.91	0.1
EPS-15	14.4	4.20	0.1

5.5 Methodology

A total of 12 experiments are conducted including three benchmark tests with only the instrumented conduit inside the backfill and four pairs of tests with geofoam inclusion as summarized in Table 5-3. In all tests, a tamped zone of 25 cm in height is created as a bedding material at the bottom of the chamber. The instrumented box is then placed over the bedding layer with a thin (1 cm) of sand material to level the gravel surface. This was insured using a water level placed in two directions over the surface of the box.

Table 5-3 Conducted tests

Test No.	**Test Type**
1	Gravel backfill (no EPS)
2	Gravel backfill (no EPS)
3	Gravel backfill (no EPS)
4	EPS22 at the top
5	EPS22 at the top
6	EPS15 at the top
7	EPS15 at the top
8	EPS15 at the top
9	EPS22 at the top and sides
10	EPS22 at the top and sides
11	EPS15 at the top and sides
12	EPS15 at the top and sides

The buried box is connected to the data acquisition system and pressure readings started at this stage. The pressure reading at the lower wall (Pad S4) is checked and compared with the expected weight of the box.

At this stage, a new geofoam block is placed on top of the box either to create the conventional induced trenching arrangement (i.e. on top only, Figure 5.13) or to simulate a second investigated layout where two additional geofoam blocks are placed on the sides of the box (Figure 5.14). The process of filling the test chamber with soil continues until the desired backfill height of 0.5 m is achieved, which is twice the height of the box. The surface pressure is then applied over the backfill to simulate an embankment of height of up to 9 m.

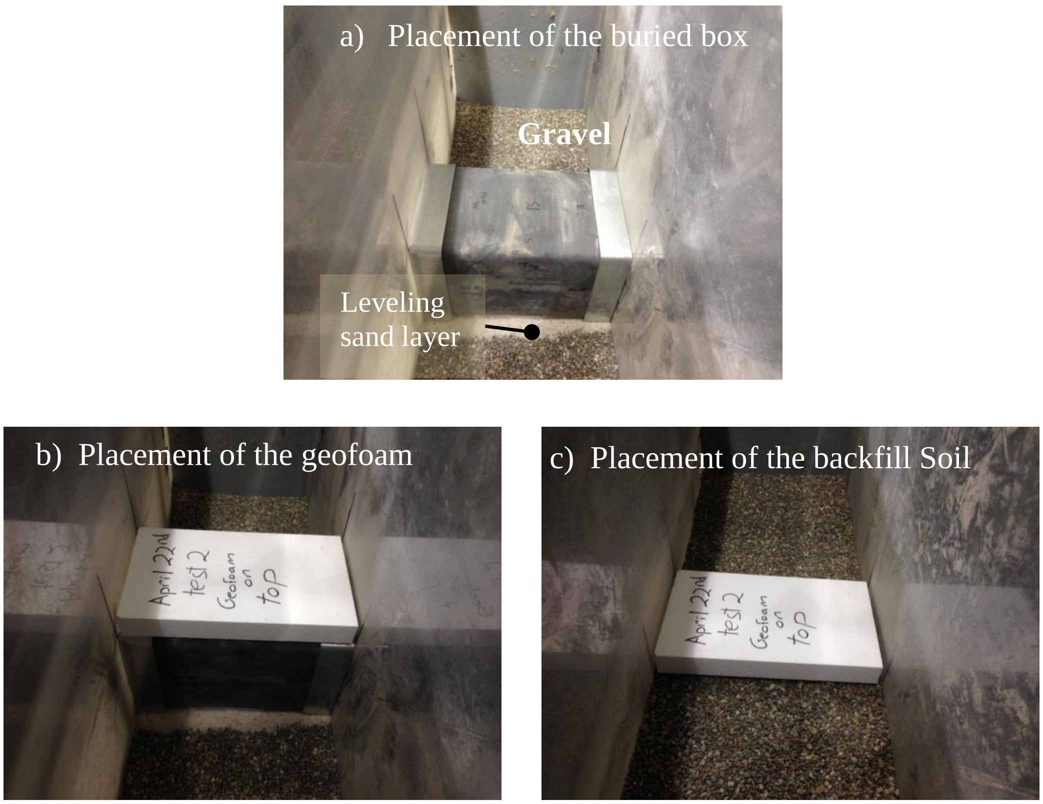

Figure 5.13 The buried box and geofoam installation process layout 1: (a) HSS placed over bedding layer; (b) geofoam layer placed over the HSS; (c) backfill placed

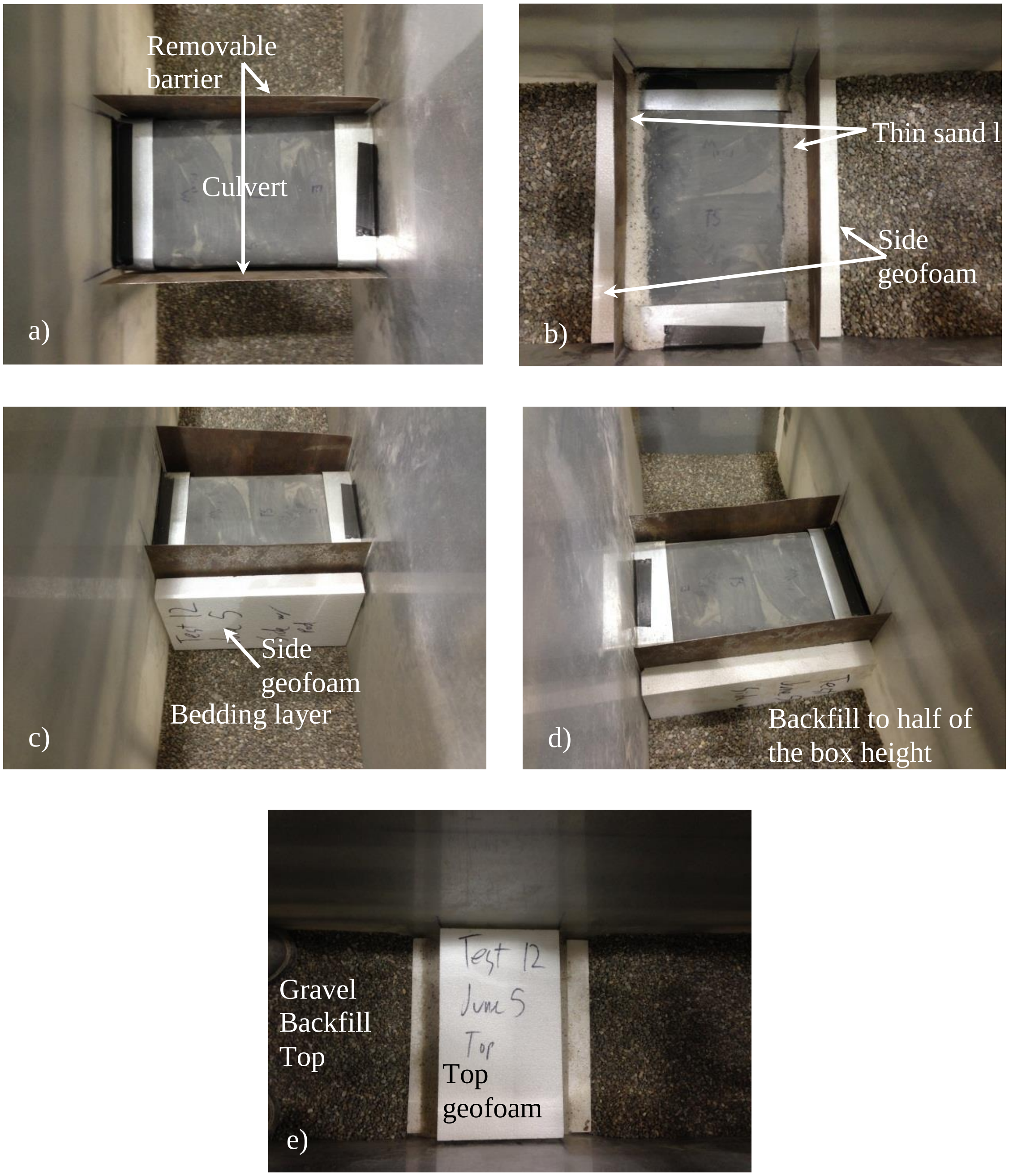

Figure 5.14 and geofoam installation process layout 2: (a) HSS placed over bedding layer; (b) geofoam layer placed on the sides; (c) backfill placed (d) sides covered with backfill (e) top layer of geofoam placed

Following the completion of the backfilling process, the earth pressure on the upper wall of the buried box was recorded. The airbag is then placed and the reaction plate is secured at the desired level at the top of the test chamber. The airbag is incrementally inflated at a rate of 1 psi (7 kPa) per minute. The test would be stopped when either the capacity of the airbag pressure was reached (20 psi) (140 kPa) or the allowable pressures of the sensing pads is exceeded. Figure 5.15 shows the setup as the test is being conducted.

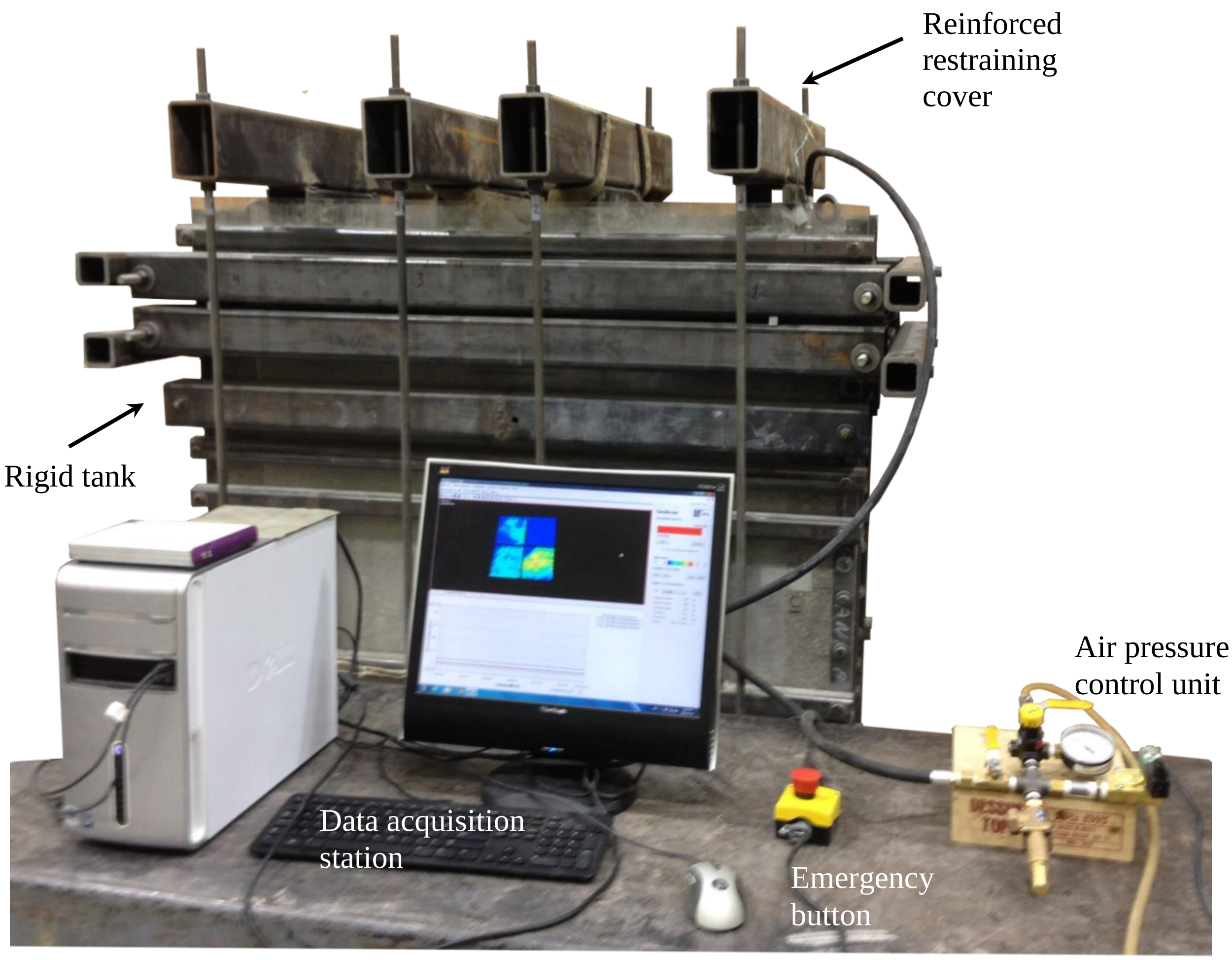

Figure 5.15 The test setup and acqusition system during the experiment

After the completion of each test, the tank is emptied using a vacuum machine connected to a collection barrel. The buried box is then retrieved and the setup is prepared for the next test. Figure 5.16 shows the pressure profile distribution when the box is placed inside the tank resting on the soil bed, thus the pad S4 (bottom slab) is recording mainly the weight of the box itself. At this stage, no pressures were recorded by pad S1 (top slab) and pad S2 (side wall) as they are not loaded. More screen shots of the measured pressure distribution on the walls of the structure as recorded in different tests are provided in Figure 5.17.

It is generally observed that pressure on the side wall is the lowest followed by the upper wall and then the lower wall. Figure 5.17 (a) represents the initial condition for the positive projecting case where soil is placed up to 0.5 m above the box before the airbag is still inflated). The rest of the figures show the contact pressures when the airbag is inflated to a maximum pressure of 20 psi which is equivalent to about 8.5 m of soil or when pad capacity reached.

The measured pressure for the positive projecting case (no geofoam) is shown in Figure 5.17 (b). It is noticed that pad S4 (lower wall) reads more pressure than S1 (upper wall) plus the weight of the buried box itself due to the drag down forces explained before in section 5.2.3. The value of the drag down forces effect will be discussed in a separate section. The pressure measured for the induced trenching method are shown in Figures 5.17(c) through 5.17(f).

Results revealed that placing the less stiff geofoam (Geospec 15) on top only (Figure 5.17c) yielded the best results in terms of pressure reduction. The second layout (top and side geofoam blocks) resulted in a pressure redistribution that led to a reverse action where the contact pressure on top and bottom slabs has increased (Figure 5.17e). It was observed that the side walls in Figures 5.17(e) and 5.17(f) experienced less pressures due to placing geofoam blocks on the sides, however, since the pressures are already low it is not considered effective enough under the investigated loading condition. It is expected that if higher in-situ lateral pressure existed (e.g. moving or creeping soil), this layout may become effective. Additional details are presented in the next sections.

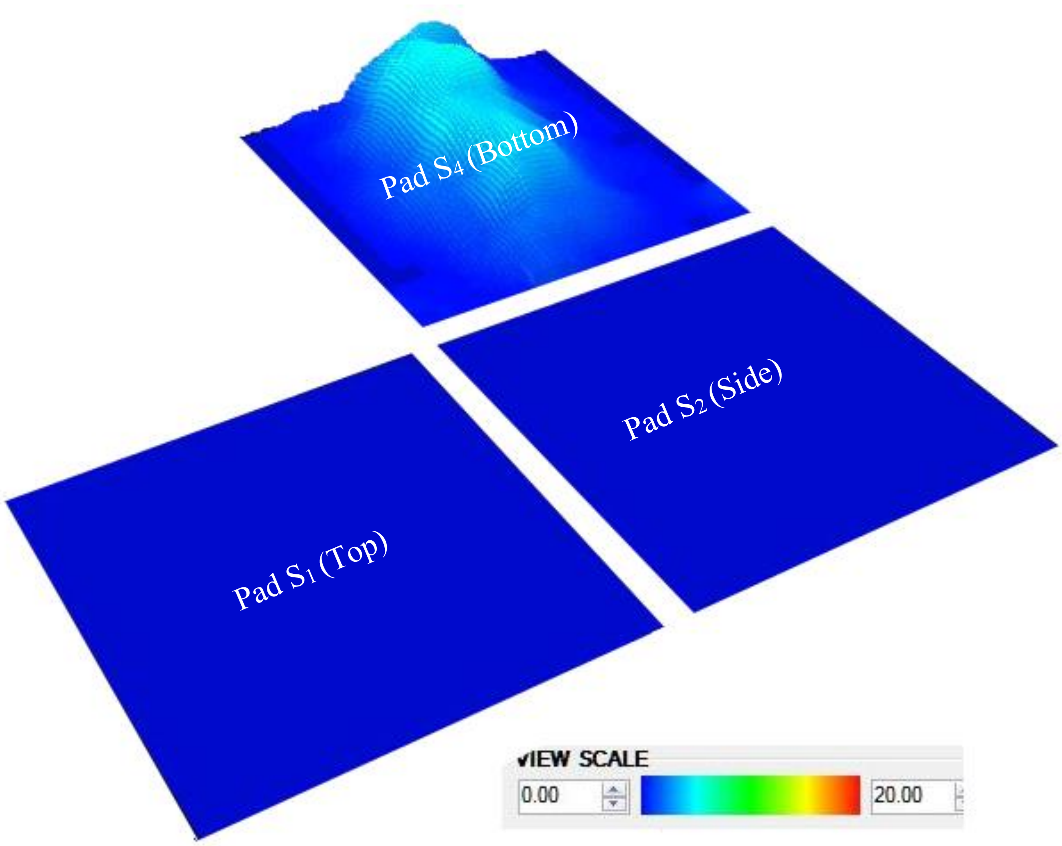

Figu 5.16 Contact pressure when the buried box is placed resting on soil

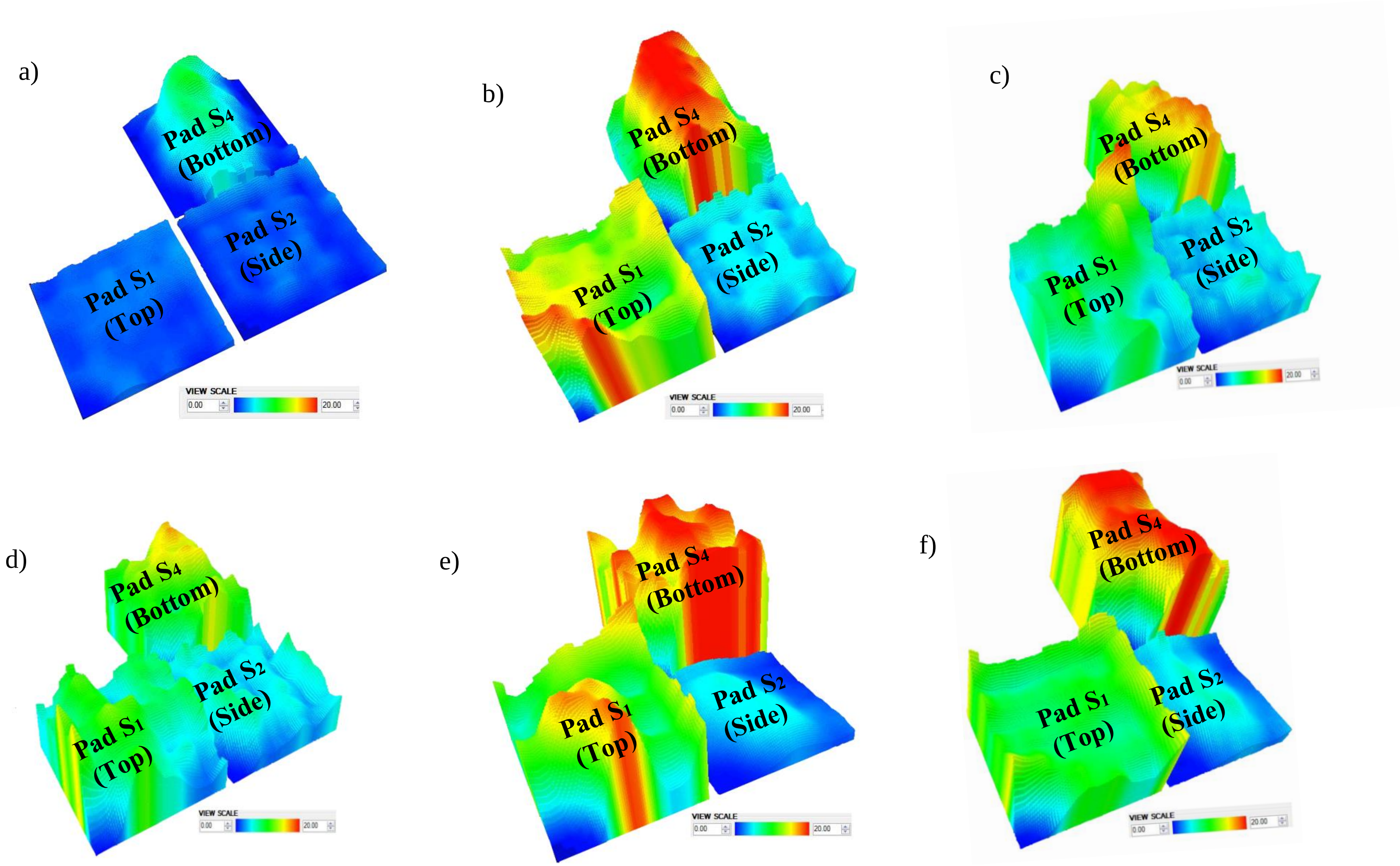

Figure 5.17 (a) initial condition (airbag empty), (b) positive projecting (Test 3), induced trench (c) stiff geofoam on Top (Test 5), (d) soft geofoam on top (Test 6), (e) (stiff geofoam top/sides (Test 10), (f) soft geofoam top/sides (Test 12)

5.6 Measured Earth Pressure Distributions

In this section positive projecting test results (no EPS inclusion) are compared with those of the induced trench installation. This was performed individually for the top, side and bottom of the box by analyzing the data recorded by pads S1, S2 and S4, respectively. The median of the recorded pressure readings as surface pressure increases is calculated at 1 psi (7 kPa) increments up to a maximum surface pressure of 20 psi (about 8.5 m of overburden pressure). Figure 5.18 shows a typical pressure distribution as captured at the upper wall of the box at applied surface pressure of 140 kPa.

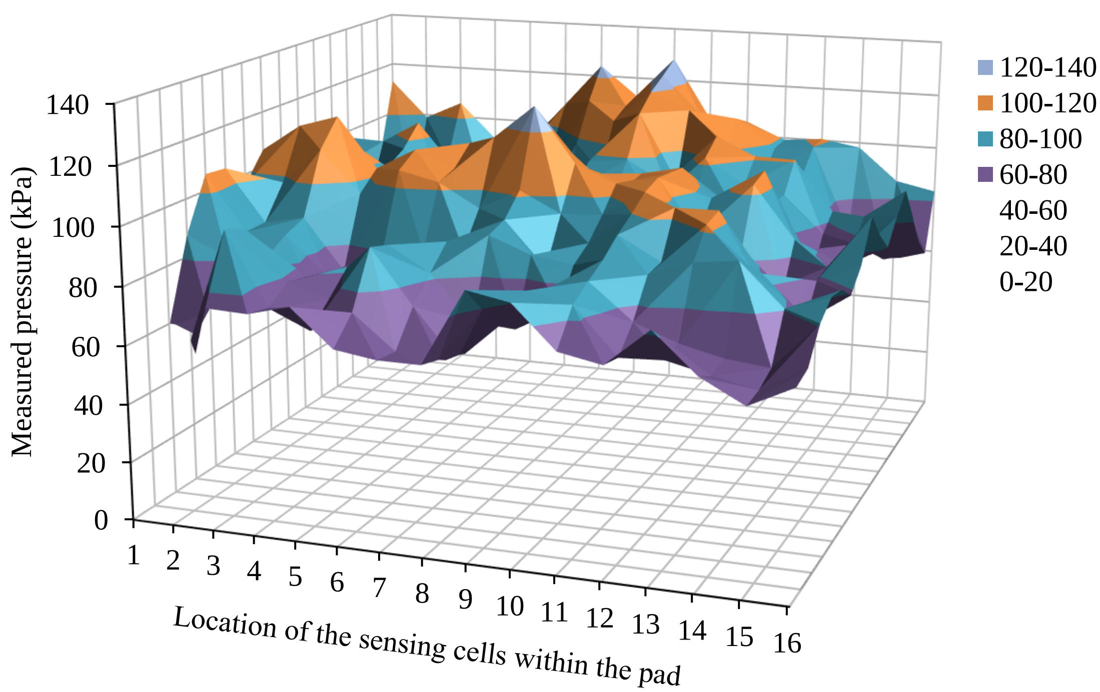

Figure 5.18 Typical pressure readings on the top wall under applied surface pressure of 140 kPa

Five groups of tests were conducted as follows:

- Gravel backfill with no geofoam.
- One EPS22 block placed on the upper wall of the buried box.
- One EPS15 block was placed on the upper wall of the buried structure.
- Three EPS22 blocks placed on the upper wall and against the side walls of the structure.
- Three EPS15 blocks placed on the upper wall and against the side walls of the structure.

The recorded pressure distribution at each load increment is averaged and presented as a point in the charts presented in Figures 5.19 to 5.24. The results for the benchmark tests with no geofoam (dark circles) are also provided for comparison purposes. The contact pressure generally increased with the increase in surface pressure. At an applied pressure of about 140 kPa (20 psi), the average readings at the upper, lower and side walls are 155, 170 and 68 kPa, respectively. The effects of placing two different geofoam materials (EPS-15 and EPS-22) above the buried structure are evaluated at the three locations (Figures 5.19, 5.21 and 5.23). Results showed that contact pressure significantly decreased from 155 kPa (no EPS case) to 60 kPa at the upper wall and from 170 kPa to 85 kPa at the lower wall when EPS-22 was introduced. This represents a reduction of about 61% and 50% for the upper and lower walls, respectively. Replacing EPS-22 with EPS-15 led to further reduction in contact pressure to 46 kPa at the upper wall and 78 kPa on the lower wall. Pressure on the side walls also decreased from 68 kPa (no EPS) to 56 kPa (EPS-22) and 45 kPa (EPS-15) representing a reduction of 17% and 33%, respectively.

Figures 5.20, 5.22 and 5.24 show the changes in contact pressure due to the placement of EPS blocks on top and next to the side walls under the same loading conditions. The changes were found to be relatively smaller compared to the case where the EPS blocks are placed only above the buried structure. The presence of EPS-22 resulted in a pressure reduction from 155 kPa at the upper wall and 170 kPa at the lower wall to 80 kPa (48%) and 150 kPa (12%), respectively. Further reduction in contact pressure was found for the case of EPS-15 with measured pressure values of 50 kPa (67%) and 111 kPa (35%) at the upper and lower walls, respectively.

The presence of the EPS geofoam blocks against the side walls was found to have a significant effect on the pressures transferred to the side walls as illustrated in Figure 5.24. The lateral pressure decreased from 68 kPa to about 18 kPa for both types of EPS materials resulting in a reduction of about 74%.

5.6.1 Upper Slab

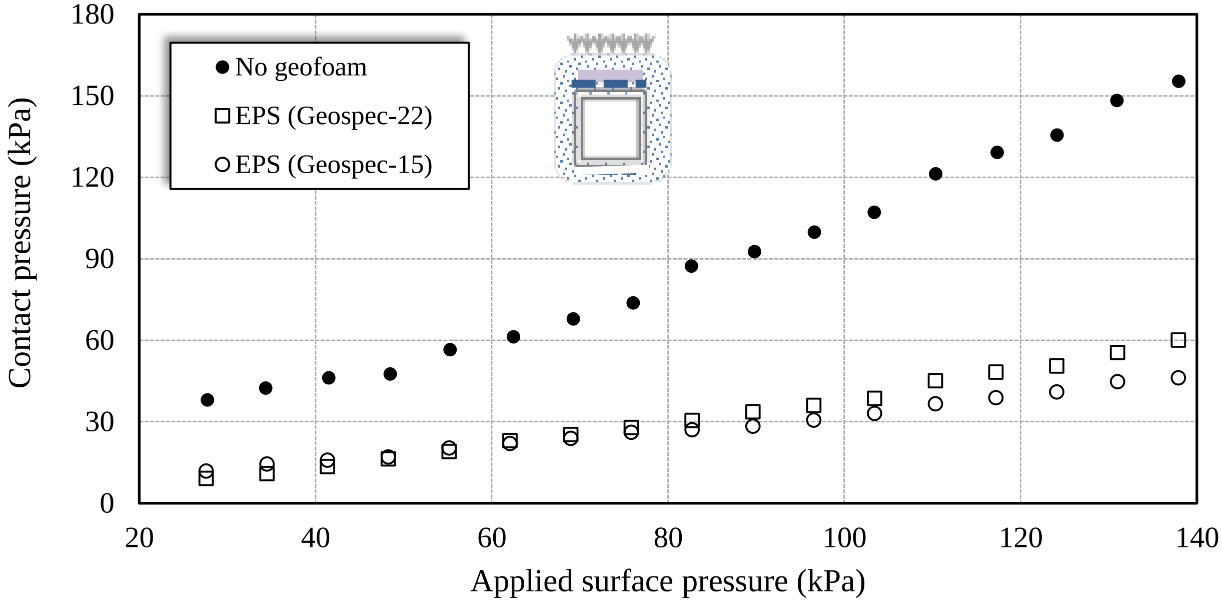

Figure 5.19 Average contact pressure on the upper wall (EPS on top only)

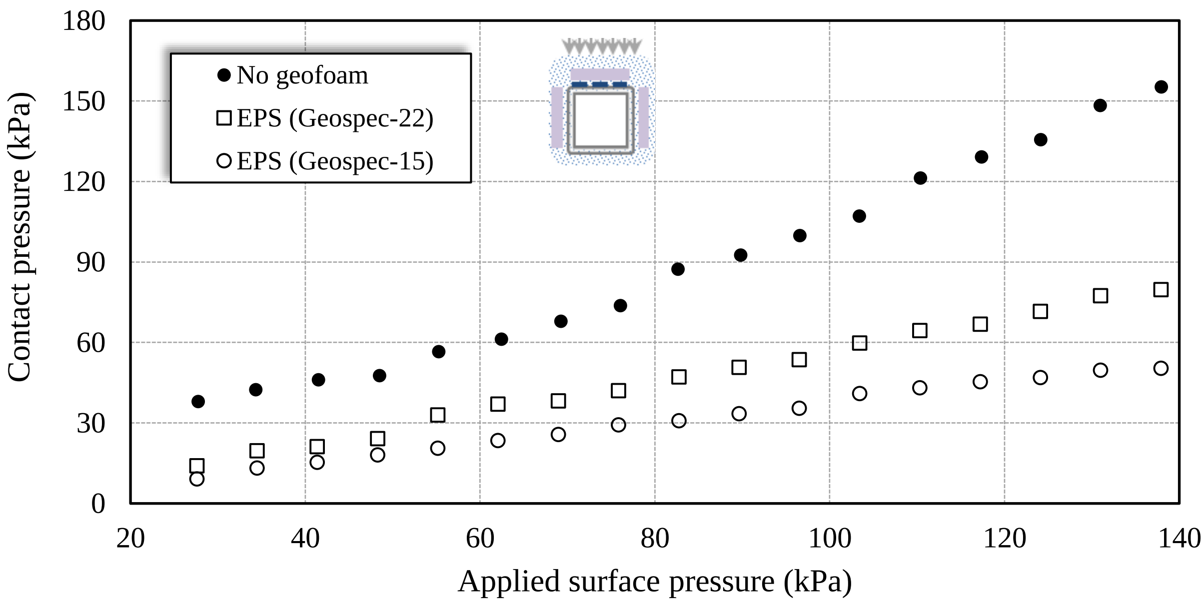

Figure 5.20 Average contact pressure on the upper wall (EPS on top and side walls)

5.6.2 Lower Slab

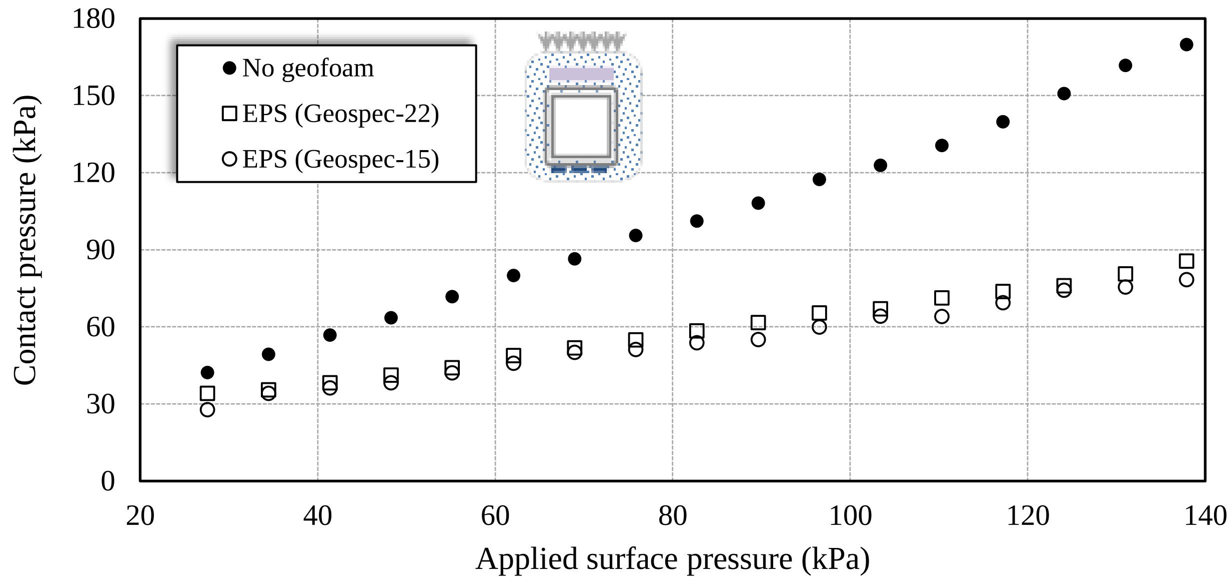

Figure 5.21 Average contact pressure on the lower wall (EPS on top only)

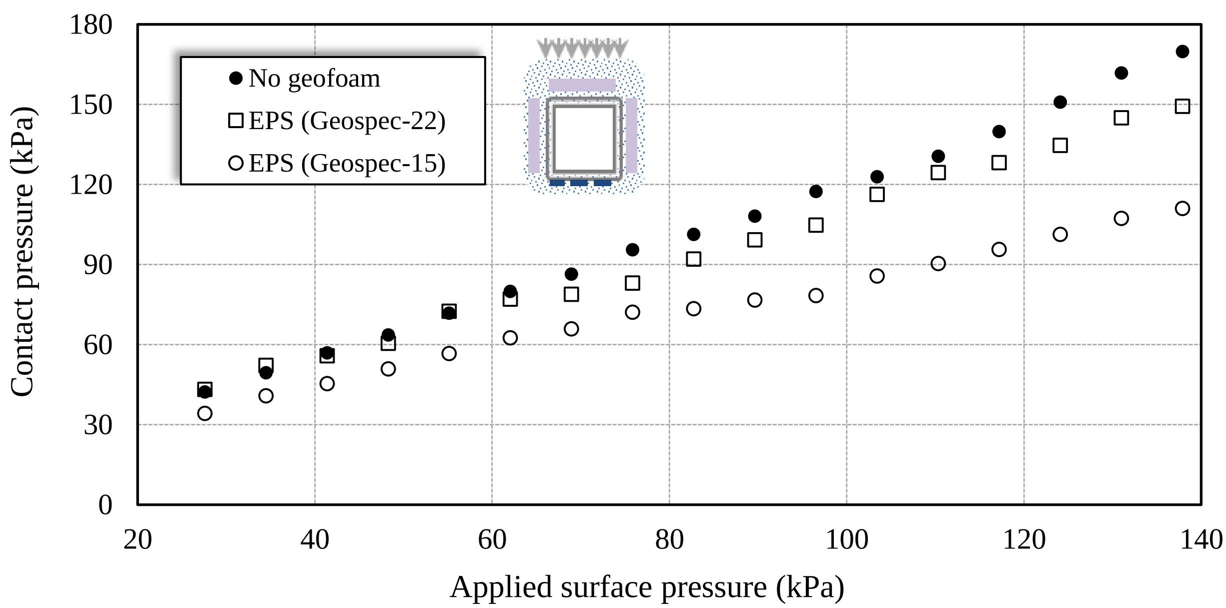

Figure 5.22 Average contact pressure on the lower wall (EPS on top and side walls)

5.6.3 Side Slab

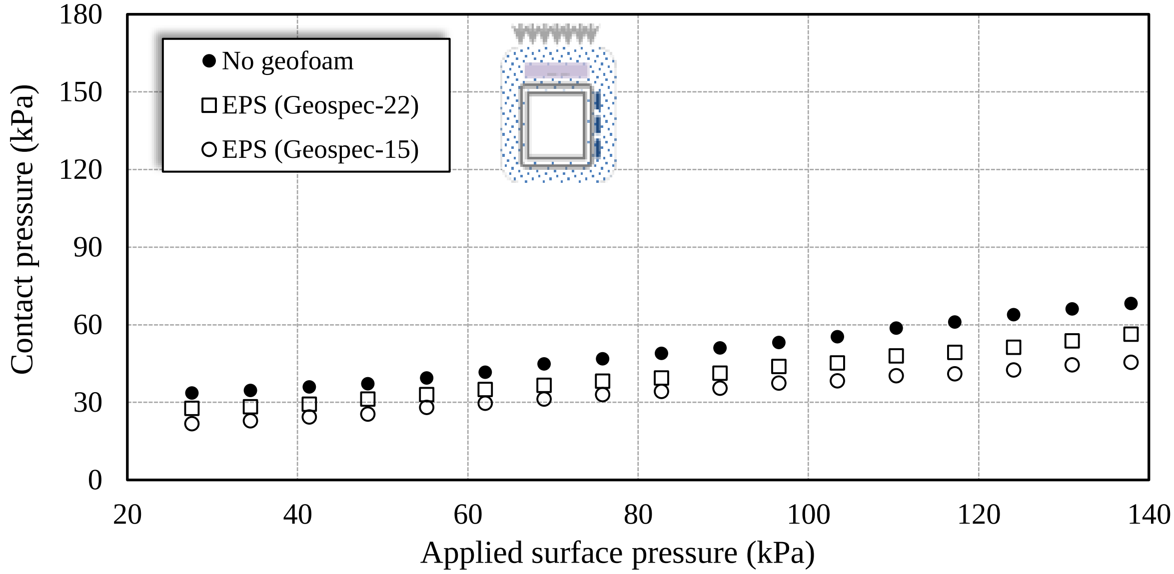

Figure 5.23 Average contact pressure on the side wall (EPS on top only)

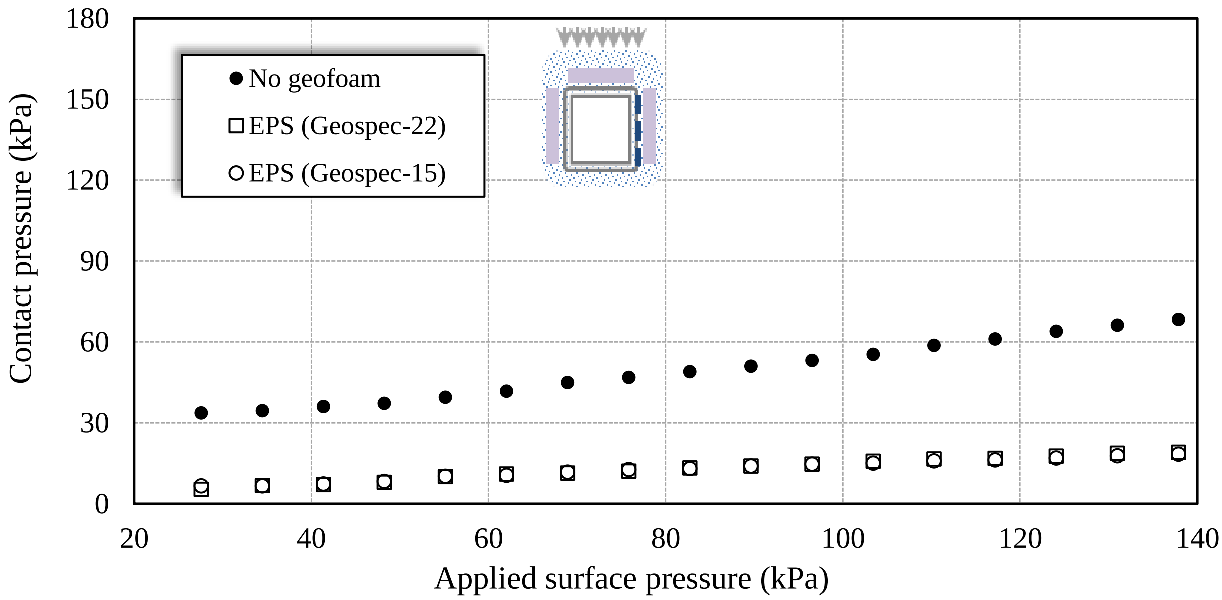

Figure 5.24 Average contact pressure on the side wall (EPS on top and side walls)

Table 5-4 summarizes the reduction amounts obtained with respect to the benchmark tests for the top and bottom slabs. It should be noted that for design purposes, the strains in the geofoam are usually specified to not exceed 1%. This means that although EPS-15 tends to provide better performance over EPS-22, the maximum surface pressure that could be carried by EPS-15 geofoam block may be limited by the strains developing in the material.

Table 5-4 Pressure changes recorded for different EPS arrangements around the structure

	EPS-22 (on top wall)	EPS-15 (on top wall)	EPS-22 (on top and side walls)	EPS-15 (on top and side walls)
Upper wall	61%	70%	48%	68%
Lower wall	50%	54%	12%	35%
Side wall	17%	34%	74%	74%

5.7 Drag down forces

The drag down forces as explained in section 5.2.3 represent the added contact pressure at the bottom slab due to the development of shear stresses along the side walls of the buried box. It is usually augmented when induced trench technique is used. The contribution of the drag down forces to the contact pressures under the buried box was estimated by comparing the measured pressures on the upper wall (adding the weight of buried box ≅ 340 N or 3 kPa) with the contact pressure measured on the lower wall. The difference between the upper and lower wall readings for the benchmark case (no geofoam) was found to be 15 kPa which corresponds to an increase in pressure of 12 kPa (about 9%) on the lower wall as a result of the drag down forces. For the induced trench condition with one block of geofoam above the box, the pressure change was found to be 22 kPa that corresponds to a pressure increase of about 30% for both EPS-15 and EPS-22. For the cases where the EPS blocks are placed over and around the structure, the change in pressure represents an increase of 45% for EPS-22 and 52% for EPS-15 due to the drag down forces.

5.8 Comparison with ACPA code and Marston/Spangler design theory:

In this section a comparison between the results of the experimental study, the Marston-Spangler theory and the ACPA code is conducted. The purpose of this comparison is to evaluate the applicability of the two theoretical methods in estimating the earth load on buried structures installed using different methods. The equations used for the calculations are provided first in the next section followed by the calculated results plotted and analysis of the results.

5.8.1 ACPA 2011 equations

Positive projecting

$$w = VAF \times PL \tag{5.1}$$

$$PL = \gamma_s \left[H + \frac{D_\circ \ (4-\pi)}{8}\right] D_\circ \tag{5.2}$$

where:

Υ_s = soil unit weight, (lbs/ft^3)

H = height of fill, (ft)

D_o = outside diameter, (ft)

Trench installation

$$w = (C_d \gamma_s B_d^2) + \left(\frac{D^2(4-\pi)}{8} \gamma_s\right) \tag{5.3}$$

$$c_d = \frac{1-e^{-2k\mu\frac{H}{B}}}{2k\mu} \tag{5.4}$$

where:

B_d = width of trench, (ft)

K = ratio of active lateral unit pressure to vertical unit pressure

μ' = tan ø', coefficient of friction between fill material and sides of trench

$K_{\mu'}$ = .165 Max for sand and gravel

5.8.2 Marston/Spangler equations

Positive projecting

$$w = (C_c \gamma_s B_d^2) \tag{5.5}$$

$$c_c = \frac{e^{2k\mu\frac{H_e}{B}}-1}{2k\mu} + \left[\left(\frac{H}{B} - \frac{H_e}{B}\right) e^{2k\mu\frac{H_e}{B}}\right] \quad \text{wherer } H > H_e \tag{5.6}$$

Where H_e is the height of plane of equal settlement. H_e depends on two variables: the settlement ratio and projection ratio. Calculating these two variables is a challenging process as specific distances need to be measured inside the backfill material. For the experimental work in this study, H_e was predefined by the soil height above the buried structure which is equal to 0.5 m.

Trench installation

$$w = \left(C_d \gamma_s {B_d}^2\right) \tag{5.7}$$

$$c_d = \frac{1-e^{-2k\mu\frac{H}{B}}}{2k\mu} \tag{5.8}$$

Induced Trench

$$w = \left(C_n \gamma_s {B_d}^2\right) \tag{5.9}$$

$$c_n = \frac{e^{-2k\mu\frac{H_e}{B_d}-1}}{-2k\mu} + \left[\left(\frac{H}{B_d} - \frac{H_e}{B_d}\right) e^{-2k\mu\frac{H_e}{B_d}}\right] \text{wherer } H > H_e \tag{5.10}$$

Figure 5.25 shows a summary of the measured and calculated results normalized with respect to the pressure of the positive projecting case (embankment technique). The Figure shows that the positive projecting method, with no compressible inclusion, results in a contact pressure that is 25% more than the overburden pressure of the soil at a given depth. As discussed in Chapter 4, this is attributed to the presence of the buried structure that is stiffer than the soil medium resulting in negative arching.

It can be seen also that there is an agreement between the Marston's theory and the ACPA 2011 code for the case of trench installation. For induced trench technique there are 3 data series, two from the experimental work conducted (EPS-22 and EPS-15) and one theoretical line (Marston Induced Trench).

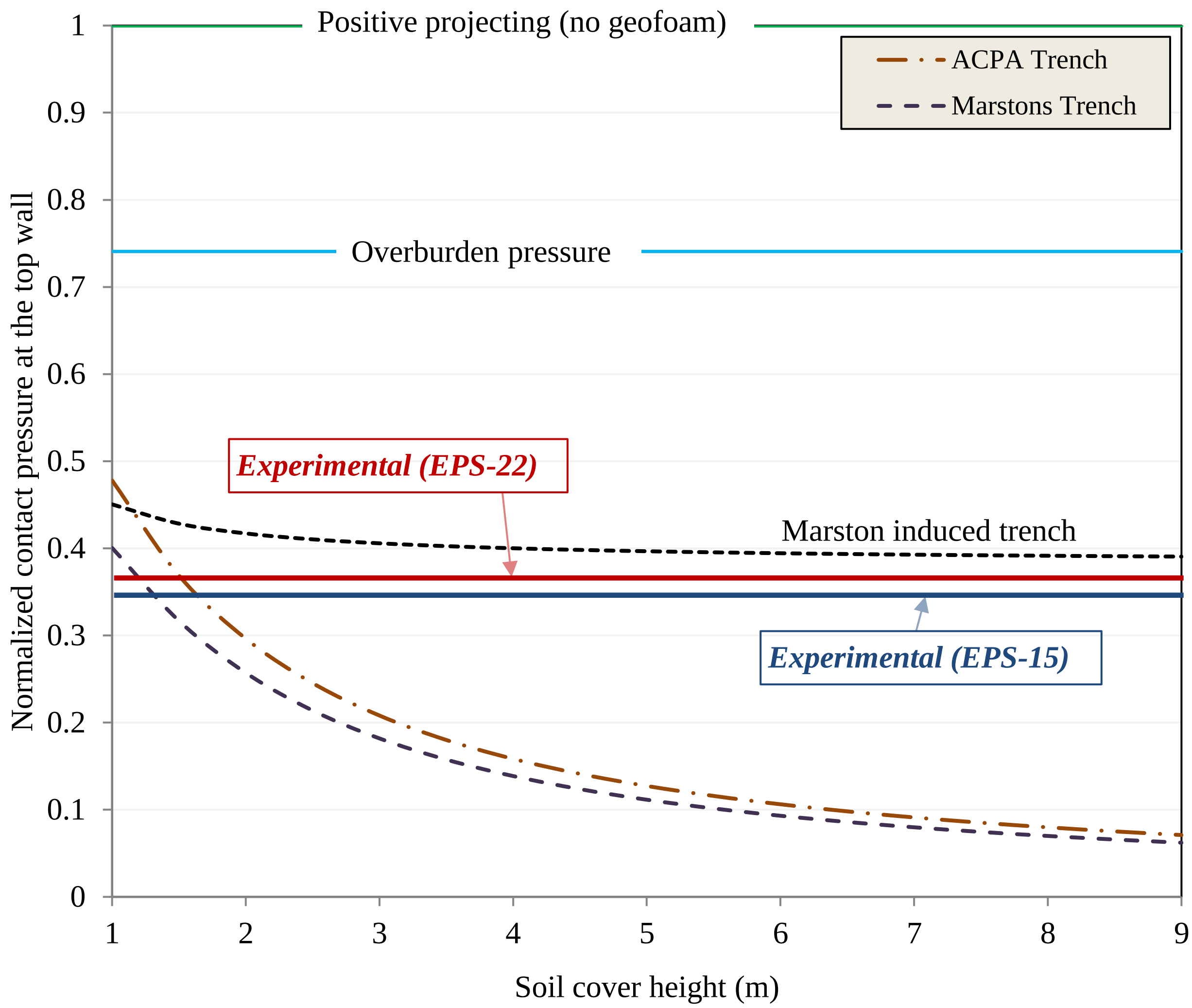

Figure 5.25 Comparison of normalized contact pressures using different methods

5.8.3 Observations

When comparing the above results several observations can be extracted.

- Marston induced trench method predicted a pressure ratio of about 0.4 or 40% of the earth load on the buried structure if no compressible material was used (positive projecting).
- The experimental results showed a pressure reduction that ranged from 0.38 for EPS-22 to 0.35 for EPS-15 as compared with the positive projecting method.

5.9 Summary and Conclusions

In this study, the induced trench installation method for a square-shaped box was modelled experimentally and earth pressures are compared with the positive projecting technique. The effect of two parameters was investigated: (1) the density of the compressible material (EPS-22 and EPS-15); (2) the layout of the EPS around the buried structure (top wall only and top and side walls). Three surfaces of the box (upper, side, and lower) were instrumented with the tactile pressure sensors. Three benchmark tests without EPS geofoam and two sets of tests for each installation layout combination were performed in the study.

The height of the embankment was simulated in the experiments by applying a uniform pressure on the surface of the soil using airbag restrained by a strong reaction frame in both the vertical and lateral directions. The experimental results showed that contact pressure acting on the upper wall of the buried box was reduced by up to 70% when EPS-15 geofoam was placed immediately above the box.

Based on the comparison between the experiments conducted and two theoretical solutions, the following is concluded:

1. Marston-Spangler theory predicts reasonably earth load on buried structures installed using trench method. Using induced trench installation results in less pressure reduction (depending on the density of the EPS material) as compared to the positive projecting method.
2. The ACPA 2011 equations calculated pressure results that are consistent with Marston's theory for buried structures installed using trench technique.
3. Using EPS 22 above the buried box resulted in a pressure reduction of 61% whereas installing EPS 15 resulted in a pressure reduction of about 70% as compared to the positive projecting method.

Overall, the results of this study demonstrate that induced trench technique for box-shaped structures reduces the contact pressures on the upper wall of the box which is in contrast with the response of positive projecting technique that usually results in an increase in earth pressure that exceeds the overburden values. It was noticed that for layout 1 (geofoam at the top of the structure), a reduction in earth pressures that ranged from 17% to 70% of the positive projecting pressure is measured. Placing additional geofoam blocks at the sides of the box was found to significantly decrease lateral pressure on the sides of the box.

These results suggest that using the classical induced trench technique with EPS geofoam placed immediately above the structure is effective in reducing earth loads on the buried structure. It is also important to highlight that the pressure reduction is smaller for the lower wall due to the drag down effect which is magnified for induced trench installations.

Chapter 6

Conclusions and Recommendations

6.1 Summary and Conclusions

The objective of the research reported in this thesis is to evaluate experimentally the earth load on buried conduits overlain by geosynthetic materials (geogrid or geofoam). Contact pressure on the walls of the structure was recorded for each case. The outcome of this study for the cylindrical as well as the square shaped conduits are summarized below.

6.1.1 Effect of geogrid reinforcement on cylindrical conduits:

A two-dimensional setup was designed and built to host an instrumented cylindrical conduit of 0.15 m diameter and backfill material. A total of four tests were conducted to study the effect of introducing a single geogrid reinforcement layer on the contact pressure acting on the pipe that is subjected to a strip load applied at the surface. The surface pressure was incrementally increased from 0 kPa to 250 kPa which caused a surface settlement under the loaded area of 10 mm and 6.4 mm for the unreinforced and reinforced soil respectively. The results showed that radial pressure acting on the pipe generally increased with the increase in applied footing load.

A reduction of 25% in contact pressure was measured at the crown after the installation of the geogrid reinforcement. At the upper haunch, however, the reduction in pressure was found to be approximately 13%.

6.1.2 Effect of EPS geofoam on cylindrical conduits:

To study the effect of using induced trench in shallow pipes under monotonic and cyclic loading, a series of 4 tests was conducted and the changes in contact pressure were recorded during the loading and unloading processes. The reduction in earth pressure was found to be maximum at the crown where the pressure decreased to only 10% of that measured in the benchmark test (90% pressure reduction).

This pressure reduction at the crown corresponded to an increase in pressure at the upper haunch by about 67% this is attributed to soil arching developed above the pipe resulting pressure redistribution increasing the load at the location between 30 and 40. A summary of the change in contact pressure is given in Table 6-1. Cyclic loading was also applied to investigate the change in load reduction on the pipe wall under repeated surface loading. It was found that the presence of geofoam block above the pipe provided consistent reduction in pressure under the imposed cyclic loading.

Table 6-1 Measured pressure changes after geofoam installation

Location	% Change in radial pressure
CR (0^o)	-90%
UH (45^o)	+67%
SL (90^o)	-35%
LH (135^o)	-24%
IN (180^o)	+15%

6.1.3 Effect of EPS geofoam on square-shaped conduits:

An experimental study was conducted to evaluate the role of installing EPS geofoam on the earth load acting on the walls of buried box section. A total of 12 tests were conducted in this section and the results are compared with ACPA design code and Marston-Spangler theory.

It was found that geofoam inclusion caused a reduction when placed above the box due to the resulting induced trenching mechanism developed. A reduction in pressure ranged from 17% on the side wall to 70% on the upper wall was measured depending on the EPS density.

Drag down forces on the side wall of square-shaped conduits

The contribution of the drag down forces to the contact pressures under the buried box, based on this study, was found to be about 9% for the case of gravel backfill only (with no geofoam). For the induced trench cases drag down forces for layout 1 represent about 30% for EPS 22 and EPS 15 (i.e placed above the box). For layout 2, the increase was found to be 45% and 52% for the EPS22 and EPS15, respectively.

Comparison with design equations

The comparison between the ACPA design code equations and Marston-Spangler theory and the experimental results concluded the following:

1. The Marston-Spangler theory reasonably predicts contact pressure on the buried structure compared with that measured in the experiments.
2. The ACPA 2011 equations provide similar results to those obtained using Marston's theory for buried structures constructed using the trench technique.

6.2 Limitations and Future Recommendations;

The work presented throughout this thesis relied on laboratory scale tests of buried conduits conducted under 1g conditions. The physical models could be considered to be either full scale representation of small diameter pipes or reduced scale tests for pipes of larger diameter. The effects of instrumentation and protection layers placed around the small diameter pipe can be reduced when pipes are tested with protection layers that do not promote any significant compression. It is, therefore, recommended that full scale or field tests be conducted to confirm the results obtained in this study.

The test chamber has been designed to represent two-dimensional loading condition over a long buried pipe. Although boundary conditions have been carefully treated in designing the test setup, extending the dimensions of the chamber and increasing the distance between the pipe wall and rigid boundaries is recommended to eliminate any boundary effects that could develop during the test.

As the work presented here focuses more on experimental and analytical investigations, numerical modeling that allows for the effect of different geometric and material parameters (e.g. pipe diameter, geogrid stiffness, EPS thickness, location with respect to the conduit, and backfill properties) is highly recommended. This analysis need to capture the 3D behavior of the biaxial geogrid and the nonlinear compressive strength of the geofoam material.

Appendix

Time loading History for experiments on circular pipes with and without geofoam (positive projecting versus induced trenching)

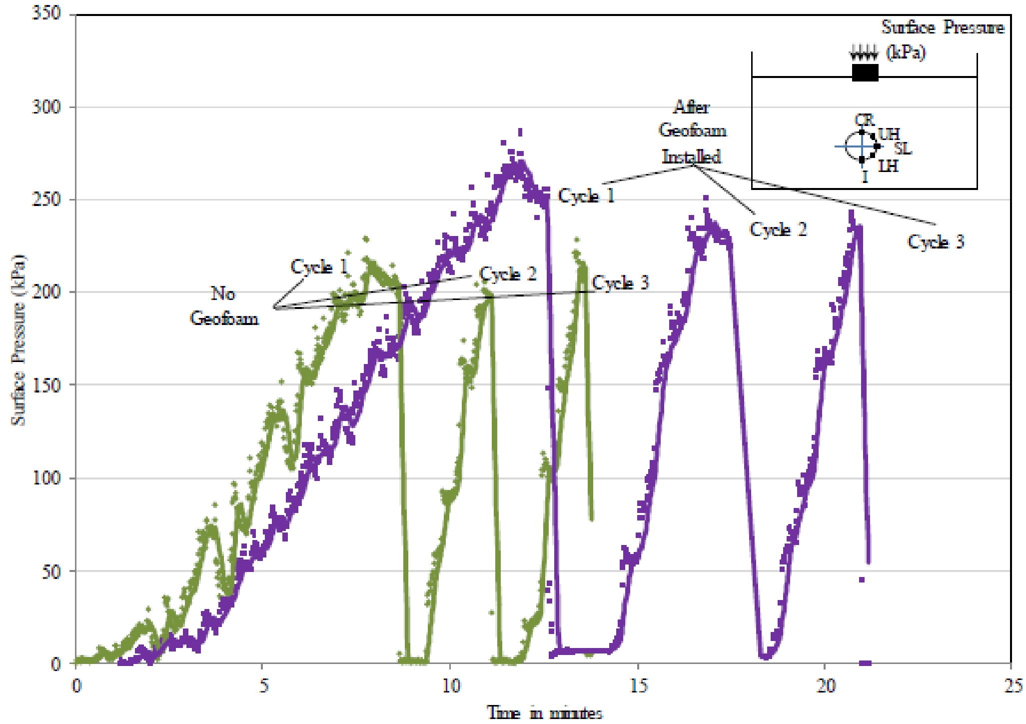

Figure A - 1

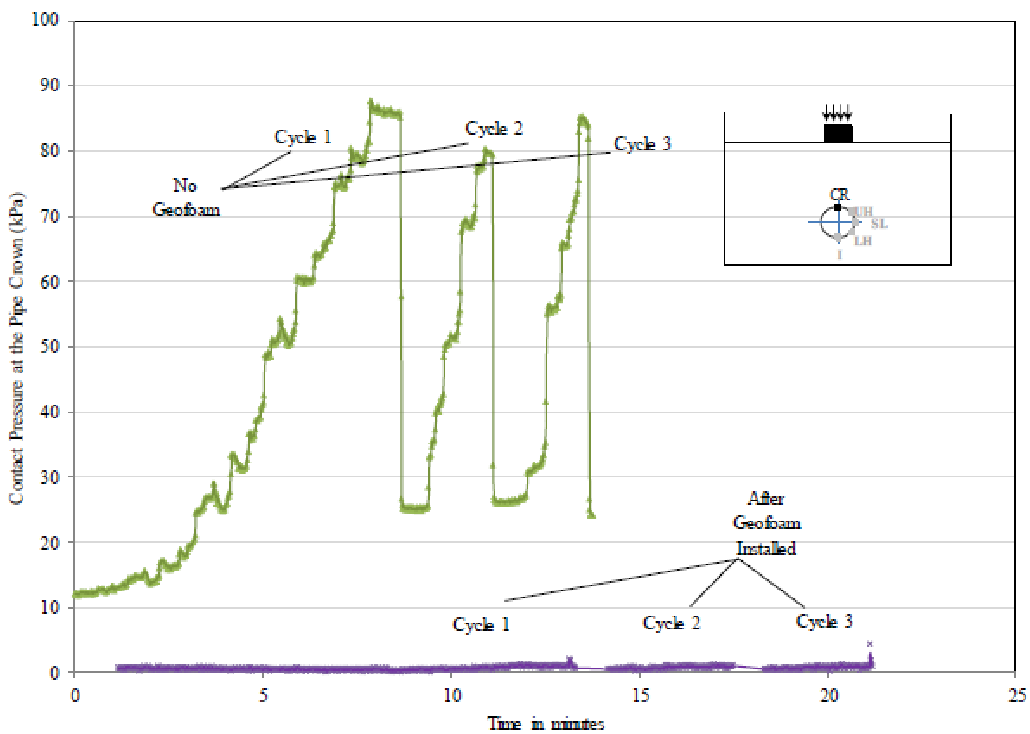

Figure A - 2

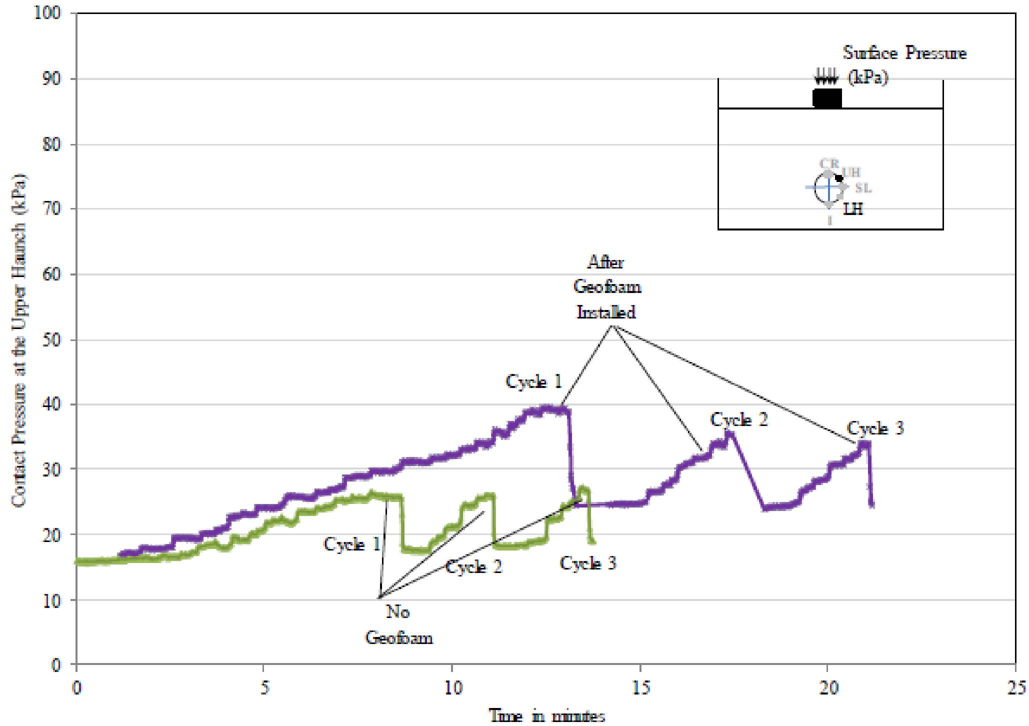

Figure A - 3

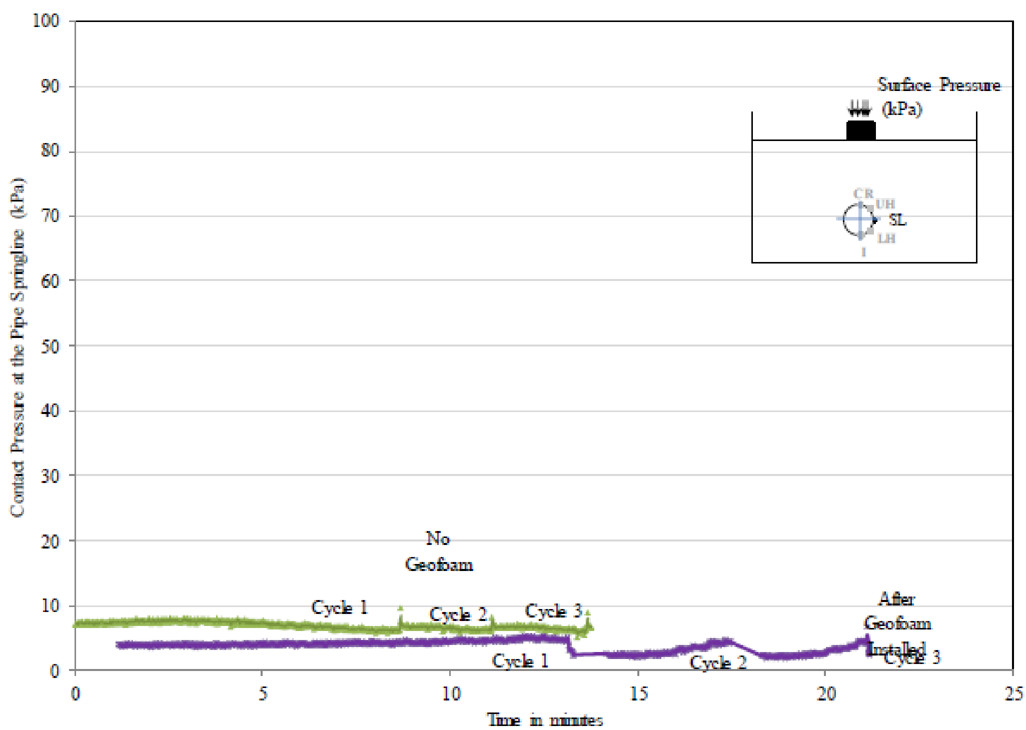

Figure A - 4

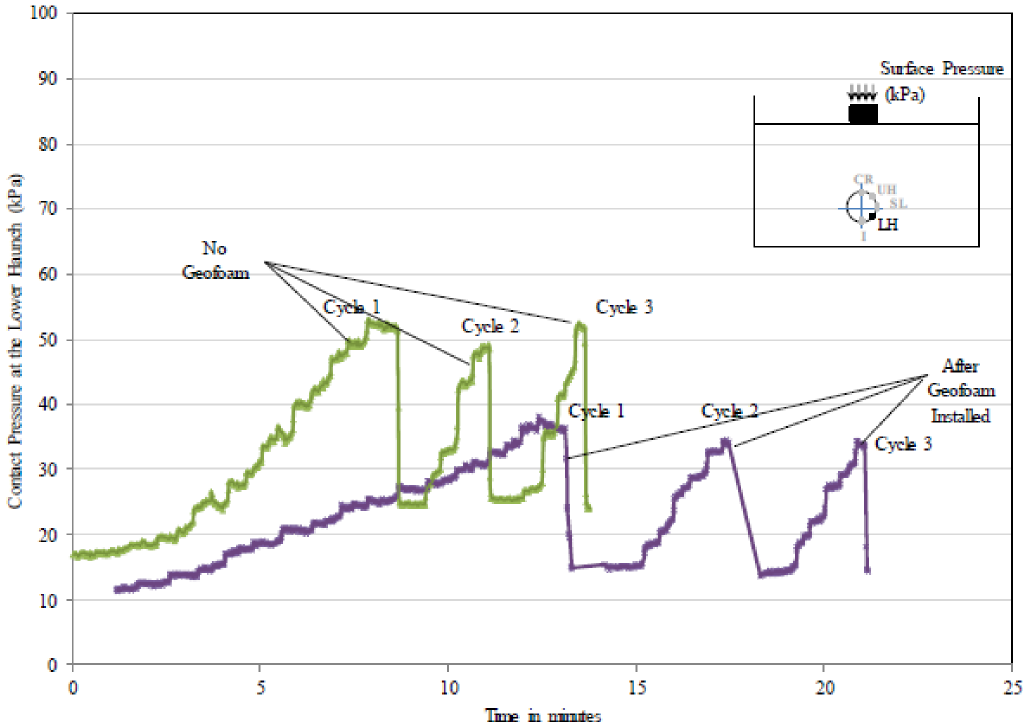

Figure A - 5

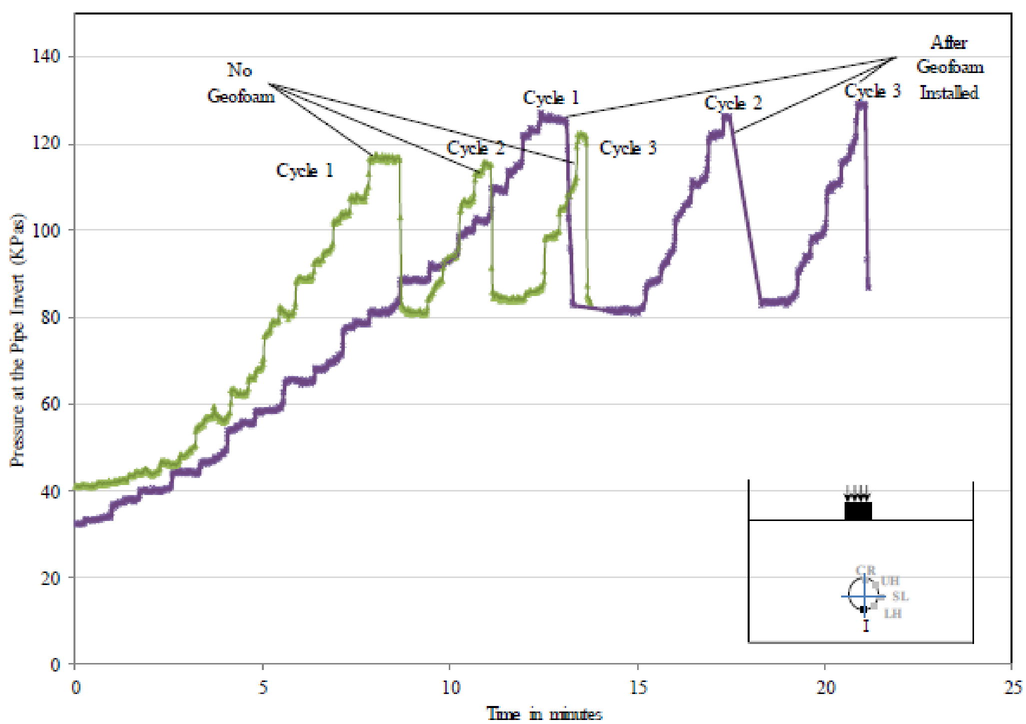

Figure A - 6

References

Abdoun, T.H., Da, H., O'Rourke M.J., Symans M.D., Thomas D., O'Rourke T.D., Palmer MC., Stewart HE., Factors influencing the behavior of buried pipelines subjected to earthquake faulting. Soil Dynamics and Earthquake Engineering 2009; 29: 415– 27.

ACPA. 2011. Concrete pipe design manual. American Concrete Pipe Association, Vienna, Va.

Adams, M.T., Collin, J.G., Large model spread footing load tests on geosynthetic reinforced soil foundations." Journal of Geotechnical and Geoenvironmental Engineering 1997; 1: 66-72.

Ahmed, M.R., Meguid M.A., Patents and techniques of contact pressure measurement in geotechnical engineering. Recent Patents on Engineering 2009; 3: 210-19.

Ahmed, M.R., and Meguid, M.A., Laboratory measurement of the load reduction on buried structures overlain by eps geofoam. 65th Canadian Geotechnical Conference 2013; Montreal, Qc, Canada (CD-ROM).

Ahmed, M.A., Tran V.D.H., Meguid, M.A., On the role of geogrid reinforcement in reducing earth pressure on buried pipes: experimental and numerical investigations. Soils and Foundations 2015; 5(33): 588-99.

Akinmusuru, J.O., Akinbolade J.A., Stability of loaded footings on reinforced soil. Journal of the Geotechnical Engineering Division 1981; (107)6: 819-27.

Alamshahi, S., Hataf, N., Bearing capacity of strip footings on sand slopes reinforced with geogrid and grid-anchor. Geotextiles and Geomembranes 2009; 27(3): 217-26.

Alawaji, H.A., Settlement and bearing capacity of geogrid-reinforced sand over collapsible soil. Geotextiles and Geomembranes 2001; 19(2): 75-88.

Arnold, M., Bartl, U., Franke, D., A solution to concurrent measurement of the normal and tangential earth pressure in model tests. Geotechnical Measurements and Modelling 2003; 321-326.

Azam, G., Hsieh, C., Wang, M., Performance of strip footing on stratified soil deposit with void. Journal of Geotechnical Engineering 1991; (117)5: 753-72.

Badie, A., Wang, M.C., Stability of spread footing above void in clay. Journal of Geotechnical Engineering 1984; (110)11: 1591-605.

Baus, R.L., Wang, M.C., Bearing capacity of strip footing above void. Journal of Geotechnical Engineering 1983; (109)1: 1-14.

Bhalla, S., Yang, Y.W., Zhao., J, Soh, C.K., Structural health monitoring of underground facilities -technological issues and challenges. Tunnelling and Underground Space Technology 2005; 20(5): 487-500.

Bourque, S., Centrifuge and numerical modeling of induced trench twin conduits. M.Sc.E. Thesis, University of New Brunswick, Fredericton, N.B 2002.

Bueno, B.S., Benjamim, C.V., Zornberg, J.G., Field performance of a full-scale retaining wall reinforced with non-woven geotextiles. Slopes and Retaining Structures under Seismic and Static Conditions, ASCE Geotechnical Special Publication 2005; Austin, Texas (CD-ROM).

Brachman, R.W.I., Moore, I.D., Rowe, R.K., interpretation of buried pipe test: small-diameter pipe in ohio university facility. Transportation Research Record 1996; 1541: 64-70.

Brachman, R.W.I., Moore, I.D., Rowe, R.K., The design of a laboratory facility for evaluating the structural response of small-diameter buried pipes. Canadian Geotechnical Journal 2000; 37(2): 281-95.

Carlson, R.W., Development and analysis of a device for measuring compressive stress in concrete. UN-11-M, PhD Thesis, Massachusetts Institute of Technology 1939.

Choo, Y.W., Abdoun, T.H., O'Rourke, M.J., Da, H., Remediation for buried pipeline systems under permanent ground deformation. Soil Dynamics and Earthquake Engineering 2007; 27: 1043–1055.

Choudhary, A.K., Jha, J.N., Gill K.S., Laboratory investigation of bearing capacity behaviour of strip footing on reinforced flyash slope. Geotextiles and Geomembranes 2010; 28(4): 393-402.

Corey, R., Han, J., Khatri D.K., Robert L., Parsons. Laboratory study on geosynthetic protection of buried steel-reinforced hdpe pipes from static loading. Journal of Geotechnical and Geoenvironmental Engineering 2014; 140(6): 04014019.

Cosentino, P., Grossman, B., Shieh, C., Doi, S., Fiber-optic chloride sensor development. Journal of Geotechnical Engineering 1995; 121(8): 610-617.

Das, B.M., Khing, K.H., Foundation on layered soil with geogrid reinforcement - effect of a void. Geotextiles and Geomembranes 1994; 13(8): 545-53.

Das, B.M., Khing, K.H., Shin, E.C., Puri, V. K., Yen, S. C., Comparison of bearing capacity of strip foundation on geogrid-reinforced sand and clay. Proceedings of the 8th International Conference on Computer Methods and Advances in Geomechanics Part 2 (of 4) 1994; Morgantown, WV, United States.

Das, B.M., Omar, M.T., The effects of foundation width on model tests for the bearing capacity of sand with geogrid reinforcement. Geotechnical and Geological Engineering 1994; 12(2): 133-41.

Das, B.M., Maji, A., Shin, E.C., foundation on geogrid-reinforced sand - effect of transient loading. Geotextiles and Geomembranes 1998; 16(3): 151-60.

Das, B.M., Shin, E.C., Strip foundation on geogrid-reinforced clay: behavior under cyclic loading. Geotextiles and Geomembranes 1994; 13(10): 657-67.

DeMerchant, M.R., Valsangkar, A.J., Schriver, A.B., Plate load tests on geogrid-reinforced expanded shale lightweight aggregate. Geotextiles and Geomembranes 2002; 20(3): 173-90.

Dore G., Juneau S., Pierre P., WO2008/017158 A1 (2008).

Dunnicliff, J., Green, G.E., Geotechnical instrumentation for monitoring field performance. Wiley, New York 1988.

Duplain, G., Van Neste R.,: US2006/7265847 (2006).

Duplain, G., US2007/7259862 (2007).

Geokon Publications on Earth Pressure Cells Model 4810, Accessed on 20 October 2015 (http://www.geokon.com/content/datasheets/4800_Series_Earth_Pressure_Cells.pdf)

Girao, P.S., Postolache, O., Pereira, J.M.D., Tactile sensors and their use in industrial, robotic and medical applications. IMEKO 20th TC3, 3rd TC16 and 1st TC22 International Conference Cultivating metrological knowledge 2007; Merida, Mexico.

Guido, V.A., D.K. Chang, D.K., Sweeney M.D., Bearing capacity of shallow foundations reinforced with geogrids and geotextiles. Second Canadian Symposium on Geotextiles and Geomembranes 1985; Edmonton, Alberta, Canada.

Guido, V.A., Kneupel, J.D., Sweeney, M.A., Plate load tests on geogrid reinforced earth slabs. Proceedings of Geosynthetics 1987; 216-25, New Orleans, Louisianam, USA.

Hanna, T.H., Field instrumentation in geotechnical engineering. Trans Tech Publications, 1985.

Hoeg, K., Stresses against underground structural cylinders. American Society of Civil Engineers Proceedings, Journal of the Soil Mechanics and Foundations 1968; 94(4): 833-58.

Ilstad, H.T., Borvik, T., Malo, K.A., A gauge for measurements of soil-structure interface force due to explosive loading. Transactions on the built environment, Structures under Shock and Impact 1994; 8: 358-364.

Inaudi, D., Glisic, B., Overview of fiber optic sensing technologies for geotechnical instrumentation and monitoring. Geotechnical News 2007; 25(3): 27-31.

Jennings, J.E., Burland, J.B., Rand soil-pressure cell for low pressures, high accuracy and long-term stability. Journal of Scientific Instruments 1960; 37(6): 193-195

Kamel, S., Meguid M.A., Investigating the effects of local contact loss on the earth pressure distribution on rigid pipes. Geotechnical and Geological Engineering 2013; 31(1): 199-212

Kang, J., Parker, F., Kang, Y.J., Yoo, C.H., Effects of frictional forces acting on sidewalls of buried box culverts. International Journal for Numerical and Analytical Methods in Geomechanics 2008; 32(3): 289–306.

Katona, M.G., Vittes, P.D., Soil–structure analysis and evaluation of buried box-culvert designs. Transp. Res. Rec 1982; 878: 1-7; Washington, D.C., United States.

Kim, K., Yoo, C.H., Design loading on deeply buried box culverts. Journal of Geotechnical and Geoenvironmental Engineering 2005; 131(1): 20–27.

Krivopal, B., US1989/5033291 (1989).

Khing, K.H., Das, B.M., Puri, V.K., Cook, E.E., Yen, S.C., The bearing-capacity of a strip foundation on geogrid-reinforced sand. Geotextiles and Geomembranes 1993; 12(4) 351-61.

Khing, K.H., Das, B.M., Puri, V.K., Yen, S.C., Cook, E.E., Foundation on strong sand underlain by weak clay with geogrid at the interface. Geotextiles and Geomembranes 1994; 13(3): 199-206.

Kohl, K.M., New, B.M., O'Rourke, T. D., Stress cell measurements for the investigation of soil-pipeline interactions during vehicular loading. Proc. Conference Geotechnical instrumentation in practice. 1990; 717-33, Nottingham, England.

Larsen, N.G., Hendrickson, J.G., A practical method for constructing rigid conduits under high fills. Paper presented at the Proceedings of the 41st Annual Meeting of the Highway Research Board 1962; Washington, D.C, United States.

Latha, G.M., Somwanshi, A., Bearing capacity of square footings on geosynthetic reinforced sand. Geotextiles and Geomembranes 2009; 27(4): 281-94.

Lazebnik, G.E., Chernysheva E., Certain errors in experimental determination of earth pressure on models of retaining walls. Power Technology and Engineering 1968; 2(4): 333-339.

Lazebnik, G.E., Smirnov, A.A., Ivanov, D.G., A set of instruments and equipment for measuring soil pressure. Soil Mechanics and Foundation Engineering 1973; 10(2): 116-121.

Lazebnik, G.E. and Tsinker G.P., Monitoring of soil-structure interaction: instruments for measuring soil pressures. 1997; Springer, 1st Edition.

Lee, F.H., Juneja, A., Wen, C., Dasari, G.R., Tan, T.S., Performance of total stress cells in model experiments in soft clays. Proceedings of the International Conference on Physical Modelling in Geotechnics: 2002; 101-106, St. John’s, Nfld., Canada.

Lee, B., Review of the present status of optical fiber sensors. Optical Fiber Technology 2003; 9(2): 57-79.

Lefebvre, G., Laliberte, M., Lefebvre, L.M., Lafleur, J., Fisher, C.L., Measurement of soil arching above a large diameter flexible culvert. Canadian Geotechnical Journal 1976; 13(1): 58-71.

Legge, T.F.H., Swart P.L., Zyl G.V., Chtcherbakov A.A., A fibre Bragg grating stress cell for geotechnical engineering applications. Measurement Science and Technology 2006; 17(5): 1173-1179.

MacLeod, T., Earth pressures on induced trench conduits. M.Sc.E. thesis, University of New Brunswick, Fredericton, N.B 2003.

Majumder, M., Gangopadhyay, T.K., Chakraborty, A.K., Dasgupta, K., Bhattacharya, D.K., Fibre Bragg gratings in structural health monitoring-Present status and applications. Sensors and Actuators 2008; 147(1): 150-164.

Marston, A., Anderson, A.O., The Theory of Loads on Pipes in Ditches and Tests of Cement and Clay Drain Tile and Sewer Pipe. Iowa State College, Ames, 1913.

Marston, M. G., The Theory of External Loads on Closed Conduits in the Light of the Latest Experiements. Iowa State University Engineering Experiemt Station, Iowa State College, Ames 1930.

Margason, G., Irwin M. J., Earth Pressure Cell. Nature Publishing Group 1964; 202(5): 483-484.

McAffee, R.P., & Valsangkar, A. J., Field performance, centerfuge test, and numerical modelling of an induced trench installation. Canadian Geotechnical Journal, 2008; 45(1) 85-101.

McGuigan, B.L., and Valsangkar, A.J., Centrifuge testing and numerical analysis of box culverts installed in induced trenches. Canadian Geotechnical Journal, 2010; 47(2): 147–163.

Miyazaki, K., Hirokawa, E., Fundamental study of reinforcement of sand layer in model test. Proceedings of the International Symposium on Earth Reinforcement 1992; Kyushu, Jpn.

Monfore, G.E., An analysis of the stress distribution in and near stress gages embedded in elastic solids. U.S. Department of Interior, Bureau of Reclamation, Research and Geology Division, Structural Research Laboratory, Report No. SP-26 1950.

Okabayashi, K., Ohtani, W., Akiyama, K., and Kawamura, M., Centrifugal model test for reducing the earth pressure on the culvert by using the flexible material. Proceedings of the 4th International Offshore and Polar Engineering Conference 1994; Osaka, Japan.

Omar, M.T., Das, B.D., Puri, V.K., Yen, S.C., Ultimate bearing capacity of shallow foundations on sand with geogrid reinforcement. Canadian Geotechnical Journal 1993; (30)3: 545-49.

Omar, M.T., Das, B.M., Yen, S.C., Puri, V.K., Cook, E.E., Ultimate bearing capacity of rectangular foundations on geogrid-reinforced sand.. Geotechnical Testing Journal 1993; 16(2): 246-52.

Olson, S.M., Hashash, Y., Polito, C., Phillips, C., Muszynski, M., Measuring pressures in the geotechnical centrifuge using tactile pressure pads. 7th Annual NEES Centrifuge Research and Training Workshop Rensselaer Polytechnic Institute, 2011.

Omega, Inc. Transactions in Measurements and Control, accessed on 20 October 2015 (http://www.omega.com/literature/transactions/volume3/pressure.html).

O'Rourke, T.D., Jezerski, J.M., Olson, N.A., Bonneau, A.L., Palmer, M.C., Stewart, H.E., O'Rourke, M.J., Abdoun, T., Geotechnics of pipeline system response to earthquakes. Proceedings Geotechnical Earthquake Engineering and SoilDynamics IV 2008; 1-38, Sacramento, CA, United States.

Padade, A.H. and Mandal, J.N., Behavior of expanded polystyrene (eps) geofoam under triaxial loading conditions. Eelctronic Journal of Geotechnical Engineering. 2012; 17: 2543-2553.

Paikowsky, S.G., Hajduk, E.L., Calibration and use of grid-based tactile pressure sensors in granular material. Geotech. Test. J., 1997; 20(2), 218–241.

Paikowsky, S.G., Palmer, C.J., Dimillio, A., Visual observation and measurement of aerial stress distribution under a rigid strip footing. Geotechnical Special Publication 2000; 94: 148-169.

Paikowsky, S.G., Tien, H.S., Experimental examination of the arching mechanism on the micro level. Geotechnical Special Publication 2002; 117: 222-228.

Paikowsky, S.G., Palmer, C.J., Rolwes, L.E., The use of tactile sensor technology for measuring soil stress distribution. Geotechnical Engineering in the Information Technology Age ASCE GeoCongress 2006; 1-6, Atlanta, Georgia, United States.

Patra, C.R., Das, B.M, Bhoi, M., Shin, E.C., Eccentrically loaded strip foundation on geogrid-reinforced sand. Geotextiles and Geomembranes 2006; 24(4): 254-59.

Peattie, K.R., Sparrows, R.W., The fundamental action of earth pressure cells. Journal of the Mech. and Phys. of Solids. 1954; 2: 141-145.

Plasti-Fab EPS Product Solutions, accessed on 20 October 2015. (http://www.plastifab.com/.)

Podoloff, R.M., Benjamin, M., Tactile Sensor for Analyzing Dental Occlusion. SOMA Engineering for the Human Body. 1989; 3(3): 1-6.

Pressure Profile Systems, Inc., accessed 20 April 2015, http://www.pressureprofile.com.

Ravet, F., Zou, L., Bao, X., Chen, L., Huang, R.F., Khoo, H.A., Detection of buckling in steel pipeline and column by the distributed Brillouin sensor. Optical Fiber Technology 2006; 12: 305–311.

Rolwes., Lawrence, E.Jr., The mechanism of load transfer in granular materials utilizing tactile pressure sensor technology. PhD Thesis, University of Massachusetts Lowell, 2002.

Sanan, B.K., An Evaluation of the effect of geofabrics on stresses and displacements in buried culverts. PhD Thesis, The University of Arizona., 1980.

Scario, J.H,. Reappraisal of Marston's formula. Journal of Transportation Engineering, ASCE 2003; 129(6): 703–712.

Scheer, A.C., and Willett, G.A.Jr., Rebuilt Wolf Creek culvert behaviour. Highway Research Record 1969; 262: 1-13 262, HRB, National Research Council, Washington, D.C.

Selig, E.T., A review of stress and strain measurement in soil. Proceedings of the Symposium on Soil-Structure Interaction, 1964; 162-186, Tucson, Arizona, United States.

Shin, E.C., Das, B.M., Experimental study of bearing capacity of a strip foundation on geogrid-reinforced sand. Geosynthetics International 2000; 7(1): 59-71.

Shin, E.C., Das, B.M., Lee, E.S., Atalar, C., Bearing capacity of strip foundation on geogrid-reinforced sand. Geotechnical & Geological Engineering 2002; 20(2): 169-80.

Sladen, J.A., Oswell, J.M., Induced trench method - a critical review and case history. Canadian Geotechnical Journal 1988; 25(3): 541-49.

Son, J.S., Parks T., US2008/7430925 B2 (2008).

Spangler, M.G., A Theory of Loads on Negative Projecting Conduits. Proceedings of the Highway Research Board, Transportation Research Board 1950; 30: 153-161, Washington, DC, United States.

Spangler, M.G., A practical application of the imperfect ditch method of construction. Highway Research Board, Proceedings of the Annual Meeting, 1958; 37: 271-277.

Spangler, M. G., R. L. Handy. Soil Engineering, 3rd ed. Intext Press, Inc., New York, 1973.

Springman, S.M., Nater P., Chikatamarla R., Laue J., Use of flexible tactile pressure sensors in geotechnical centrifuges. International Conference on Physical Modelling in Geotechnical Engineering 2002; 113-118, St. Johns, Canada.

Tachi S., Kawakami N., Kajimoto H., Kamiyama K., Mizota T., WO2005/2538040 (2006).

Tadros, M.K., Benak, J.V., Gilliland, M.K., Soil pressure on box culverts. *ACI Struct. J. 1989;* 86(4), 439–450.

Talesnick, M., Measuring soil contact pressure on a solid boundary and quantifying soil arching. Geotechnical Testing Journal 2005; 28(2): 171-179.

Talesnick, M., Hanna H., Avraham N., Dancygier, Yuri S.K., Measuring soil pressure on a buried model structure for the validation of quantitative frameworks. Journal of Geotechnical and Geoenvironmental Engineering 2008; 134(6): 855-865.

Talesnick, M.L., Xia, H.W., Moore, I.D., Earth pressure measurements on buried HDPE pipe. Geotechnique, 2011; 61(9): 721-732.

Talesnick, M.L., Xia, H.W., Moore, I.D., Earth Pressure Measurements on Buried Hdpe Pipe. Geotechnique, 2012; 62(12): 1139-42.

Taylor, D.W., Pressure distribution theories, earth pressure cell investigation, and pressure distribution data. U.S. Waterways Experiment Station 1947.

Taylor, R. K., Induced Trench Method of Culvert Installation. In Highway Research Record, HRB, National Research Council, 1973; 510(41-55), Washington, D.C. United States.

Tekscan, Inc. (2012). I-Scan & High-Speed I-Scan User Manual v. 7.5x, Tekscan Inc., Boston, Mass, accessed on 20 October 2015 (https://www.tekscan.com/products-solutions/systems/i-scan-system)

Tessari, A., Sasanakul, I., Abdoun, T., Advanced sensing in geotechnical centrifuge models, In 7th International Conference on Physical Modeling in Geotechnics 2010; 395-400 Zurich, Switzerland.

Tobar, T., Meguid, M.A., Experimental Study of the earth pressure distribution on cylindrical shafts. J. Geotech. Geoenviron. Eng. 2011; 137(11): 1121–1125.

Turan, A., El Nagar, M.H., Dundas, D., Investigation of induced trench method using a full scale test embankment. Geotech Geol Eng. 2013; 31: 557-568.

Vaslestad, J., Load reduction on buried rigid pipes below high embankments. ASCE Specialty Conference, Pipeline Division 1991; 47-58, Denver, Colorado, United States.

Vaslestad, J., Johansen, T.H., Holm, W., Load reduction on rigid culverts beneath high fills: long-term behavior. Transportation Research Record, 1415, Transportation Research Board, 1993; 1415:56-68, Washington, DC, United States.

Vaslestad, J., Yesuf, G.Y., Yohansen, T.H., Wendt, M., Damtew, T., Instrumented field test and soil structure interaction of concrete pipe with high fill. Proceedings of the 17th international conference on soil mechanics and geotechnical engineering: The academia & practice of geotechnical engineering 2009; 1802-1805, Alexandria, Egypt.

Wang, M.C., Badie, A., Effect of underground void on foundation stability. Journal of Geotechnical Engineering 1985; 111(8): 1008-19.

Wang, M.C., Hsieh, C.W., Collapse load of strip footing above circular void. Journal of Geotechnical Engineering 1987; 113(5): 511-15.

Weiss, K., Worn, H., The working principle of resistive tactile sensors cells. Proc. IEEE International Conference on Mechatronics & Automation 2005; 471-476, Portsmouth, UK

White, N.M., Boltryk P., Sensors in adaptronics. in: adaptronics and smart structures. Springer Berlin Heidelberg 2007; 301-369.

Yamamoto, K., Kusuda, K., Failure mechanisms and bearing capacities of reinforced foundations. Geotextiles and Geomembranes 2001; 19(3): 127-62.

Yamamoto, K., Otani, J., Bearing Capacity and failure mechanism of reinforced foundations based on rigid-plastic finite element formulation. Geotextiles and Geomembranes 2002; 20(6): 367-93.

Yoo, C.H., Parker, F., Kang J., Bedding and fill heights for concrete roadway pipe and box culverts. Final Report, ALDOT Project No. 930-592. Highway Research Center, Auburn University, AL, U.S.A., 2005.